SPRINGER BRIEFS IN MATERIALS

Jean-Michel Guenet

Organogels
Thermodynamics, Structure, Solvent Role, and Properties

Springer

SpringerBriefs in Materials

The SpringerBriefs Series in Materials presents highly relevant, concise monographs on a wide range of topics covering fundamental advances and new applications in the field. Areas of interest include topical information on innovative, structural and functional materials and composites as well as fundamental principles, physical properties, materials theory and design. SpringerBriefs present succinct summaries of cutting-edge research and practical applications across a wide spectrum of fields. Featuring compact volumes of 50 to 125 pages, the series covers a range of content from professional to academic. Typical topics might include:

- A timely report of state-of-the art analytical techniques
- A bridge between new research results, as published in journal articles, and a contextual literature review
- A snapshot of a hot or emerging topic
- An in-depth case study or clinical example
- A presentation of core concepts that students must understand in order to make independent contributions

Briefs are characterized by fast, global electronic dissemination, standard publishing contracts, standardized manuscript preparation and formatting guidelines, and expedited production schedules.

More information about this series at http://www.springer.com/series/10111

Jean-Michel Guenet

Organogels

Thermodynamics, Structure, Solvent Role, and Properties

Springer

Jean-Michel Guenet
CNRS-Université de Strasbourg
Strasbourg
France

ISSN 2192-1091 ISSN 2192-1105 (electronic)
SpringerBriefs in Materials
ISBN 978-3-319-33176-8 ISBN 978-3-319-33178-2 (eBook)
DOI 10.1007/978-3-319-33178-2

Library of Congress Control Number: 2016937940

Printed on acid-free paper

This Springer imprint is published by Springer Nature
The registered company is Springer International Publishing AG Switzerland

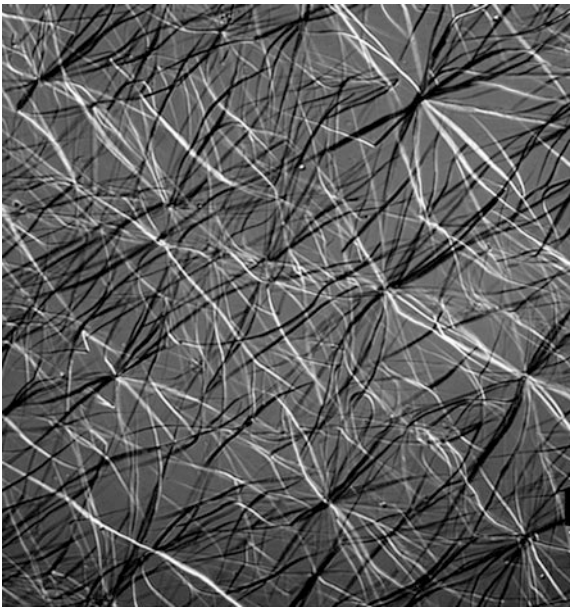

About the Author

Prof. Jean-Michel Guenet is Directeur de Recherche at CNRS and former head of the Institut Charles Sadron, Strasbourg, France, a CNRS-owned laboratory associated with the Université of Strasbourg. He has a degree in materials science engineering from Paris XIII University (1974), and obtained a Ph.D. degree in 1980 at Université de Strasbourg (formerly Université Louis Pasteur). He spent a year at Bristol University, UK, under the guidance of Prof. A. Keller as a postdoctoral fellow. He was Visiting Scientist at NIST with Prof. G.B. McKenna, Gaithersburg, USA, in 1985; a Visiting Professor at Université de Mons-Hainaut, Belgium, with Prof. M. Dosière from 1995 to 2004; and Invited Professor at Shizuoka University, Japan, with Prof. H. Itagaki in 2002 and 2009. He has authored about 170 papers, and has also written two books *Thermoreversible Gelation of Polymers and Biopolymers* (Academic Press, 1992), and *Polymer-solvent Molecular Compounds* (Elsevier, 2008). In 1990, he was awarded the Dillon Medal of the American Physical Society for his work on polymer gels. He has also founded in 1996 of a series of conferences formerly entitled *Polymer-solvent Complexes and Intercalates* which has been renamed POLYSOLVAT in 2008. Since 2008 this series of conferences is sponsored by IUPAC as being one of its kind.

To my grandchildren Antoine, Lucas,...
À mes petits enfants Antoine, Lucas,...

Preface

This monograph should not be regarded as a comprehensive review of the papers published on the recent topic of organogels. Rather, it aims at highlighting the physics aspect of organogelation while most of the papers covering this field deal chiefly with the synthesis and the characterization aspects. As a rule, the way investigations, experimental, and theoretical approaches, together with the interpretations of the experimental data are tackled, depends drastically on the researcher background. Here formation mechanisms, thermodynamic, molecular structure, morphology, and physical properties are presented and discussed from the view of a polymer physicist whose main interest has been on the study of polymer thermoreversible gels for many years and who has entered the field of organogelation a few years ago. Therefore, organogels are systematically examined in the light of the knowledge gathered on the physics aspect of polymer thermoreversible gelation whenever this appears relevant for their understanding. *To be sure, this is not the story of organogels, but rather a story on organogels.*

Some reminders will be given throughout on basic aspects of thermodynamics, with special emphasis on phase diagrams, radiation scattering techniques, and rheology. This relies on the author's feeling, as well as with his own experience, that many readers might not be too familiar with these aspects.

This book therefore pursues two goals: provide researchers already involved in the field with an alternative view on these systems and give an easy access gate to newcomers. It aims at reaching a broad audience, from students to senior scientists.

As emphasized above, it is not the purpose of this monograph to provide the reader with an exhaustive list of references. Rather, those references that are thought to illustrate some aspects in the best way will be quoted. Therefore, it should be clearly understood that the absence of some references does not convey any negative judgment. Recent reviews are available [1–3] and even a book edited by Terech and Weiss [4], and another one edited by Liu and Li [5]; both consist of chapters collected from different authors.

Systems designated as hydrogels will be mentioned throughout but no specific chapter will be devoted to them. The term hydrogels is often broadly used and

encompasses different systems from self-assembling molecules to biopolymers gels such as agarose, carrageenans, and the like. Here only those hydrogels comparable to organogels are considered, namely excluding those systems for which ionic force comes into play.

Finally the author wishes to acknowledge the following people for kindly providing him with figures and data: A. Ajayaghosh, A. Banerjee, J.L. Bantignies, L. Bouteiller, D. Collin, C. Daniel, N. Giuseppone, X.Y. Liu, B. Lotz, U. Maitra, S. Malik, E.W. Meier, P. Mésini, Nonappa, J.L. Pozzo, M. Schmutz, A. Thierry, R.G. Weiss.

References

1. Terech, P., Weiss, R.G.: Low molecular mass gelators of organic liquids and the properties of their gels. Chem. Rev. **97**, 3133–3159 (1997)
2. Babu, S.S., Praveen, V.K., Ajayaghosh, A.: Functional π-gelators and their applications. Chem. Rev. **114**, 1973–2129 (2014)
3. Weiss, R.G.: The past, present and future of molecular gels. What is the status of the field, and where is it going? JACS **136**, 7519–7530 (2014)
4. Terech, P., Weiss, R.G. (eds.): Molecular Gels: Materials with Self-assembled Fibrillar Networks. Springer (2006)
5. Liu, X.L., Li, J.L.: Soft Fibrillar Materials: Fabrication and Applications. Wiley-VCH (2013)

Contents

Chapter 1
Introduction

When Horace Walpole coined the word "serendipity" in 1754 he probably did not realize to what extent this word would apply to many scientific discoveries. Organogels are certainly among these "*pleasant surprises*" and/or "*unexpected discovery occurring by design*" that have triggered a growing enthusiasm amidst researchers these past 15 years. In some aspects, the discovery of organogels is reminiscent of that of polymers. Polymers were in most cases the results of unwanted reactions that deeply disturb organic chemists in their studies. Polymers obey the "bodenkörper" rule devised by German chemist Wilhelm Ostwald, which means the "physical body at the bottom," namely the *precipitate at the bottom*. Similarly, scientists attempting to synthesize new molecules, in many cases for the purpose of getting systems with liquid crystalline properties, faced the same situation when they stumbled upon solutions that jammed, turning into unexpected, undesired gels. They eventually called these systems organogels as they would form in organic solvents with organic molecules. Sometimes the term "*molecular gels*" is used as opposed to gels formed from polymers.[1]

This topic is becoming more and more attractive as witnessed by the exponential growth of the number of papers published these past few years when the only keyword "organogel" is selected. This number has grown from only a few papers in the late 1990s to more than 200 papers a year nowadays (see Fig. 1.1).

As with polymers the formation of these gels arises from so-*called physical interactions*, such as hydrogen bonds, van der Waals interactions, π-stacking, and the like, that are of much lower energy than *chemical interactions* through covalent bonds.[2] As a result, these gels are thermoreversible in the sense that heating up produces melting of the gel into the original solution while cooling down allows

[1]It is here worth stressing that the proper term for physical gels prepared from polymers or biopolymers is *Polymer/biopolymer thermoreversible gels* and not polymer organogels.
[2]In the case of polymers there exists "chemical gels" where chains are chemically-cross-linked by covalent bonds. These gels are then thermally-irreversible.

J.-M. Guenet, *Organogels*, SpringerBriefs in Materials,
DOI 10.1007/978-3-319-33178-2_1

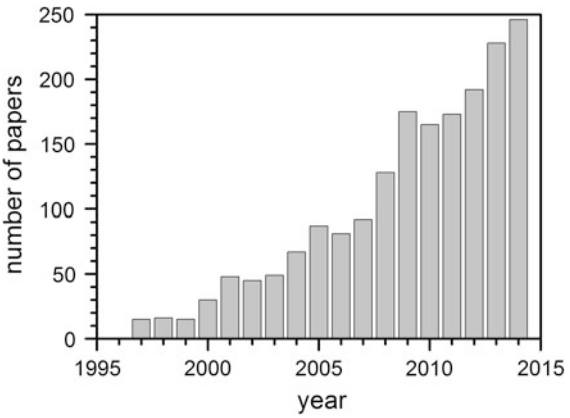

Fig. 1.1 Number of papers published when keyword "organogels" is entered. Data from ISI Web of knowledge [1]

reformation of the gel. This process, designated as SOL–GEL transition, can be carried out infinitely without altering the molecular structure of the components.

These gels are typically of fibrillary morphology as are polymer thermoreversible gels. Their macroscopic resemblance is striking as shown in Fig. 1.2. Yet, their gelation mechanism differs: organogelation is a nearly-one-dimensional process in most cases while polymer gelation arises chiefly from hampering chain folding [2]. Also, the fibrils cross-sections of organogels are in most cases significantly larger. This is reminiscent to some extent of birds and bats: both have wings but evolution followed differing paths to achieve this particular feature.

The question that may torment researchers is why do these oligomolecules form fibrillary gels just like larger polymer molecules? It turns out that most molecules involved in the gelation process may be described as "***chimera***". Like this Greek mythology monster, they bear different facets, in other words chemical groups, as portrayed for some of them in Fig. 1.3. As a consequence, the nature of the interactions is likely to result in unusual ordering properties. Parts of the molecules

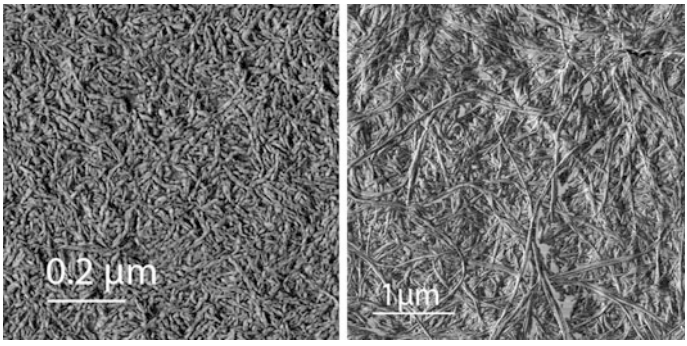

Fig. 1.2 AFM pictures of xerogels from isotactic polystyrene/*trans*-decalin thermoreversible gels (*left*) and OPV/benzyl methym ether. (J.M. Guenet, unpublished results)

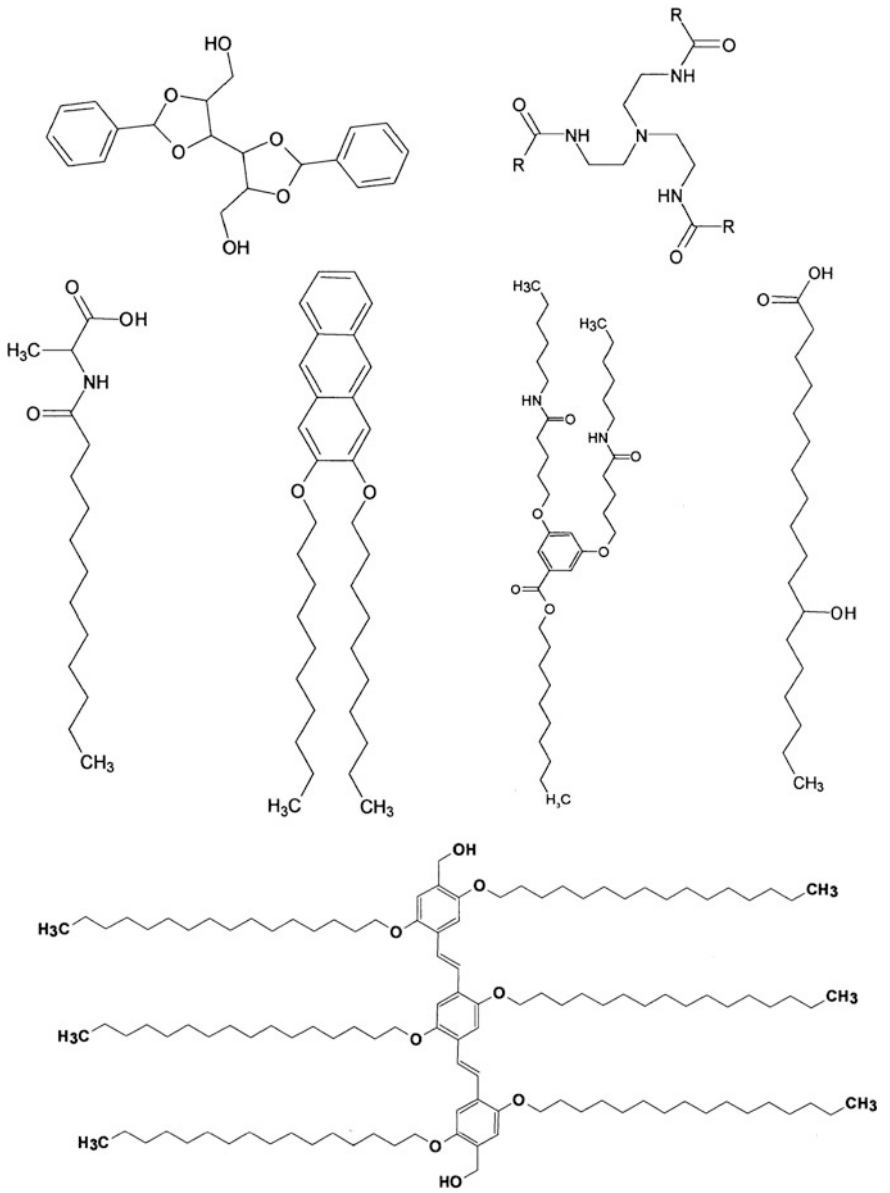

Fig. 1.3 Chemical structures of selected organogelators. *Top left* 1,2 dibenzyl sorbitol [3], *top right* a trisamide [4]; *middle left* N-n-Dodecanoyl (L)-alaninate [5], *middle center left* 2,3-Bis-n-decyloxyanthracene [6], *middle center right* 3,5-Bis-(5-hexylcarbamoyl-pentyloxy)-benzoic acid decyl ester [7], *middle right* 12-Hydroxystearic Acid [8]; *bottom* oligo phenylene vinylene C16 [9]

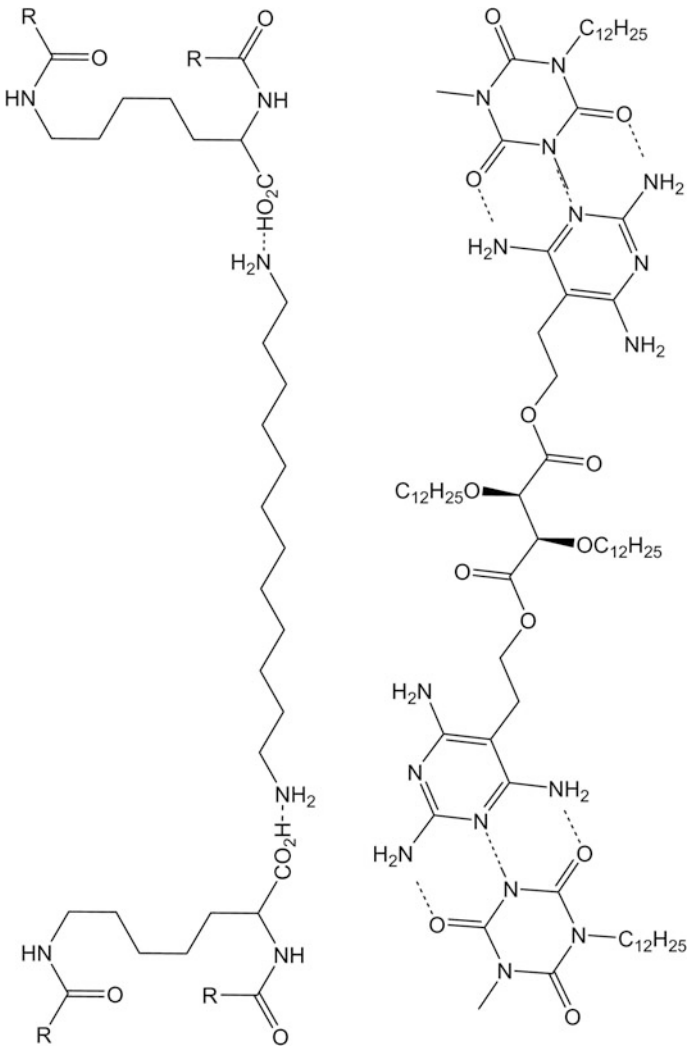

Fig. 1.4 Chemical structures of organogelators composed of two complementary molecules. Interactions between partners are achieved through hydrogen bonds as shown. *Left* tert-butyl carbamate functionalized lysine derivative with dodecyl chains attached via carbamate bonds [10]; *right* JANUS-II compound [11, 12]

may be able to establish hydrogen bonds, while other parts are likely to interact through π-staking, and/or van der Waals interactions, and the like. Clearly, the crystallization behavior is likely to be a complex process. The rather odd chemical structure of these molecules might be the clue for understanding the organogelation phenomenon.

Even more complex systems made up of two molecules can also produce organogels. Some examples of these molecules are shown in Fig. 1.4. These molecules first assemble strongly with a well-defined partner through hydrogen bonds by a recognition process, and then form fibrillary structures. Some can be large molecules as those studied by Smith and coworkers [10] or smaller molecules as reported by Sarazin et al. [11]. Needless to say that in this case the gelation phenomenon is more complex than a simple crystallization. Two options are to be envisaged: (1) the molecule and its partner may first assemble, thus forming supramolecular polymers that eventually aggregate; (2) the molecule and its partner co-crystallize producing a fibrillar morphology. We shall see that option 1 may prevail in these systems.

All these aspects will be tentatively addressed in this monograph.

References

1. Data from ISI Web of Science: https://isiknowledge.com
2. Guenet, J.M.: Thermoreversible Gelation of Polymers and Biopolymers Academic Press London (1992); Guenet, J.M.: Polymer-solvent Molecular Compounds. Elsevier, London (2008)
3. Thierry, A., Straupe, C., Lotz, B., Wittmann, J.C.: Phys. Gelation - Path Towards Ideal Dispers. Additi. Polym. Polym. Commun. **31**, 299 (1990); VanderHart, D., Douglas, J.F., Hudson, S.D., Antonucci, J.M., Wilder E.A.: NMR Charact. Form. Kinet. Struct. Di-O-Benzylidene Sorb. Gels Self-Assem. Org. Solv. Langmuir. **27**, 1745 (2011)
4. Feng, L., Cavicchi, K.A.: Investigation of the relationships between the thermodynamic phase behavior and gelation behavior of a series of tripodal trisamide compounds. Soft Matter **8**, 6483 (2012)
5. Pal, A., Ghosh, Y.K., Bhattacharya, S.: Molecular mechanism of physical gelation of hydrocarbons by fatty acid amides of natural amino acids. Tetrahedron **63**, 7334 (2007)
6. Lescanne, M., Colin, A., Mondain-Monval, O., Fages, F., Pozzo, J.L.: Structural Aspects of the gelation process observed with low molecular mass organogelators. Langmuir **19**, 2013 (2003)
7. Diaz, N.; Simon, F.-X.; Schmutz, M.; Rawiso, M.; Decher, G.; Jestin, J.; Mesini, P.J. *Self-Assembled Diamide Nanotubes in Organic Solvents*. *Angew, Chem. Int. Ed.*, **2005**, *44*, 3260
8. Terech, P., Pasquier, D., Bordas, V., Rossat, C.: Rheological properties and structural correlations in molecular organogels. Langmuir **16**, 4485 (2000)
9. Ajayaghosh, A., George, S.J.: J. Am. Chem. Soc. **123**, 5148 (2001)
10. Hardy, J.G., Hirst, A.R., Smith, D.K.: Exploring molecular recognition pathways in one- and two-component gels formed by dendritic lysine-based gelators. Soft Matter **8**, 3399 (2012)
11. Sarazin, D., Schmutz, M., Petitjean, A., Lehn, J.M., Guenet, J.M.: Structure of supramolecular polymers generated via self-assembly through hydrogen bonds Mol. Cryst. Liq. Cryst. **468**, 539 (2007)
12. Lehn, J.M.: *Supramolecular chemistry: concepts and perspectives*. VCH, Weinheim (1995)

Chapter 2
Gels: A Definition

Polymer thermoreversible gels and organogels are produced from solutions where the solvent is by far the major component, typically above 90 % up to 99.9 % with some biopolymers. By cooling these solutions, they turn into a solid-like material at a relatively well-defined temperature. It is customary to read in some papers that a given component *gelled a given solvent*.

Every book or review dealing with gels systematically quotes Dorothy Jordan Lloyd [1] who tackled the question of defining a gel and who eventually came to the conclusion that "*The colloidal condition, the gel, is one which is easier to recognize than to define*". The reason lies in the fact that there is usually no clear-cut definition resting on a minimum of physical parameters while simply handling and touching a gel allows one to realize that it is neither a viscous solution nor a piece of glue nor a paste.

It is therefore worth devoting some space so as to try and provide the reader with a thorough insight into the way these systems can be, or rather may be defined. A *definition*, also called an *extensive definition* in the present case, serves to specify the *extension of a concept*. It allows one to establish a list naming every object that is a member of a specific set. In this monograph two ways of defining organogels are discussed: the *rheological aspect* and the *topological-thermodynamic aspect*. The former is the classical approach based on the rationale that a connected array of objects should possess a solid-like behavior, something testable by mechanical observations. The latter derives from the fact that organogels are thermally-reversible networks, and so relies both upon its topology, with respect to the accepted definition of a network, and upon its formation and melting properties.

These two ways of tentatively defining a gel go beyond the all too often used tube tilting or tube upside down test which may be misleading. That a solution or a suspension does not flow anymore through some jamming process does not prove at all that a gel has formed. For instance, humid sand passes the tube tilting test and yet nobody would seriously consider it a gel.

J.-M. Guenet, *Organogels*, SpringerBriefs in Materials,
DOI 10.1007/978-3-319-33178-2_2

2.1 Rheological Definition

The very first rheological apparatus granted by nature to man is one's fingers. Compressing a system between one's finger and thumb allows one to decide whether one his dealing with a viscous solution or a gel. Yet, this apparatus is far from perfection, and often deceiving as it provides no information on long relaxation processes.

In the case of polymers, rheological properties are considered to differentiate a gel, whose existence arises from chemical or physical cross-linking, from a highly viscous solution. Typically, a gel is a solid-like system that can be studied by classical techniques such as oscillatory, relaxation ,and creeping experiments [2]. From these experiments parameters such as G', G'', $\tan \delta = G'/G''$, E or J can be derived where G' and G'' are the storage modulus and the loss modulus, E the Young's modulus, and J the compliance. Relaxation experiments are carried out by application of a given deformation ε which relates the resulting stress to the Young's modulus ($\sigma(t) = E(t)x\varepsilon$) while creep experiments are performed by application of a given stress σ_o which relates the compliance to the deformation $\gamma(t)$ ($J(t) = \gamma(t)/\sigma_o$). In order to identify the typical behavior of a solid, two criteria must be strictly fulfilled:

(1) **criterion 1**: in oscillatory experiments G' must be much larger than G', usually over a decade, which implies that stress–strain relaxation is chiefly governed by an elastic process [3];
(2) **criterion 2**: in a relaxation experiment $E(t_\infty) = \text{const} = E(t_o)$, or in a creep experiment $J(t_\infty) = 1/E = 1/E(t_o)$ emphasizing the solid-like behavior as opposed to what is seen in highly viscous solutions.

For instance, vulcanized rubber used in the making of car tyres fulfills all these criteria, while native rubber displays a strong relaxation. Vulcanization is obtained through chemical cross-linking thus establishing covalent bonds between the rubber chains. Covalent bonds are of sufficient energy to prevent from disentanglements by reptation that otherwise occurs in native rubber entailing permanent deformation. As a rule, chemically cross-linked gels, namely of the same type of molecular architecture as cross-linked rubber yet highly swollen by a solvent, behave the same [4].

Strangely enough, despite the abundant literature on organogels, not so many rheological experiments have been reported so far. Terech et al. [5] and later Collin et al. [6] have studied in depth about these systems either by oscillatory experiments by means of a classical cone–plate apparatus (Terech et al.) or with a piezorheometer where opposite ceramics vibrate in the shear mode (Collin et al.). These experiments are performed in a limited range of frequency typically from 10 to 500 Hz with classical cone–plate rheometer, while a piezorheometer allows one to extend the frequency range from 0.2 to 1000 Hz. A typical variation of G' and G'' as shown in Fig. 2.1 is observed in both studies.

Although G' looks virtually constant and is much larger by approximately a decade than G'', the behavior shown in Fig. 2.1 can be deceiving despite the large

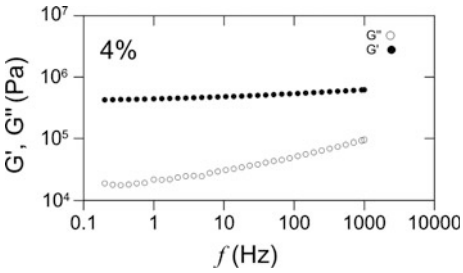

Fig. 2.1 Variation of the storage modulus G' (●) and the loss modulus G'' (○) as a function of shear frequency for experiments carried out by means of a piezorheometer at very low strain (10^{-5}). The organogel is a 4 % mixture of a modified peptide (w/v) in tetraline. From Collin et al. [6]

frequency range swept. Apparently, criterion 1 is obeyed, yet relaxation experiments over longer period of times, namely as if the frequency range were extended to much lower values, may reveal subsequent relaxation down to $E(t_\infty) = 0$. The organogel may therefore experience irreversible, permanent deformation which implies that the rheological approach is possibly not appropriate for a non-questionable definition of these systems.

This behavior has already been observed by Guenet and McKenna [7] with gels from isotactic polystyrene, a stereoregular polymer that display significant relaxation when submitted to a given deformation: usually the stress falls to zero after 24 h. Yet, the very primitive handling and/or touching test unquestionably shows one is dealing with a gel.

Recent results by Collin et al. [6] have observed a similar behavior. Their experiments consist in applying a given deformation, and then submitting the sample to a vibrating shear mode. This is seen in Fig. 2.1. Yet, by compressing further, the response is identical to the previous one (Fig. 2.2). Clearly, application of a compressive deformation has led to an irreversible modification of the organogel. Would the gel have not undergone irreversible deformation, then G' should have drastically increased. This behaviour is equivalent to the stress relaxation phenomenon

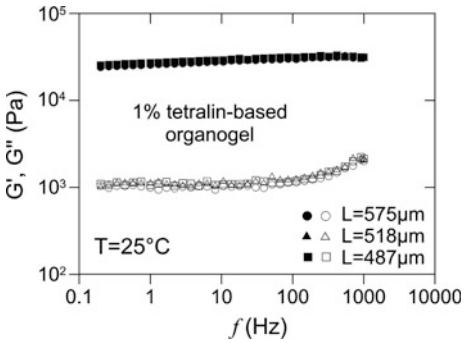

Fig. 2.2 Variation of G' and G'' of a 1 % tetralin-based organogel as a function of frequency for different thicknesses resulting from a gradual static compression of the sample. The measurements were performed at 25 °C. From Collin et al. [6]

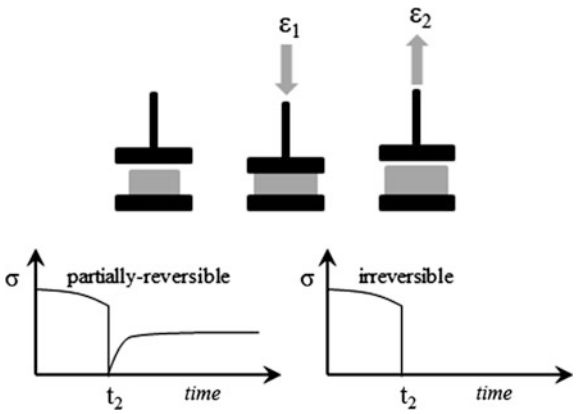

Fig. 2.3 Rheological test designed by Daniel et al. [8]. A cylinder-like piece of gel is placed between two plates. A deformation ε_1 is applied to the sample and the stress σ is measured as a function of time. At $t = t_2$ the *upper plate* is pulled up to a deformation ε_2, which entails a sharp drop of the stress σ. For a partially reversible system, a stress will gradually reappear (*graph left*), while for an irreversible system (a paste for instance) the stress remains 0 independent of ε_2 (*graph right*). [8]

observed with iPS gels. Therefore, these organogels do not meet criterion 2 although they meet criterion 1, at least when low shear deformation are used.

Guenet and coworkers realized that failure to meet these rheological criteria was due to the degree of interaction between the object involved in the gel architecture. They accordingly proposed another test involving compression measurements for determining the degree of interaction by investigating the degree of recovery after submitting the gel to a deformation [8]. Indeed, if applying a deformation to the organogel entails destruction of connecting bonds this can be evaluated through the simple test schematized in Fig. 2.3.

This test consists in measuring the stress resulting from the compression of a cylindrical sample to a deformation ε_1, and then at $t = t_2$ moving the piston to a deformation ε_2 with $\varepsilon_2 < \varepsilon_1$. A stress should reappear if connecting bonds are still present. Conversely, if these bonds have been destroyed or if they did not exist in the first place, then the stress remains zero. This test was successfully applied to thermoreversible gels from stereoregular polymers. It could be equally used for characterizing organogels.

This test allows one to offer a way of measuring the degree of reversibility, $r(\varepsilon_1)$ for a given deformation. It suffices to determine at which value of ε_2 set at always the same time t_2 there is no recovery at all. Then, $r(\varepsilon_1)$ is simply $r(\varepsilon_1) = \varepsilon_1/\varepsilon_2$. Admittedly, this kind of analysis is tedious and time-consuming but it provides one with tangible data of the system under study.

It is worth stressing that destruction of interfibrillar bonds is possible under mechanical constraint because these bonds are of energy lower than covalent bonds. In the literature, these systems are often said to be *thixotropic*. Actually, the same

phenomenon occurs with solid ice. It is well-known that a weight will sink down through a piece of ice through local destruction and reformation of the hydrogen bonds. This phenomenon is well-known in glaciers. The same occurs with thermoreversible polymer gels and organogels: van der Waals or hydrogen interfibrillar bonds can be disrupted, yet may reform. This is sometimes described as a yield stress phenomenon [5] although recovery may take place with time, which is reminiscent of a healing process through the reformation of interfibrillar bonds.

It is worth emphasizing that systems may show a storage modulus higher than the loss modulus in a large frequency range in oscillatory experiments [9] while they do not pass the test designed by Daniel et al. [8]. An extension to very low frequencies, which is equivalent to very long relaxation times may reveal that G'' becomes larger than G' in the end. Usual rheometers do not give access to very low frequencies so that a relaxation experiment is more informative in most cases. This will be discussed in more details in Chap. 6.

2.2 Topological-Thermodynamic Definition

Rheology and/or the test developed by Guenet and coworkers are clearly not sufficient to decide whether a system can be considered gel or not. The topology together with the thermodynamic of these systems brings probably a better way of tackling the question. This definition was already proposed by Guenet and coworkers for polymer thermoreversible gels [10].

It is customary to regard a gel as a network of connected objects. The definition of a network that is provided by any dictionary is

> a large system of lines, tubes, wires, etc., that cross one another or are connected with one another (Longman dictionary [11]).

Note that this definition is basically the same in French, Spanish, and German, and possibly in many other languages, which makes it universal. In all cases, elongated objects are involved in the formation of a gel. Therefore the gel status can be inferred from structural or morphological investigations. This ***is the topological criterion***. A typical example is given in Fig. 2.4 left.

In addition, polymer thermoreversible gels, and similarly organogels, are thermally-reversible systems: they can be melted and reformed at will. As a result, one has to introduce an additional criterion to differentiate these gels from those that are thermally-irreversible such as polymer chemical gels. This is the ***thermodynamic criterion*** which states that: *the formation and melting of these gels proceed* via *first order transitions*,[1] *and that the process is perfectly reversible* [10]. A typical example is given in Fig. 2.4 right.

[1]Not to be confused with *first order reactions* that describe chemical processes.

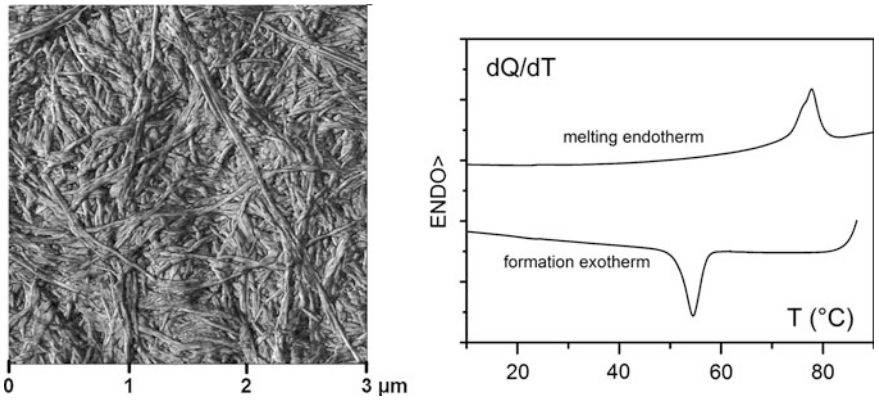

Fig. 2.4 *Left* AFM picture of a xerogel from an oligophenylenevinylene molecule in benzyl methyl ether (C = 0.4 % w/v) (OPVE, synthesized by Ajayaghosh et al. [12]). Micrometric fibrils are seen with cross-sections in the nanometric range; *right* typical DSC traces obtained on cooling (formation exotherm) and heating (melting endotherm). These are typical examples of first order thermodynamic transitions. The associated enthalpies are given by the area under the peaks after proper calibration. Case presented here a tripod molecule (BHPB-10 synthesized by Mésini and coworkers [13]) in fluorotoluene (Courtesy Guenet, private communication)

This particularly means that one should be able to detect formation exotherms and melting endotherms in calorimetric investigations, yielding the formation and melting temperatures together with the associated enthalpies.

These two criteria make it possible to differentiate gels from deceiving systems such as phase-separated glasses (may show network architecture but no first-order phase transitions) and spherulitic systems (may show first-order phase transition but no network architecture. It seems therefore unfortunate that papers may describe spherulitic systems as gel which eventually throws the scientific community into confusion [14].

It is worth elaborating further concerning the latter system, namely assemblies of spherulites. Tilting test tube will show the absence of flow. In experiments with classical rheometers, this system may also exhibit apparent elastic properties, particularly at very small deformation. The reason lies simply in the imbrications of spherulites within one another, something reminiscent of the burrs of burdock that keep sticking to clothes. Yet, these assemblies eventually behave like a paste. A striking example is given by Daniel et al. for systems prepared with syndiotactic polystyrene (sPS) on the one hand, and poly phenylene oxide (PPO), on the other hand in 1,2 dichloroethane [15].

As shown in Fig. 2.5, sPS/1,2 dichloroethane solutions form fibrillar networks unlike PPO/1,2 dichloroethane solutions from which spherulites are obtained. Daniel et al. have further dried the samples by exchanging the solvent with supercritical CO_2 extraction. The advantage of this solvent extraction procedure lies in the absence of surface tension effects so that the original morphology is usually kept. As can be seen in Fig. 2.5, only sPS systems retain their initial shape while

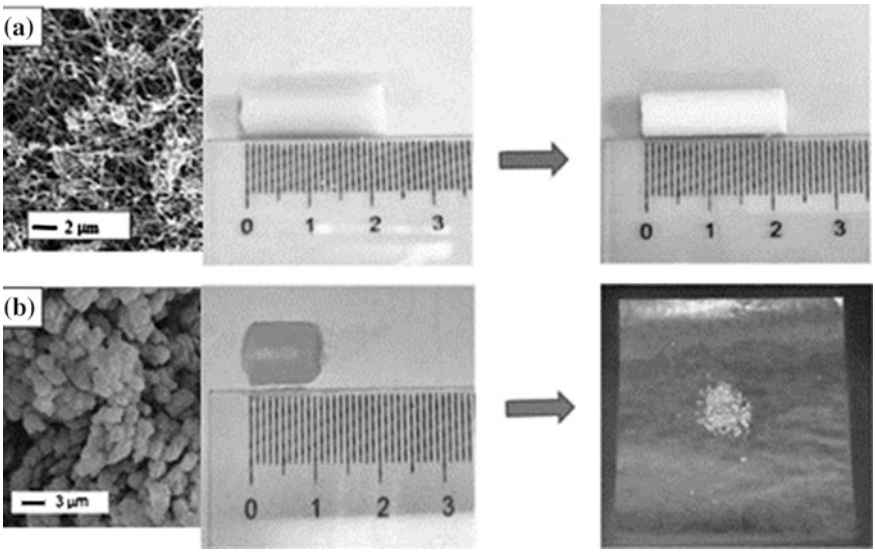

Fig. 2.5 Comparison between sPS/1,2 dichloroethane systems (*upper figures*, **a**) and PPO/1,2 dichloroethane systems (*lower figures*, **b**) after supercritical CO_2 extraction. *Left* SEM pictures showing a fibrillar morphology for the sPS systems, and a spherulitic morphology for the PPO systems. *Middle* both systems before extraction; *right* systems after extraction. Only the sPS system retains its initial shape (courtesy by Daniel from Daniel et al. [15])

PPO systems become powdery. This outcome clearly shows that spherulitic assemblies produced from solutions cannot be considered a network based on the current definition by language dictionaries.

It is worth stressing that connections between spherulites will occur in polymers solutions for very high concentrations and in the solid state because of the high level of chain entanglements. Such entanglements do not exist for oligomolecules so that increasing the organogelator concentration will not create any connections between spherulites.

2.3 Summary

If we refer back to the necessity of deriving a definition, namely to specify the *extension of a concept* and to establish a list naming every object that is a *member of a specific set,* then the topological-thermodynamic definition is probably best suited to reach this goal. To be sure, a large majority of papers published on these systems display AFM pictures that exhibit typical fibrillar morphology. Yet, it still remains of interest to find out to which extent these fibrils are interconnected, a property which is best determined by rheological experiments.

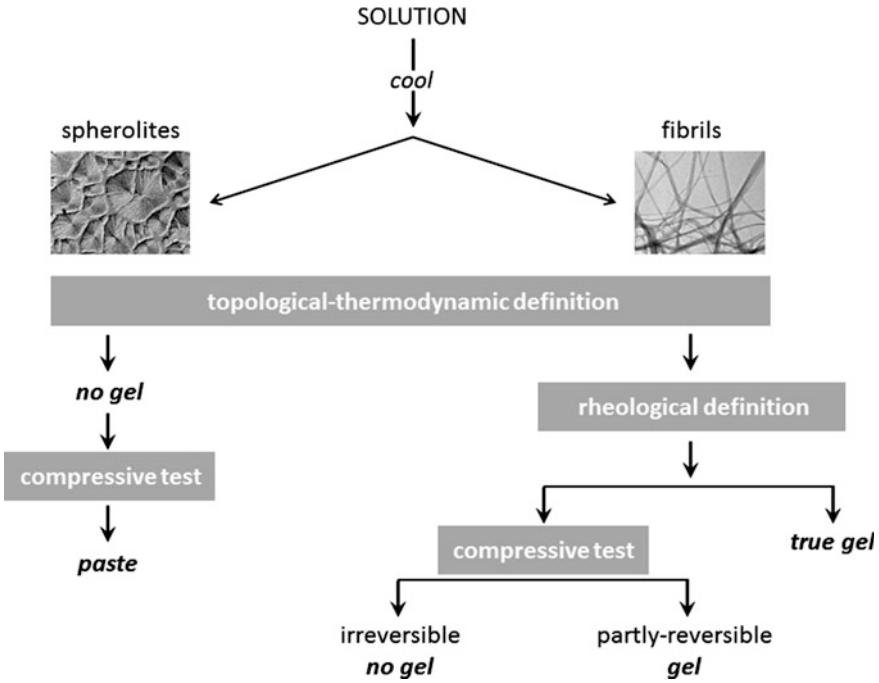

Fig. 2.6 Sketch of the cascade of definitions and test that should be used for evaluating the gel status of a crystallizing system. Irreversible and partly-reversible stand for the degree of gel shape recovery after compression. As shown, the first level of definition should be the thermodynamic-topological definition, and then followed by the rheological definition

Admittedly, a set of randomly dispersed fibrils with no interfibril connections might not be worth considered a gel either unless some "sticking" process operates. Such a case is reminiscent of the *Mikado game* where sticks are in contact but without any specific interaction otherwise. Application of a double criterion to spherulitic systems, namely topological definition and the compressive test, allows one to discard them definitely from the realm of gels [8]. The sketch in Fig. 2.6 summarizes the cascade of criteria and test that should allow one to decide about the gel status of the system under study. Systems studied by Collin et al. [6] ought to be therefore discarded on the basis of this set of criteria.

This tentative set of criteria developed above for defining a gel brings one back to the remark by Lloyd about the difficulty in designing a nice, self-containing definition. After all, we are in the realm of soft matter where defining things is ultimately a complex task.

In any case it must be clear that only interconnected fibrillar systems only ought to be regarded as gels. They do represent a specific set.

References

1. Lloyd, D.J.: In: Alexander, J. (ed.) Colloid Chemistry: Theoretical and Applied, vol. 1, p. 7. The Chemical Catalog Co, New York (1926)
2. Barnes H.A., Hutton J.F., Walters, K.: An Introduction to Rheology. Elsevier Science Publishers, Amsterdam (1989)
3. Ferry, John D.: Viscoelastic Properties of Polymers. Wiley, New York (1980)
4. Candau, S., Bastide, J., Delsanti, M.: Structural, elastic, and dynamic properties of swollen polymer networks. Adv. Polym. Sci. **44**, 27–71 (1982)
5. Terech, P., Pasquier, D., Bordas, V., Rossat, C.: Rheological properties and structural correlations in molecular organogels. Langmuir **16**, 4485–4494 (2000)
6. Collin, D., Covis, R., Allix, F., Jamart-Grégoire, B., Martinoty, P.: Jamming transition in solutions containing organogelator molecules of amino-acid type: rheological and calorimetry experiments. Soft Matter **9**, 2947 (2013)
7. Guenet, J.M., Mckenna, G.B.: The concentration dependence of the compression modulus of iPS/cis-decalin gels. J. Polym. Sci. Polym. Phys. Ed. **24**, 2499 (1986)
8. Daniel, C., Dammer, C., Guenet, J.M.: On the definition of thermoreversible gels: case of syndiotactic polystyrene. Polymer **35**, 4243 (1994)
9. Guenet, J.M.L: unpublished observations
10. Guenet, J.M.Thermoreversible: Gelation of Polymers and Biopolymers. Academic Press, London (1992)
11. Dictionary of English language and culture, Longman Group UK ltd, Harlow (1992)
12. Dasgupta, D., Srinivasan, S., Rochas, C., Ajayaghosh, A., Guenet, J.M.: Hybrid thermoreversible gels from covalent polymers and organogels. Langmuir **25**, 8593 (2009)
13 Diaz, N., Simon, F.X., Schmutz, M., Rawiso, M., Decher, G., Jestin, J., Mesini, P.J.: Self-assembled diamide nanotubes in organic solvents. Angew Chem. Int. Ed. **44**, 3260 (2005)
14 Huang, X., Terech, P., Raghavab, S.R., Weiss, R.G.: Kinetics of 5α-cholestan-3β-yl N-(2-Naphthyl)carbamate/n-alkane oganogel formation and its influence on the fibrillary networks. J. Am. Chem. Soc. **127**, 4336 (2005)
15. Daniel, C., Longo, S., Cardea, S., Vitillo, J.G., Guerra, G.: Monolithic nanoporous-crystalline aerogels based on PPO. RSC Adv. **2**, 12011–12018 (2012)

Chapter 3
Thermodynamic and Kinetic Aspects

As was mentioned in the previous chapter, organogel formation and melting proceed chiefly from first-order transitions. This implies that more or less ordered structures are produced which involves kinetic and thermodynamic processes. Here, a brief outline of these aspects is provided. The reader can peruse specialized books devoted to each particular topic that are given in the reference section.

3.1 Some Basic Principles

The basic principles needed for studying the thermodynamic aspects are discussed in the next two sections. One principle deals with the order of the transition and correspondingly whether crystalline systems or supramolecular polymers are under study. The second principle gives some indications about the nucleation and growth process involved in a crystallization phenomenon.

3.1.1 Order of the Transition

It seems important to state first that the **order of a thermodynamic transition** should not be confused with **the order of a reaction**. The latter is the measure of the kinetics of a chemical reaction.

In thermodynamic events, two main transitions are usually observed: the **first-order transition** for which the derivative of the free energy is discontinuous and **second-order transitions** where only the second derivative and higher derivatives of the free energy are discontinuous. The former occurs in crystal

J.-M. Guenet, *Organogels*, SpringerBriefs in Materials,
DOI 10.1007/978-3-319-33178-2_3

melting and solid–solid phase transformation, while the latter are seen in glass transition,[1] some cases of phase transformation, in certain cases in nematic-liquid transition, para- and ferro-magnetic transitions, etc.

A first-order phase transition is, strictly speaking, *irreversible* in the sense that it does not occur at the same temperature on cooling and on heating for a pure system. As will be developed below, this arises from the need of a homogeneous nucleation step for pure systems. These transitions always create some degree of order or modify the existing order. In DSC experiments, the heat capacity C_p must exhibit a peak as a function of temperature, either on cooling or on heating. This peak corresponds to the *latent heat* of the transition, and is endothermic on heating (absorbing heat) and exothermic on cooling (releasing heat) for stable phases. Occurrence of an exothermic peak while heating implies that a *transition from a metastable to a stable phase* takes place. Conversely, an endothermic peak always occurs when passing from *a stable phase to another stable phase* (for instance solid-to-liquid, solid–solid transformation, etc).

Second-order phase transitions are always reversible as the transition temperature does not depend upon whether it is recorded on cooling or heating. It appears in DSC experiments as a jump of the heat capacity.

It is worth mentioning that organic chemists tend to speak of *cooperative processes* for designing *first-order transitions* and *non-cooperative* for designing *second-order transitions, isodesmic* being also used for supramolecular polymers…

In first-order transitions, such as crystallization, growth of the system occurs simultaneously in the three directions of space. Note that kinetic effects may come into play, which does not affect at all the order of the transition. In the case of organogels obtained through crystallization the gelation process, the fibrils growth, does not therefore proceed in two steps: formation of one-dimensional supramolecular polymers, and then lateral aggregation.

The 1-D formation of supramolecular polymers is rather of the second-order type. A typical example was observed for a bicopper complex in organic solvents [1]. These molecule pile up on top of one another so as to form long 1-D chains that yield a very viscous solution without further molecular order. These supramolecular polymers are dynamic polymers as the interaction between bicopper complex molecules is of the order of kT. The behavior of these supramolecular polymers is well accounted for through a theory originally developed by Cates [2, 3]. This theory states that the length distribution is rather large and obeys a Boltzmann statistics. Also, the average length depends upon temperature, T, and concentration, C, through:

$$< L > \sim C^{1/2} \exp(E_{\text{scission}}/2kT) \tag{3.1}$$

[1]Strictly speaking the glass transition is not a thermodynamic event but the behavior of C_p is similar to a second-order transition.

where E_{scission} is the dissociation energy required to separate two bicopper complex molecules.

Exceptions to the simultaneous crystallization in 3-D may be observed. As will be seen in Chap. 4, organogels formed by means of two complementary molecules may possibly be formed by a two-step process.

3.1.2 Nucleation and Growth

The formation of ordered structures always involve a *nucleation step*, namely the creation of a nucleus, needed to trigger the gelation process and then followed by a *growth step*. Basically, there are two types of nucleation process: *homogeneous* nucleation and *heterogeneous* nucleation [4].

The *homogeneous nucleation* phenomenon has been studied long ago by Gibbs who derived the well-known equation from the free energy of the system [5]

$$\rho_c = \frac{\sigma T_m^o}{\Delta H_f \Delta T} \tag{3.2}$$

where ρ_c is the critical radius, namely the smallest radius necessary for triggering crystal growth. Other terms are the surface free energy, T_m^o the melting temperature for the infinite crystal, ΔH_f the melting enthalpy and ΔT the undercooling,[2] i.e., $T_m^o - T$, T being the temperature at which the sample is cooled.

When the system is cooled to below T_m^o, concentration fluctuations start growing that create small "embryo crystals." As long as these "embryo crystals" have not reached the critical size given by Eq. (3.2), they will vanish. Equation (3.2) implies that high undercooling is usually necessary for reaching the required critical nucleus. This is, however, balanced by the other terms: high surface free energy and high melting temperature increase, ρ_c, while high melting enthalpy decreases, ρ_c.

When homogeneous nucleation is at play a *hysteresis* will be observed between the formation temperature and the melting temperature. This is why first-order transitions are considered irreversible. It should be therefore kept in mind that *only the melting temperature is a thermodynamic parameter* since the formation temperature may vary with the preparation conditions.

The stationary nucleation rate *Ist* is also an important parameter. It depends on temperature, W the barrier energy, and viscosity $\eta(T)$ through

$$I\text{st} \sim \eta^{-1}(T) \exp\left(\frac{W}{kT}\right) \tag{3.3}$$

[2]Chemists tend to use "supersaturation" instead of undercooling for solutions. Supersturation is rather obtained through solvent evaporation, but the net result is the same.

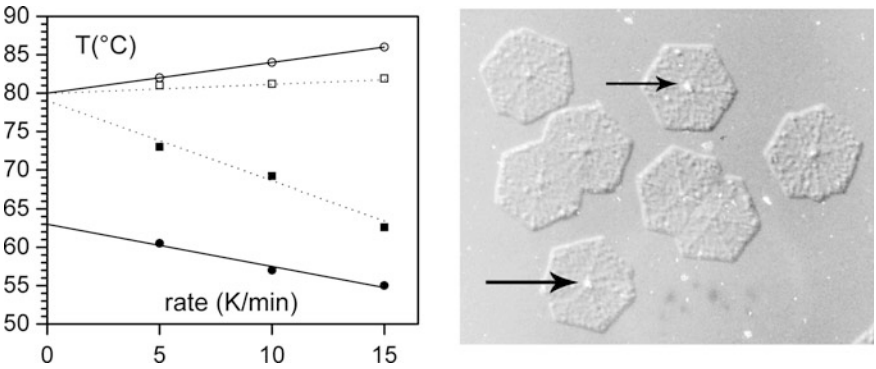

Fig. 3.1 *Left* variation of the formation (●) and melting (○) temperatures measured as a function of scanning rate in cooling and heating DSC experiments for an OPV/benzyl alcohol system. Naphathalene crystallization (■) and melting (□) are provided or the sake of comparison. A large hysteresis between equilibrium formation and melting temperatures is seen for OPV/BA systems unlike naphthalene. *Right* iPS single crystals grown on heterogeneous nuclei (*arrows*). Guenet, unpublished results

This means that increasing the undercooling first increases the nucleation rate until viscosity takes over and entails a decrease of this rate.

This also implies that macroscopic formation of the gel depends upon the number of nuclei per unit volume: the time needed to grow fibrils long enough for achieving connectedness depends on their number and also on the diffusion coefficient of the molecules. Consequently, the growth rate of the network is directly related to the undercooling ΔT. As will be stressed below, knowledge of the phase diagram is an essential step in the investigation of these systems. For instance, comparison with different solvent must be made at identical ΔT in order to be meaningful.

Heterogeneous nucleation starts on an existing impurity[3] provided that there is a favorable interaction with the system and allowing for an adequate positioning of the molecules for promoting crystalline growth. The case of the heterogeneous nucleation of single crystals from isotactic polystyrene (iPS) is shown in Fig. 3.1. Epitaxy is often involved in heterogeneous nucleation as it favors crystal growth. Favorable wetting of the impurity by the undercooled solutions is also a key factor (surface nucleation). In the case of ice formation, it is known that dust play this role. Provided that the impurity possesses a size larger than the critical radius, nucleation occurs as soon as the system is cooled to below the melting temperature. *No hysteresis* is therefore observed under equilibrium conditions (i.e., zero cooling rate).

In DSC experiments carried out at finite heating and/or cooling rates, the formation temperature is always significantly lower than the melting temperature due to various inertia effects. This simple technique allows one to settle the issue as to

[3]Impurity here means a foreign component usually under a solid form.

whether homogeneous or heterogeneous nucleation is involved. In the case of heterogeneous nucleation , simultaneous extrapolation to zero heating rate and to zero cooling rate should give the same value. Conversely, in the case of homogeneous nucleation , values obtained from heating and cooling runs will differ [6].

The latter situation is more than often observed in organogels, which therefore suggests that homogeneous nucleation is at play. A typical example is given in Fig. 3.1 for an OPV organogelator in benzyl alcohol where the value of the hysteresis is found to be about 17 °C. For the sake of comparison, the behavior of naphthalene is given for which no hysteresis is observed because heterogeneous nucleation is involved in this case.

The fact is that not so many "impurities" possess a surface structure liable to interact with or wet favorably an organogelator molecule, and correspondingly to orientate it in the right way for starting crystalline growth. Homogeneous nucleation of organogels has some interesting outcomes as will be detailed in the chapter devoted to the structure.

In the case of a *liquid-liquid phase transition*, any impurity will trigger the separation process so that heterogeneous nucleation is basically always involved. Further, there exists a domain below the miscibility gap delimited by the so-called *spinodal* line where the physically unstable [7]. If the system can be quenched unaltered within this domain, then it will phase separate through a diffusion process often referred to as *spinodal decomposition*. This peculiar situation is usually difficult to be observed because the system must reach this domain free of any phase-separated material. S*pinodal decomposition* was earlier thought to be the driving mechanism for polymer thermoreversible gelation, but was later considered as one among other possible mechanisms [8] or even discarded.

In most cases, the growth of these gels is quite fast. Terech has studied the kinetics in differing solvents [9] for a given volume fraction of the organogelator.

The opacity curves in Fig. 3.2 show that gelation is achieved within a few minutes, but depends upon the solvent type. As discussed above, the comparison

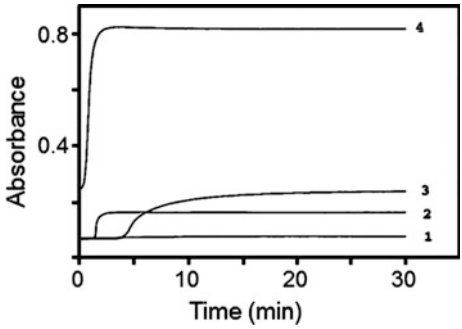

Fig. 3.2 Kinetic variation of the optical opacity, measured at λ = 550 nm (optical path = 1 mm), during the aggregation reaction of 1,2-Hydroxystearic Acid/hydrocarbon systems. The organogels possess a volume fraction φ_v = 1.77 %. 1 = toluene; 2 = dodecane; 3 = nitrobenzene; 4 = hexafluorobenzene. From Terech et al. [9]

would be meaningful if the undercooling would be the same. The temperature–concentration phase diagram would probably reveal that ΔT is significantly lower in nitrobenzene with respect to dodecane and hexafluorobenzene. The curve for toluene seems to remain virtually flat, although gelation takes place in this solvent, because the refractive index of the organogelator and the solvent match. Adequate enlargement reveals a slight increase.

3.2 The Temperature–Concentration Phase Diagrams

Whenever multicomponent systems are investigated the *temperature–concentration phase diagram* should be mapped out first. Indeed, results and conclusions are likely to depend dramatically upon the domain of temperature and concentration (in some cases also pressure) where a system is studied. Also, the melting behavior when determined from only one concentration may be deceiving and may lead to erroneous conclusions as will be discussed below.

The best suited technique for establishing phase diagrams is Differential Scanning Calorimetry (DSC) which allows one to determine the thermal behavior of the investigated systems, namely the formation and melting temperatures, as well as the associated enthalpies. The phase diagram has to be, however, often completed with observations from techniques such as optical microscopy, X-ray diffraction, and Infra-red experiments, to quote but a few.

As will be also detailed, the construction of the phase diagram is made possible by using Gibbs' phase rule, particularly by considering the ***variance v***, an essential parameter, which reads [5]:

$$v = N - \varphi + \tau \tag{3.4}$$

where N is the number of components, φ the number of phases and τ the number of intensive variables that can be used. In most cases only one variable, namely the temperature T, is used so that $\tau = 1$. Yet, other intensive variables can be applied to the system, such as pressure, electric field, magnetic field, etc

The ***variance*** corresponds to the spatial dimension of the locus where phases coexist in a T, C phase diagram. For a binary system if $v = 2$ then $\varphi = 1$, i.e., one phase existing on a T, C surface. If $v = 1$ then $\varphi = 2$, i.e., two phases coexisting on a line at T = const OR C = const. For T = const the line is designated as a non-variant event. Finally, for $v = 0$ then $\varphi = 3$, which implies that three phases coexist for T = const AND C = const, namely on a point. A maximum of three phases should be detected for a two-component system, a situation encountered in most of the investigations on organogels. Some studies are also often performed in binary solvents in which case a maximum of four phases may be observed.

Another important contribution by Gibbs is the ***lever rule***. It allows one to calculate the proportions of the different phase. This rule will be detailed below and also used in the Chap. 6 (rheology). From this rule it can be demonstrated that the

enthalpies associated with the first-order transitions observed in a given system must vary linearly with concentration. This was further developed by Tammann who suggested plotting the enthalpies as a function of concentration so as to determine the compositions of the different phases (known as Tammann's diagram). Observing linear variation is also a way of asserting that the system stands at equilibrium or near-equilibrium. For instance, if the degree of crystallinity varies drastically with concentration, then a linear variation is unlikely to be seen.

These rules are valid for very large systems under equilibrium conditions. Another aspect to be taken into account is the finite size of the objects, something relevant to organogels where fibrils have cross-sectional dimension in the sub-micron range. Gibbs established a relation for the melting temperature under these conditions

$$T_m = T_m^o\left[1 - \frac{S\sigma}{V\Delta H_m}\right] \tag{3.5}$$

where T_m and T_m^o are the melting temperatures of a finite and of an infinite crystal, respectively, S and V the surface and volume for the objects, σ and ΔH_m the surface free energy and the melting enthalpy. For long, cylindrical fibrils Eq. (3.5) reduces to

$$T_m = T_m^o\left[1 - \frac{2\sigma}{r\Delta H_m}\right] \tag{3.6}$$

and for fibrils of rectangular cross-section of length and width l_a and l_b.

$$T_m = T_m^o\left[1 - \frac{2(l_a + l_b)\sigma}{l_a l_b \Delta H_m}\right] \tag{3.7}$$

The corrective term related to the fibril cross-section may be important or negligible depending on σ and ΔH_m. As we shall see below, the cross-sectional size may vary with the preparation temperature (more nuclei, smaller crystal sizes). It is therefore recommended to evaluate properly the size effect before pursuing the mapping out of the phase diagram further.

A complete temperature–concentration phase diagram should therefore display the temperatures corresponding to the different first-order thermal events, together with the associated enthalpies as a function of concentration. To be sure, the concentration must be expressed either in *weight/total weight* or *mole/total moles*, as these parameters do not vary with temperature. The relevancy of Tammann's plot requires that the enthalpies must not be divided by the concentration but always be per gram of sample, NOT per gram of the organogelator.

Indications as to the stability of the phases can be obtained when mapping out the phase diagram on heating by DSC. In principle, the transformation of a stable phase into another stable phase must give off an endothermic event. If an exothermic event is observed it means that the phase was metastable: *transformation on heating of a*

metastable phase into a stable phase always produces an exotherm. A typical example in polymer systems is provided by the crystallization on heating of amorphous polyethylene terephthalate where the metastable liquid transforms into a crystalline phase by giving off an exotherm.

3.2.1 Some Relevant Theoretical Phase Diagrams

It is not intended here to give an exhaustive list of possible phase diagrams, but rather to focus on typical examples that may be experimentally encountered. Four types are presented: the simplest case of a solid–liquid phase transition, the case of systems displaying a liquid–liquid phase separation (monotectic transformation), the case where molecular compounds are formed, and the case where the organogelator possesses two crystalline forms. Organogels pertaining to these three types of diagram have been already discussed in the literature as will be detailed below.

These phase diagram are those obtained on heating for reasons developed above. In many cases the formation diagram is rather the same except it is shifted to lower temperatures. In-depth descriptions can be found in text books by Reisman [10] and/or Adkins [11], and in books devoted to polymer systems [12].

3.2.1.1 Solid–Liquid Phase Transition

The *liquid–solid phase transition* is the simplest case encountered in many systems. The transition is noted on heating:

$$\text{solid} + \text{liquid} \rightarrow \text{liquid}$$

A typical phase diagram is shown in Fig. 3.3. It displays the characteristic shape observed for the *liquidus* (full line), namely the line where the very last crystals melt. As a rule, a strong downturn at low concentration is seen while a moderate increase occurs for higher concentrations. The downturn is more or less conspicuous depending on the solvent melting point. The dotted line emphasize where the gel, i.e., an infinite network, exists, while above aggregates, finite structures, are found.

The aspect of the endotherm expected to be recorded in a DSC experiment is shown in red. This endotherm typically consists of one broad peak due to the extension of the melting process over a large range of temperature due to the extension of the liquidus. In no case does this convey the notion of crystals size dispersion as is all too often concluded when experiments are restricted to one or two concentrations.

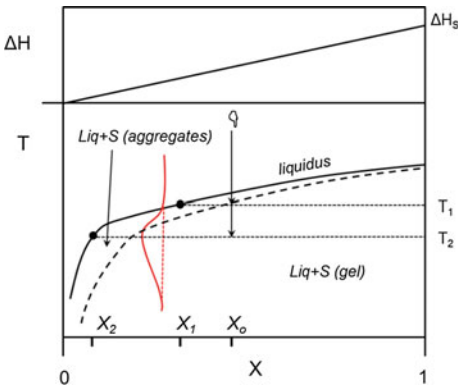

Fig. 3.3 Temperature–concentration phase diagram. *Upper case* Tammann's diagram where ΔH_s stands for the melting enthalpy in the pure solid state. In *red* is shown the type of endotherm expected to be observed in a DSC experiment. The *dotted line* highlights the fact that at a given temperature only aggregates remain, and correspondingly no macroscopic gel exists. Further details are given in the text

By applying the *Gibbs lever rule*[4] the fraction of each phase at temperature T_1, the solid phase $\varphi_s(T_1)$ and the liquid phase $\varphi_l(T_1)$, for a binary mixture of starting concentration X_o are derived through:

$$\varphi_l(T_1) = \frac{1 - X_o}{1 - X_1} \quad \varphi_s(T_1) = \frac{X_o - X_1}{1 - X_1} \tag{3.8}$$

Applying the same principle for T_2 shows, as intuitively expected, that the solid phase has increased at the expense of the liquid phase. Consequently, the concentration of the dilute phase decreases. This analysis provides one with data that can be of further exploited in accounting for results such as those obtained in rheology experiments as will be discussed in Chap. 6.

3.2.1.2 Monotectic Transition

Another type of phase diagram that can be encountered in organogels is drawn in Fig. 3.4. Here a *liquid–liquid phase transition* occurs prior to gelation/crystallization. The transition that occurs at $T = T_M$ is designated as a monotectic transformation, and is summarized as follows:

$$S + L_1 \rightarrow S + L_2$$

[4]The term lever rule comes from the similarity with a lever in balance for which the ratio of output to input force is given by the ratio of the distances from the pivot to the points of application of these forces.

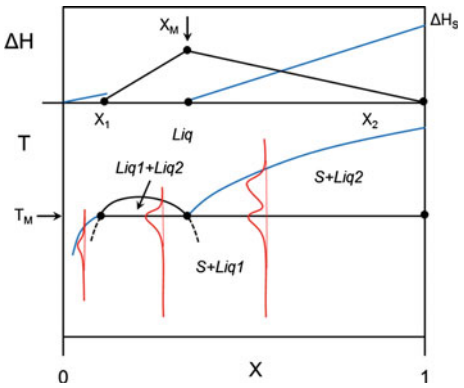

Fig. 3.4 Temperature–concentration phase diagram showing a monotectic transition. Within the miscibility gap two liquid phases of differing composition coexist. *Dotted lines* indicate the metastable extension of the binodal curve. In the *upper case* Tammann's diagram where ΔH_s stands for the melting enthalpy in the pure solid state. This diagram allows one to determine the concentration X_M as well as X_1 and X_2 highlighted with *black dots* (here $X_2 = 1$). In *red* is shown the aspect of the endotherm expected to be observed in a DSC experiment. Further details can be found in the text

It arises from the existence of a miscibility gap delimited by a bowl-shaped line, named binodal, where the system decomposes into two liquid phases, L_1 and L_2 where L_1 is of lower concentration than L_2. By further cooling crystallization occurs to form eventually a solid phase in equilibrium with L_1. At T_M a non-variant event therefore occurs in a large range of concentration whose existence derives from the expression of the variance (relation 3.4). The shape of the phase diagram, in particular the existence of a non-variant event at T_M, results from the application of Gibbs phase rules.

The shapes of the expected DSC thermograms are again red-labeled. For concentrations lower than X_M, only one endotherm should be observed. Conversely, above X_M a partial and sudden melting of the solid phase take place at T_M followed by the gradual and final melting of the same phase, hence the occurrence of two endotherms. The occurrence of two endotherms might be deceiving if one restricts to the study of one concentration, as it does not mean that two different crystalline species are present in the system. Again, mapping out the phase diagram is an essential step in the study of binary systems.

The enthalpy associated with the monotectic transition plotted by means of Tammann's diagram must vary linearly and reach a maximum at $X = X_M$. Its variation also allows one to determine the value of the solid phase concentration, X_s. The case considered here corresponds to $X_s = 1$, the case $X_s < 1$ would correspond to a system where solvent is occluded within the crystals, yet not forming a molecular compound (a so-called *solid solution*).

The *liquid–liquid phase separation* is also nucleation-controlled, yet, as opposed to crystallization, any impurity will do the trick. As a result, this phase separation

process is chiefly heterogeneously nucleated. The occurrence of the *liquid–solid phase separation* may be of either nucleation type but depends strongly on the cooling rate. By slowly cooling the liquid–liquid phase separation can proceed to higher stages, designated as the *Ostwald ripening*, while a rapid reduces its extension. Indeed a rapid cooling allows the mixture to spend a limited time within the miscibility gap, and reach rapidly the domain where *liquid–solid phase separation* occurs. Interestingly, as was theoretically shown by Cahn [13], under these conditions the *liquid–liquid phase separation* must take place prior to crystallization in a concentration range $X_1 \leq X \leq X_M$ due to the existence of the metastable extensions of the binodal curve (see Fig. 3.4). Yet, the *liquid–liquid phase separation* cannot proceed further as it is rapidly arrested by crystallization before reaching higher stages. This implies that the rate at which the system is cooled will definitely have an impact on the final morphology of the system. This effect is well-known in the making of ceramics where the arrest of the liquid–liquid phase separation by crystallization allows one to obtain finely dispersed structures [14].

3.2.1.3 Molecular Compounds

A molecular compound is formed through the co-crystallization at the molecular level of two or more species. The resulting crystal structure differs from the lattice of the pure components. Molecular compounds are also often designated in the literature as *solvated crystals*, *crystallosolvates*, *co-crystals*, *inclusion compounds*, *chlatrates*, *intercalates*, etc. There are two types of molecular compound: *congruently melting* and *incongruently melting*. Basically, the former behaves as a pure compound while the latter transforms into another phase, a solid phase or another less-solvated compound, prior to final melting.

A typical phase diagram for a *congruently melting* molecular compound is shown in Fig. 3.5. This compound is characterized by a well-defined stoichiometry,

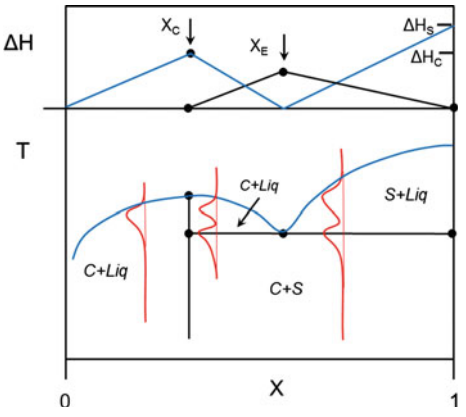

Fig. 3.5 Temperature–concentration phase diagram for a congruently melting molecular compound. Expected DSC traces are shown in *red*. Further details in the text

which stands for the number of molecules A versus the number of molecules B in the co-crystal. At $X = X_c$ the event is:

$$\text{Compound} \rightarrow \text{Liquid}$$

From the Tammann's diagram one extracts a stoichiometric concentration *Xc* as shown in Fig. 3.5. Here, it is worth stressing that extrapolation of the melting enthalpy to $X = 1$ from the compound domain is likely to be different from that of the solid phase ΔHs. If it is so, this might be a clue for assuming the occurrence of a molecular compound as will be shown in what follows [15].

The phase diagram shows the formation of an eutectic system with the compound and a solid phase at higher concentrations, this is just a possible situation among many others. As above, the expected DSC traces are also presented. At X_c only one melting endotherm is observed which corresponds to the melting of the pure compound. For concentration larger than X_c another endotherm appears which corresponds to the eutectic formed between the compound and the solid. The first endotherm will be non-variant with concentration. Again, the composition of the eutectic can be determined from the Tammann's diagram.

An *incongruently melting* compound is also characterized by a stoichiometric composition that may not be a rational number. As shown in Fig. 3.6 right, the compound transforms into another phase without melting, i.e., without going through a liquid state. At $X = X_c$ the event is:

$$\text{Compound} \rightarrow \text{Solid} + \text{Liquid}$$

Again the stoichiometric composition can be derived from the Tammann's diagram as shown in Fig. 3.6.

An experimental example of incongruent melting is observed in syndiotactic polystyrene/benzene gels where a compound transforms into another, less-solvated compound around the boiling point of benzene [16].

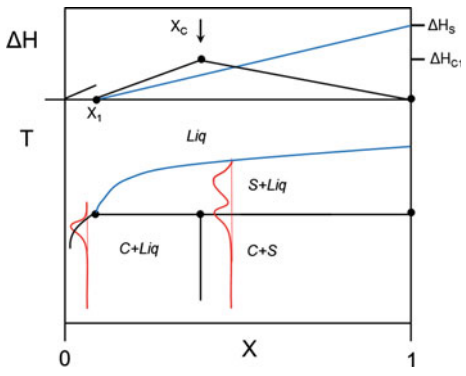

Fig. 3.6 Temperature–concentration phase diagram for an incongruently melting molecular compound. Expected DSC traces are shown in *red*. Further details in the text

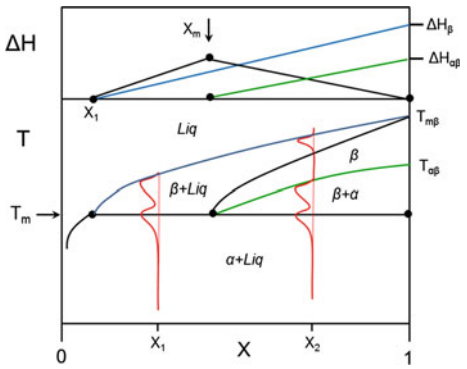

Fig. 3.7 Temperature–concentration phase diagram for a metatectic transition. X_m stands for the metactectic concentration where the α form + liquid transforms into the β form at $T = T_m$. $T_{\alpha\beta}$ is the temperature at which the α form transforms into the β form in the pure solid state. Again, the expected DSC traces are given in *red*. Further details in the text

3.2.1.4 Case for Two Crystal Forms: Metatectic Transition

In some cases the organogelator may possess two differing crystalline forms, α form and β form, in the solid state [17]. This will have an impact on the phase diagram, the simplest case being the occurrence of a *metatectic transition* (Fig. 3.7). This transition is written as

$$\alpha + \text{liq} \rightarrow \beta$$

Two noticeable events are shown in the phase diagram. At $X = X_1$, the first event at $T = T_m$ is the transformation of α form + liquid into the β form + liq, and then followed by the melting of the β form. At $X = X_2$ the first event is again the metatectic transition where α form + liquid transforms into α form + β form. On further heating, the α form definitely transforms into the β form. A monophase domain is then crossed without any thermal event until the line where the β form starts to melt is reached. At X_2 a complex thermal behavior is observed which again may not be clearly understood if the phase diagram is not mapped out in a large range of concentrations, especially if X_m turns out to be low enough.

3.2.2 Theoretical Expression for the Liquidus

Although the entire calculation of the phase diagram is in most cases either exceedingly difficult or even out of reach, it is always of interest to derive a theoretical expression for the terminal melting of a system, namely the liquidus line.

The simplest model was derived by van't Hoff, Le Chatelier and Schröder for ideal systems. It reads:

$$Log\,X = -\frac{\Delta H_m}{R}\left[\frac{1}{T(X)} - \frac{1}{T_m}\right] \tag{3.9}$$

where ΔH_m is considered to be the melting enthalpy (sometimes designated as dissolution enthalpy) and T_m the melting temperature of the pure system. Plotting Log X as a function of $1/T(X)$, the value found for the melting temperature at a concentration X, should therefore give a linear variation.

Equation (3.9) is strictly valid for ideal systems, namely for systems with similar type of interactions and also of close molar volume. This is clearly not the case for organogelators so that *the use of this relation is irrelevant and meaningless*. It cannot even be taken as a first approximation. This irrelevancy of this equation in the case of polymer thermoreversible gels was already stressed by Guenet [8]. He advocated that the approach derived by Flory for semi-crystalline polymer solutions is certainly more relevant. Flory's relation reads [18]:

$$\frac{1}{T_m} - \frac{1}{T_m^o} = \frac{RV_p}{\Delta H_m V_s} \times \left[\left(1 - \varphi_p\right) - \chi_1\left(1 - \varphi_p\right)^2\right] \tag{3.10}$$

where T_m^o is the melting point of the pure polymer, φ_p its volume fraction, V_p its molar volume, ΔH_m the melting enthalpy of the pure polymer, V_s the solvent molar volume and χ_1 the polymer–solvent interaction parameter.

Clearly, this equation differs drastically from Eq. (3.9) since it takes into account nonideal interactions. Yet, it cannot be applied to organogels since this theory states that long chains are already present in the liquid state. Unless, organogelators would form supramolecular polymers prior to gelation, a new theory has to be developed.

Equation (3.9) is, however, all too often used in the interpretation of the liquidus curve for organogels. That in many cases the plot Log X vs $1/T(X)$ gives a straight or near-straight line does not mean that this equation applies. Indeed, the temperature range is usually very narrow so that this type of representation is liable to appear linear. Values of ΔH_m are derived from this plot, although the true value can be, and must be obtained from DSC experiments.

Feng and Cavicchi were also perfectly aware of the limitation of the present theories, and made an attempt to improve the thermodynamic description of these systems by considering the theory for regular solutions [19]. By introducing an interaction parameter χ, they come up with the following relation:

$$\ln X + (1 - X)^2\chi = \frac{\Delta H_m}{R}\left(\frac{1}{T_m^o} - \frac{1}{T_m(X)}\right) \tag{3.11}$$

where χ reads

$$\chi = \frac{V}{RT}\left(\delta_{\text{org}} - \delta_s\right)^2 \tag{3.12}$$

where δ with appropriate subscripts are the solubility parameters of the organogelator and of the solvent. Although this is an interesting approach, it relies on a parameter, the solubility parameter, which may not be an appropriate parameter in view of the complex chemical structure of organogelators. Indeed δ is calculated with

$$\delta = \left(\frac{\sum F_i}{\sum V_i}\right)^{0.5} \tag{3.13}$$

where F_i and V_i are the contribution from each chemical unit to the cohesive energy density and their molar volume.

Clearly, δ is an average value which relies typically on a mean-field approach. It may work rather well with the triaryl amine molecules these authors studied because of their relatively high degree of symmetry (see below).

A theory specifically developed for organogel is still missing. The complexity of the chemical structure of organogelators may, however, require the use of molecular simulation as an analytical theory might be out of reach.

3.2.3 *Experimental Phase Diagrams*

As was stressed above, mapping out the temperature–concentration phase diagram should be the first step in the investigation of organogels. Unfortunately, this is seldom the case. Very few experimental phase diagrams are thus available in the current literature. Here phase diagrams illustrating the theoretical cases described above are considered.

The diagram mapped out by Feng and Cavicchi [19] is shown in Fig. 3.8. It is a typical phase diagram observed in many systems as described in Fig. 3.3 for the

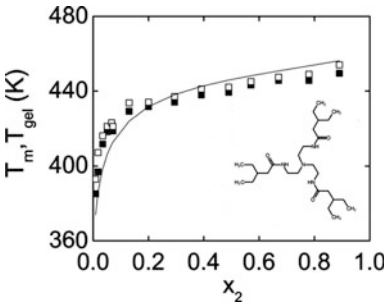

Fig. 3.8 Temperature concentration phase diagram for a triarylamine (chemical structure shown inside) in propylene glycol. T_m is the melting temperature measured by DSC (□) and T_{gel} (■) the temperature at which the gel turned into a SOL. x_2 is the mol fraction. The *solid line* is calculated by means of Eq. (3.11). From Feng and Cavicchi [19]

simplest case of a **liquid–solid transformation**. Also, Eq. (3.8) allows Feng and Cavicchi to reproduce to a good approximation their experimental data. This type of phase diagram implies that the fibrils of the gels are made up with *non-solvated crystals*. In this diagram are reported both the melting temperatures from DSC experiments and the SOL-GEL transition. The latter always occurs at lower temperature. This is expected as emphasized in Fig. 3.3. The total melting occurs in two steps: first disappearance of the infinite network, leaving finite aggregates, and then the gradual melting of the remaining aggregates. The DSC endotherm contains both, while rheology is only sensitive to the first step.

Dasgupta et al. investigated OPV systems in different solvents in relation with the chemical structure of the OPV molecule, namely the nature of the terminal groups [15]. Their findings can illustrate the case where a **molecular compound** is possibly formed. This OPV molecule shown in Fig. 3.9 possesses terminal groups capable of establishing hydrogen bonds. They consider a solvent that mimics this terminal group, namely benzyl alcohol, which also displays propensity for hydrogen bond formation. They compared the outcomes with those obtained from benzyl methyl ether, for which the hydrogen bond forming ability is drastically reduced, and *trans*-decahydronaphthalene for which hydrogen bond formation is totally absent.

The temperature–concentration phase diagram in Fig. 3.10 reveals two types of behavior. OPV organogels prepared in benzyl methyl ether and in *trans*-decahydronaphthalene possess virtually identical formation and melting temperature, as well as formation and melting enthalpies. Conversely, OPV organogels prepared in benzyl alcohol have higher formation and melting temperatures together with higher melting and formation enthalpies. Clearly, the fact that benzyl alcohol mimics the OPV end groups has a strong bearing on the thermodynamic properties

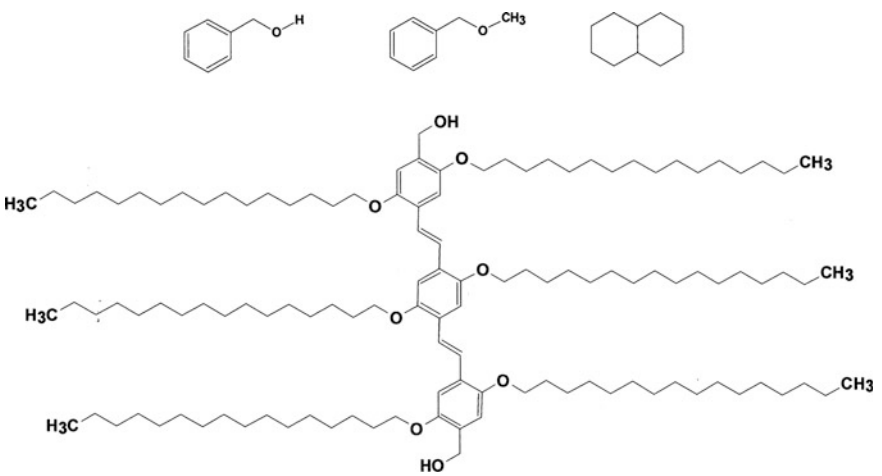

Fig. 3.9 *Upper figures* from *left* to *right*, benzyl alcohol, benzyl methyl ether, *trans*-decahydronaphthalene. *Lower figure* OPV molecule with terminal OH groups (OPVOH)

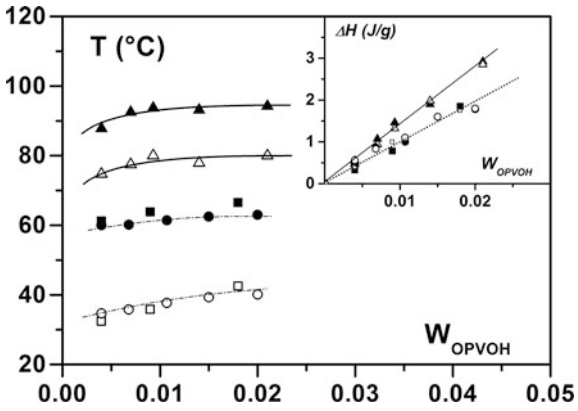

Fig. 3.10 Temperature–concentration phase diagram for OPVOH (see Fig. 3.9 for chemical structure) in different solvants. *Inset* Tamman's diagram for the formation and the melting enthalpies. In both diagrams *filled symbols* stand for the melting and *open symbols* for the formation. *Triangle* = OPVOH/benzyl alcohol, *square* = OPVOH/*trans*-decahydro-naphthalene, *dot* = OPVOH/benzyl methyl ether. From Dasgupta et al. [15]

of the organogel. Interestingly, extrapolation to 100 % OPV yields the experimental enthalpies obtained for OPV (solid state $\Delta H = 181 \pm 10$ J/mol) in the case of benzyl methyl ether and *trans*-decahydronaphthalene ($\Delta H = 172 \pm 10$ J/mol), while a larger value is obtained in benzyl alcohol ($\Delta H = 240 \pm 10$ J/mol).

This behavior is reminiscent of situations that can occur in the case of molecular compound as highlighted in Fig. 3.5. Extrapolating the experimental formation and melting enthalpies from a concentration range where a compound is formed is not to give the value of the pure component. Results reported by Dasgupta et al. [15] therefore suggest the formation of a **molecular compound in benzyl alcohol** but not in the other two solvents. To be sure, the occurrence of a molecular compound relies only on circumstantial evidence so far. Further investigations are needed to confirm this assumption.

The hypothetical occurrence of a compound would most probably originate in the specific interaction that can be created between the benzyl alcohol molecules and the terminal group of the OPVOH organogelator.

It is worth stressing that benzyl alcohol may not globally be a good solvent towards OPVOH, particularly for the aliphatic moieties. This, however, does not prevent from the formation of a molecular compound provided that a part of the organogelator molecule displays strong affinity towards a specific solvent molecule. Similarly, it ought to be remembered that the melting point depends upon solvent quality: the higher the quality, the lower the melting point. Benzyl methyl ether and *trans*-decahydronaphthalene are certainly better solvents compared to benzyl alcohol, hence a lower melting temperature for their organogels. Conversely, the values of the melting enthalpies do not depend upon the solvent quality. They are an intrinsic property for a given crystalline structure.

Inclusion compounds were also mentioned by Maitra et al. for bile acid esters derivatives. Yet, these authors observed that the formation of compounds with these molecules tend to hinder the gelation phenomenon [20].

The study reported by Christ et al. [21] on BHPB-10/*trans*-decahydronaphthalene illustrates the case when a **liquid–liquid phase separation** is involved in the gelation process (chemical structure of the molecule is given in Fig. 2, middle center right).

The existence of a miscibility gap, namely the occurrence of a liquid–liquid phase separation, is seen by optical microscopy through the observation of droplets (see Fig. 3.11). It is also indirectly revealed by DSC experiments through the occurrence of a non-variant first-order event at $T = 43$ °C on cooling and $T = 66$ °C on heating. A similar non-variant event is seen by optical microscopy slightly shifted in temperature. At $T = 49$ °C, a drastic change takes place in the system: the droplets burst out to produce a network. The propagating front can be easily recognized on the optical microscope picture. As expected for a liquid1 + liquid2 → liquid1 + solid transformation a hysteresis of about 23 °C by DSC and 11 °C for optical microscopy experiments is seen for the position of the monotectic line determined on cooling ("*formation monotectic line*") and that determined on heating ("*thermodynamic monotectic line*"), since homogeneous nucleation is clearly at play in these systems as discussed in Sect. 3.1.2. There is therefore a domain noted $(\text{liquid1} + \text{liquid2})_{\text{meta}}$ where liquid2 is in a metastable state while cooling. Conversely, this effect is virtually absent within experimental uncertainties for the liquid1 + liquid2 → liquid

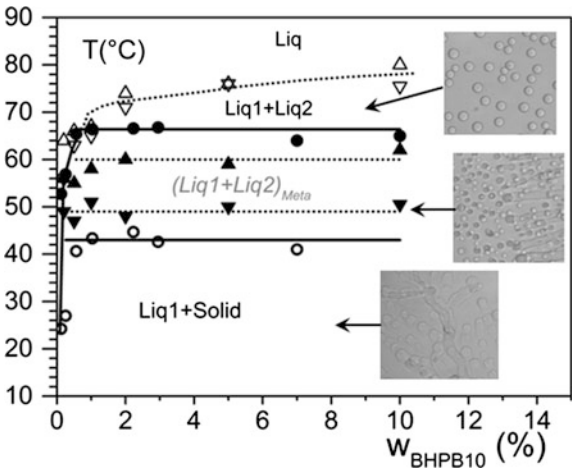

Fig. 3.11 Temperature-concentration phase diagram for BHPB-10/*trans*-decahydro-naphthalene. *Full* (heating) and *open* (cooling) *circles* together with *full lines* stand for DSC data. *Triangles* and *dotted lines* stand for data obtained by optical microscopy at 2 °C/min. Orientation of the *triangles* indicates whether the system is cooled (*down*) or heated (*up*). *Insets* show optical microscope pictures taken in the indicated domains (*upper* in the miscibility gap, *lower* in the gel domain, *middle* at T_{gel} on cooling). From Christ et al. [21]

transformation as the binodal line is little dependent upon the cooling or heating process (see Sect. 3.1.2 for further details).

The large hysteresis between formation and melting *further supports the involvement of a homogeneous nucleation process for triggering organogelation*. Another interesting feature arises from the path followed for preparing the gel, particularly at which rate the system is cooled. Slow cooling produces a coarse structure as shown in Fig. 3.11. Conversely, if the solution is quenched rapidly to below the "*formation monotectic line*" in such a way as by-passing the miscibility gap, then the structure of the organogel differs drastically: structures are much thinner and highly dispersed. This arises from the fact that the liquid–liquid phase separation is rapidly arrested by crystallization. Such an effect was already well-known in the making of ceramics [14] where fine dispersion of one component into the other is sought. The cooling rate can therefore be an appropriate parameter for tuning the gel structure as can equally be the quenching temperature (more details in Chap. 4).

3.3 Summary

The mapping out of the temperature–concentration phase diagram ought to be regarded as the first and most important part in the study of organogels. To quote but one example: the occurrence of a molecular compound can be easily derived from its shape without recourse to X-ray diffraction investigation [12]. This step provides one with a wealth of information.

Performing DSC experiments may appear as an easy and simple task although in many cases it turns out to be trickier than it looks. First, DSC runs must be performed at different rates to find out whether any kinetic effect is interfering. Ideally, the temperatures related to first-order events should be extrapolated to zero rate in order to obtain an "equilibrium" temperature. Second, one should be certain that size effects do not come into play since these are prone to modify these temperatures (see relations (3.5) and (3.6)). The Tammann's diagram is therefore essential for completing the phase diagram. For instance, if the melting temperature versus concentration displays a maximum, which is absent in the Tammann's diagram, something may be wrong. Conversely, nonlinear variations of the enthalpies in this diagram also indicate some underlying problem not taken into account such as kinetic effects. Third, additional investigations by simple techniques, such as optical microscopy, should be carried out so as to strengthen the conclusions drawn from the DSC findings. For instance, a liquid–liquid phase separation could go unnoticed from calorimetry traces but will be detected by means of a simple optical microscope.

Finally, an important rule, all too often forgotten, ***a given crystal structure possesses a characteristic melting enthalpy whose value is independent of the solvent used***. If the enthalpy varies with the solvent type, then this is a clear indication that a molecular compound is involved provided that any other effect is carefully discarded.

References

1. Terech, P., Schaffhauser, V., Maldivi, P., Guenet, J.M.: Rheological and neutron scattering investigations of the jelly state of binuclear copper complexes in cyclohexane. Europhys. Lett. **17**, 515 (1992)
2. Cates, M.E.: Reptation of living polymers: dynamics of entangled polymers in the presence of reversible chain-scission reactions. Macromolecules **20**, 2289 (1987); Cates, M.E.: Dynamics of living polymers and flexible surfactant micelles: scaling laws for dilution. J. Phys. Fr. **49**, 1593 (1988)
3. Terech, P., Schaffhauser, V., Maldivi, P., Guenet, J.M.: Living polymers in organic solvents. Langmuir **8**, 2104 (1992)
4. Schmelzer, J.W.P.: Phase transitions, and nucleation. In: Hubbard, A. (Ed.) Encyclopedia of Surface and Colloid Science, pp. 4017–4029. Marcel Dekker, New-York (2002)
5. Gibbs, J.W.: Elementary Principles in Statistical Mechanics. Charles Scribner's Sons, New York (1902)
6. Francois, J., Gan, Y.S., Guenet, J.M.: The sol–gel transition and phase diagram of the system aPS-CS2. Macromolecules **19**, 2755 (1986) (experimental examples)
7. Cahn, J.W., Hilliard, J.E.: Free energy of a nonuniform system. I. Interfacial free energy. J. Chem. Phys. **28**, 258 (1958)
8. Guenet, J.M.: Thermoreversible Gels from Polymer and Biopolymers. Academic Press, London (1992)
9. Terech, P., Pasquier, D., Bordas, V., Rossat, C.: Rheological properties and structural correlations in molecular organogels. Langmuir **16**, 4485–4494 (2000)
10. Reisman, A.: Phase Equilibria. Academic Press, New York (1970)
11. Atkins, P.W., de Paula, J.: Physical Chemistry, 9th edn. Oxford University Press, Oxford (2010)
12. Guenet, J.M.: Polymer-Solvent Molecular Compounds. Elsevier, London (2008)
13. Cahn, J.W.: The metastable liquidus and its effect on the crystallization of glass. J. Am. Ceram. Soc. **52**, 118 (1969)
14. Zarzycki, J.: Phase-separated systems. Disc. Farad. Soc. **1970**, 122 (1971)
15. Dasgupta, D., Srinivasan, S., Rochas, C., Ajayaghosh, A., Guenet, J.M.: Solvent-mediated fiber growth in organogels. Soft Matter **7**, 9311 (2011)
16. Daniel, C., De Luca, M.D., Brulet, A., Menelle, A., Guenet, J.M.: Thermoreversible gelation of syndiotactic polystyrene in benzene. Polymer **37**, 1273 (1996)
17. Sarbu, A., Biniek, L., Guenet, J.M., Mesini, P.J., Brinkmann, M.: Reversible J- to H-aggregate transformation in thin films of a perylene-bisimide organogelator. J. Mater Chem. C. **3**, 1235 (2015)
18. Flory, P.J.: Principles of Polymer Chemistry. Cornell University Press, New York (1953)
19. Feng, L., Cavicchi, K.A.: Investigation of the relationships between the thermodynamic phase behavior and gelation behavior of a series of tripodal trisamide compounds. Soft Matter **8**, 6483 (2012)
20. Nonappa, Lahtinen M., Behera, B., Kolehmainen, E., Maitra, U.: Unraveling the packing pattern to gelation using SS NMR and X-ray diffration: direct observation of the evolution of self-assemble fibres. Soft Matter **6**, 1748 (2010)
21. Christ, E. et al. Origin of invariant gel melting temperatures in the c-T phase diagram of an organogel. Langmuir (2016). http://dx.doi.org/10.1021/acs.langmuir.6b00995

Chapter 4
Molecular Structure and Morphology

The recommendations expressed for defining the pore size characteristics will be considered here for describing organogels based on the fact that these systems are porous materials. Consequently, it will be considered that *microscopic* level involves distances below 2 nm, *mesoscopic* from 2 to 50 nm, and *macroscopic* larger than 50 nm [1].

The most relevant approach for throwing some light on the phenomenon of organogelation remains therefore to discuss first the level of order in the *microscopic* structure, namely the crystalline structure, then describe the *mesoscopic* structures which deals with the fibrils structure together with the gel junctions, and finally end up with the resulting *macroscopic* structure, namely the gel morphology. As expected, the latter is tightly related to the former two.

Again, selected examples that highlight specific situations are exposed. This chapter is by no means intended to provide an exhaustive list of the data available in the literature on this topic.

4.1 The Microscopic Structure

Despite their complex chemical structure, most of the organogelators possess a *well-defined crystalline structure* in the bulk state. Many examples can be found in the literature [2–6]. For instance, Maitra et al. [3] have shown that powder diffraction patterns for a series of gelators derived from bile acid esters display a large number of reflections that allow the determination of the molecular arrangement (Fig. 4.1). The diffraction patterns of the gel, the xerogel, and the bulk state may be sometimes close enough [3] and sometimes not [4]. In any case, the fibrils of organogels are usually highly crystalline.

The degree of order depends, however, on the solvent type. A striking example is given by organogels prepared from OPV molecules in various solvents.

J.-M. Guenet, *Organogels*, SpringerBriefs in Materials,
DOI 10.1007/978-3-319-33178-2_4

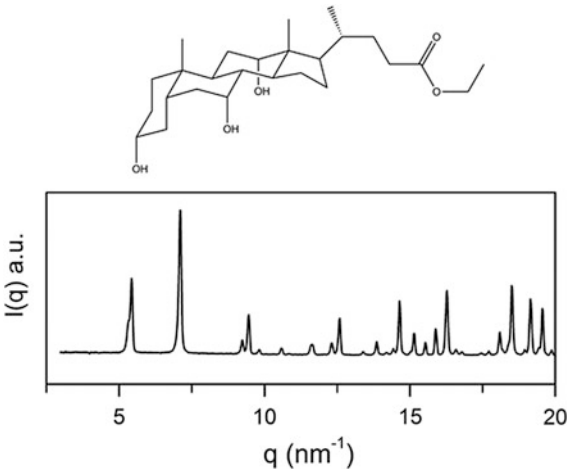

Fig. 4.1 X-ray diffraction pattern of an organogel from (ethyl 3a, 7a, 12a-trihydroxy-5b-cholan-24-oate prepared in various solvents (data provided by Nonappa and Maitra [1])

Dasgupta et al. [6] have observed by means of SAXS experiments that the crystal structure differs whether one uses benzyl alcohol or *trans*-decahydronaphthalene (see Fig. 4.2).

Ajayaghosh and coworkers [7] had already observed that the gel color, and correspondingly that of the SOL, can be tuned by toying with the chemical structure of the terminal groups. The GEL color is also sensitive, although to a lesser extent, to the solvent type.

For the sake of clarity, the OPV molecules will be described as follows: the succession of benzyl rings and double bonds will be named "*the central core,*" while the aliphatic moieties will be designated as "*aliphatic wings*".

The SAXS diffraction patterns in Fig. 4.2 obtained on wet gels of 1 % at ESRF synchrotron radiation facility show that three peaks can be easily identified for OPVR/benzyl alcohol organogels while only one peak, rather poorly defined, is observed in *trans*-decahydronaphthalene. According to Dasgupta et al. this means that the high degree of order between layers containing the π-stacking is largely disrupted in the case of *trans*-decahydronaphthalene gels as opposed to that in benzyl alcohol gels. These authors further surmise that this arises from the solvation of the aliphatic moieties by *trans*-decahydronaphthalene, a good solvent to paraffinic systems. Conversely, benzyl alcohol is not a good solvent to these moieties, so that it is not occluded inside the structure.

The chemical structure of the *terminal groups* of OPV molecules of the type shown in Figs. 4.2 and 4.3 play a decisive role in the molecular arrangement in the bulk state, and correspondingly in the organogels.

Comparison of the diffraction pattern in the low-q range between gels both prepared in benzyl alcohol reveals conspicuous differences. To be sure, OPVR/benzyl alcohol gels display a far better molecular order than OPVOH/benzyl

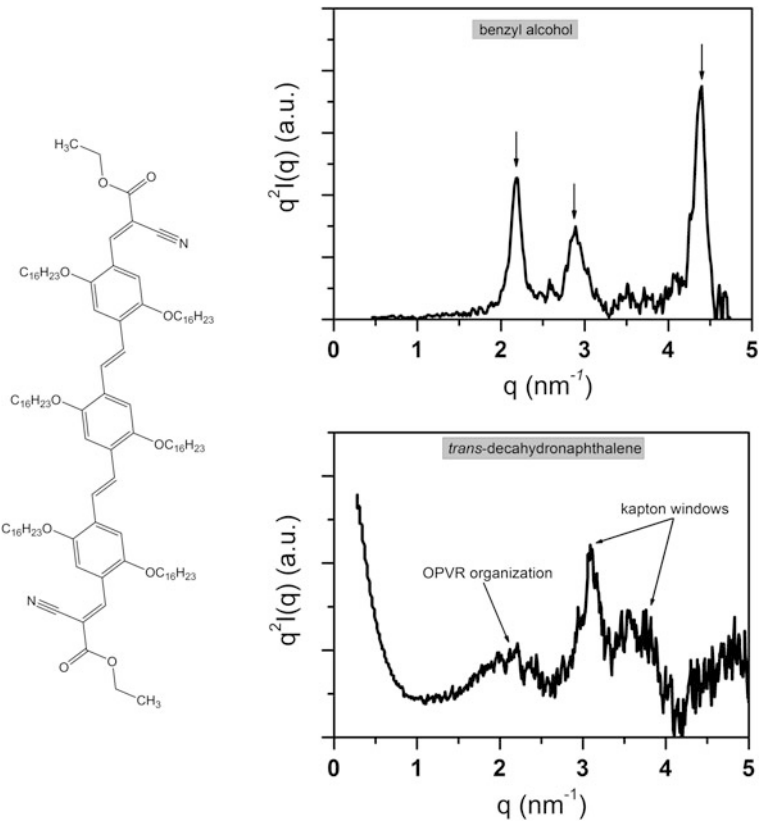

Fig. 4.2 *Left* the OPV molecule studied in 1 % gels (named OPVR). *Upper right* SAXS diffraction pattern in benzyl alcohol, *lower right* in gels from *trans*-decahydronaphthalene. In the latter case, only one peak corresponds to the gel and the other two are due to the kapton windows of the SAXS set-up. From Dasgupta et al. [6]

alcohol gels since three well-defined peaks are seen for the former against one for the latter in the explored q-range. Noticeably, the position of the first peak, which is related to the distance between molecules in the [100] plane of the crystal lattice,[1] differs in both systems (Fig. 4.4). For the [110] distance the OPVOH molecules must stand upright, while those of OPVR (Fig. 4.2) must be tilted in order to account for the lower distance as portrayed in Fig. 4.4. The crystal structure of the OPVR molecules in the benzyl alcohol organogels is most probably of the triclinic type.

Dasgupta et al. further account for the diffraction pattern in the case of OPVR/benzyl alcohol gels by assigning the second peak at $d = 2.17$ nm to the

[1]The *c axis* is taken as the axis perpendicular to the π-stacking, see Fig. 4.4.

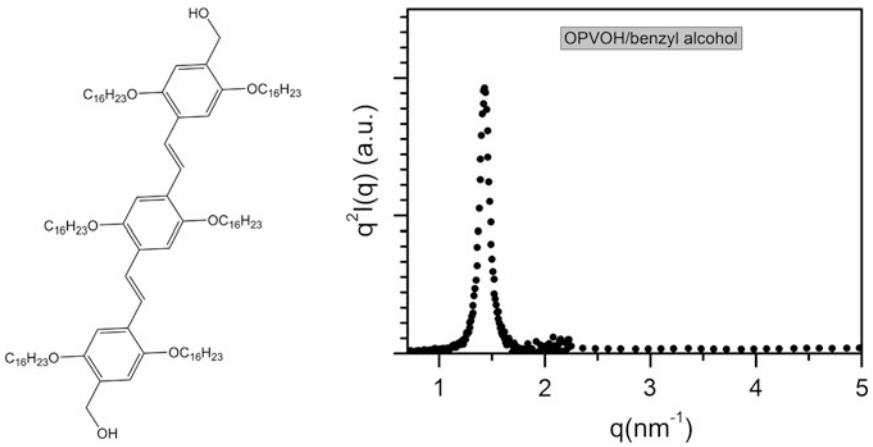

Fig. 4.3 *left* chemical structure of OPV molecule (named OPVOH), *right* diffraction pattern in the SAXS range, $C_{OPVOH} = 0.4 \times 10^{-2}$g/cm^3. From Dasgupta et al. [8]

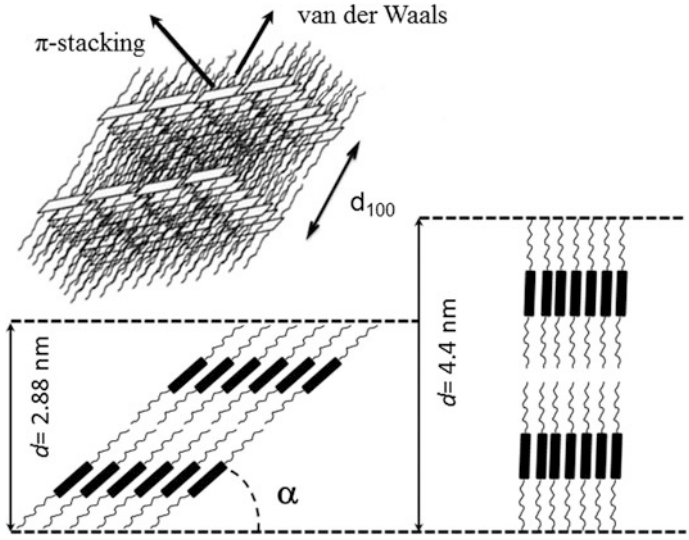

Fig. 4.4 *Top* schematic representation of the molecular arrangement in OPVOH organogels as determined by Ajayaghosh and coworkers [5]. Rectangles stand for the "central core" and threads represent the aliphatic wings. *Bottom* the molecules as seen parallel to the central core; *left* OPVR molecules with a tilt angle of about $\alpha \approx 41°$, *right* the OPVOH molecules standing upright, from Dasgupta et al. [6, 8]

[010] plane of the crystalline lattice (related to the length of the *central core + terminal groups*), while they surmise that the third one may be the second order of the first reflection or may correspond to the [002] plane.

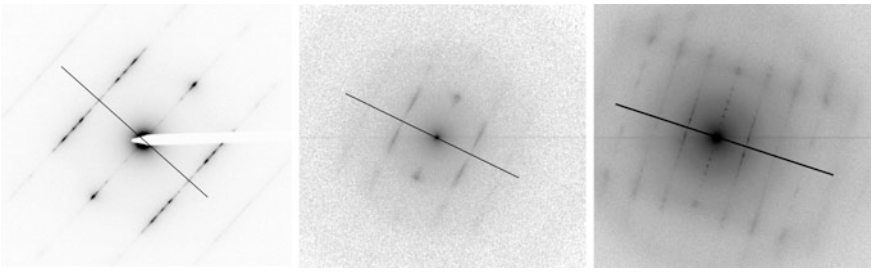

Fig. 4.5 TEM diffraction patterns obtained on xerogels from OPVR/benzyl alcohol (*left*), OPVOH/benzyl alcohol (*middle*), and OPVMe/benzyl alcohol (*right*). In OPVMe, the OH group is replaced by an OCH_3 group. The *straight lines* stand for the fibril long axis. After *left* diffraction pattern from Dasgupta et al. [6], and Guenet and Thierry unpublished (*middle* and *right* diffraction patterns)

That three peaks are seen with OPVR suggests a high organization in the three dimensions of space while only one direction seems to be privileged for OPVOH systems. The very narrow peak indicates that there is a high organization along the direction involving van der Waals interactions, namely the [100] plane (see Fig. 4.4). That the growth direction involving H-bonds between terminal groups is not privileged is possibly related to the hypothetical formation of a compound with benzyl alcohol. If the solvent molecules are not properly placed, then orientation defects can be introduced, thus breaking the order over some distance. The local structure has definitely a direct bearing upon the morphology of these systems as detailed in what follows.

The high organization of the OPV molecules in xerogels has been observed by Guenet and coworkers by performing microdiffraction in transmission electron microscopy (TEM) [6]. As can be seen in Fig. 4.5 the patterns consist of narrow diffraction spots, something reminiscent of single crystals. Interestingly, the diffraction pattern obtained with OPVOH systems is not so well-defined compared with that of OPVMe, where the OH group has been replaced by an OCH_3 group, thus preventing H-bonds formation, and correspondingly a compound formation with benzyl alcohol.

Recently, Wan and coworkers [9] have reported X-ray diffraction studies (Fig. 4.6) on a sugar-appended organogelator. They have observed a change in molecular packing when going from the gel, for which the molecular structure was found to be the same as solution-grown crystals in acetonitrile, to the xerogel. In the latter case, they suggest that drying the gel promotes the interdigitation between the aliphatic moieties of the molecules.

The results may suggest the occurrence of some molecular compounds. Indeed, drying a gel is likely to remove the solvent from the crystal lattice so that a change in the parameters is expected together with a change in the aspect of the diffraction pattern. One can indeed notice in Fig. 4.6 that the diffraction pattern is not so well-defined as is in the case of the wet gel or the crystal.

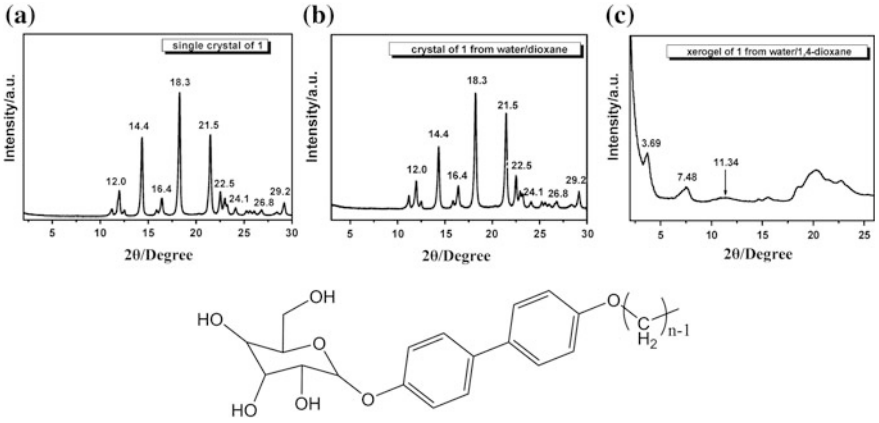

Fig. 4.6 X-ray diffraction pattern of (**a**) a single crystal of 1 from acetonitrile (2 mg/mL), (**b**) a crystal of 1 from water/1,4-dioxane (8/2, v/v, 5 mg/mL), and (**c**) a xerogel of 1 from water/1,4-dioxane (8/2, v/v, 5 mg/mL). From Wan and coworkers [9]

4.2 The Mesoscopic Structure(s)

Basically, the mesoscopic structure deals with the determination of the shapes of the organogel fibrils as well as the way they interact as a function of various parameters such as temperature, concentration, solvent type, and the like. Several techniques can be used in this aim: AFM, TEM, SAXS, SANS to quote but a few. Typically, the range of distance explored lies within 2–50 nm. In this section, a clear emphasis is put on systems studied by means of scattering techniques, nondestructive techniques, and electron microscopy and/or AFM, "destructive" techniques. Their combination guarantees a better structural description of the organogel mesoscopic structure.

4.2.1 The Fibril's Shape

The fibril's shape, namely its cross-section and its degree of curvature, can be studied by destructive techniques such as AFM and TEM, in some cases by high-resolution SEM, but also by nondestructive small-angle scattering techniques, such as X-ray and/or neutron scattering (SAXS, SANS) that are quite suited for exploring the mesoscopic range. As a rule, AFM and TEM need relatively dilute system so as to be able to observe individual fibrils while scattering techniques can be applied to more concentrated systems. In any case, the combination of all these techniques is always rewarding.

AFM and/or SEM investigations reveal that organogel fibrils are straight or nearly straight in distance range below 100 nm [5–10]. Under these conditions, the

data from small-angle scattering studies can be interpreted by using models developed for cylindrical objects. Fournet [11] obtained the following general expression for cylinders of length L and radius r:

$$I(q) \sim \int_o^{\frac{\pi}{2}} \frac{\sin^2(qL\cos\phi)}{q^2L^2\cos^2\phi} \frac{4J_1^2(qr\sin\phi)}{q^2r^2\sin^2\phi} \sin\phi \, d\phi \tag{4.1}$$

where q is the modulus of the scattering vector ($q = \frac{4\pi}{\lambda} \sin 2\theta$) and ϕ the angle between the cylinder axis and the scattering vector.

Interestingly, for the case $L \gg r$ and $qL \gg 1$ only those cylinders whose long axis is perpendicular to the scattering vector contribute to the scattering intensity. Then $\phi \approx \pi/2$ in relation (4.1) so that the second term in the integral of (4.1) can be extracted while equating $\sin\phi = 1$. After performing the integration of the first term (4.1) becomes [12, 13]:

$$I(q) \sim \frac{\pi\mu_L}{q} \frac{4J_1^2(qr)}{q^2r^2} \tag{4.2}$$

where μ_L is the mass per unit length of the cylindrical object. Relation (4.2) can be written in a general form where σ is a length related to the cross-section of the object:

$$I(q) \sim \frac{\pi\mu_L}{q} \varphi(q\sigma) \tag{4.3}$$

with

$$\varphi(q\sigma) = \int_\sigma \rho(\sigma) J_o(q\sigma) 2\pi\sigma \, d\sigma \Big/ \int_\sigma \rho(\sigma) 2\pi\sigma \, d\sigma \tag{4.4}$$

where $\rho(\sigma)$ is the scattering density, and J_o the Bessel function of 1st type and zeroth order.

The assumption made to derive relation (4.2) has another important consequence. In a randomly distributed array of long cylinders the probability for having two neighboring cylinders oriented perpendicular to the scattering vector is rather weak. As a result, the intermolecular scattering terms can be generally neglected [14], and one is therefore fulfilling the "isolated cylinder scattering" condition.

The function $\varphi(q\sigma)$ reads for the following cross-section shapes (Fig. 4.7):

Disc of radius r corresponding to a *solid cylinder*:

$$\varphi(qr) = 4J_1^2(qr)/q^2r^2 \tag{4.5}$$

Circle of radius r corresponding to a *thin-walled cylinder (sleeve)*

$$\varphi(qr) = J_o^2(qr) \tag{4.6}$$

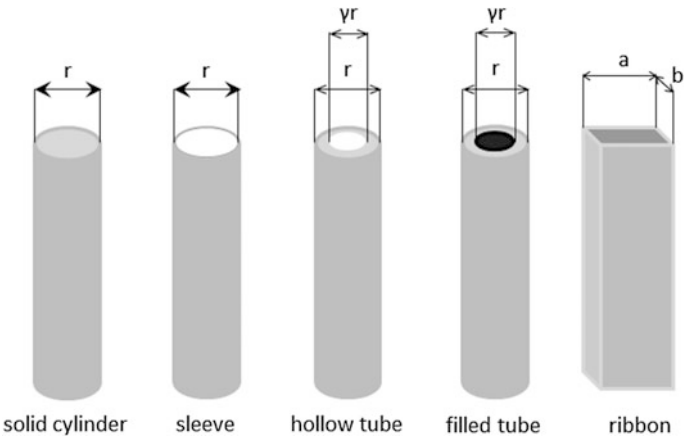

Fig. 4.7 Various shape of cylinders that can be used as models for interpreting scattering curves in organogels for mesoscopic structures

Hollow disc of outer radius r and inner radius γr corresponding to a *tube*

$$\varphi(qr) = \left[\frac{2}{(1-\gamma^2)qr} \times (J_1(qr) - \gamma J_1(\gamma qr)\right]^2 \tag{4.7}$$

Cylinders can also consist of a hollow tube filled by a solid cylinder of different contrast and density. The scattering curve in the case of SANS can be totally different by using a hydrogenous or a deuterated solvent. If the scattering amplitudes are A_{out} for the hollow cylinder and A_{in} for the inner solid cylinder, then $\varphi(qr_{\text{out}})$ reads:

$$\varphi(qr_{\text{out}}) = \left[\frac{2A_{\text{in}}\gamma}{A_m qr_{\text{out}}} J_1(q\gamma\, r_{\text{out}} + \frac{2A_{\text{out}}}{A_m qr_{\text{out}}}(J_1(qr_{\text{out}} - \gamma J_1(q\gamma\, r_{\text{out}})\right]^2 \tag{4.8}$$

with

$$A_m = \gamma^2 A_{\text{in}} + \left(1-\gamma^2\right)A_{\text{out}} \tag{4.9}$$

The consequence is the possible observation of "negative apparent cross-sectional radius as (4.8) reads for $qr_{\text{out}} \ll 1$:

$$\varphi(qr_{\text{out}}) = 1 - \frac{q^2}{4}\left[\frac{r_{\text{out}}^2}{A_m}\left(A_{\text{in}}\gamma^4 + A_{\text{out}}\left(1-\gamma^4\right)\right)\right] \tag{4.10}$$

The term is bracket can be negative, so that the intensity may show an upturn instead of a downturn in a Kratky plot (see Fig. 4.11 for instance).

A rectangle of length a and width b, corresponding to a *straight ribbon*:

$$\varphi(qr) = \frac{2}{\pi}\int_o^{\pi/2}\left[\frac{\sin qa/2\cos\theta}{qa/2\cos\theta}\times\frac{\sin qb/2\sin\theta}{qb/2\sin\theta}\right]^2\sin\theta\, d\theta \tag{4.11}$$

In the case of bundles of parallel cylinders the expression of the scattered intensity reads [15]:

$$I(q) \sim \frac{\pi\mu_L}{q}\varphi(q\sigma)\frac{1}{n^2}\sum_{j=1}^{n}\sum_{i=1}^{n}J_o(qs_{ij}) \tag{4.12}$$

where s_{ij} is the distance between the centers of the cylinders, and J_o is again the Bessel function of first kind and of zeroth order.

Fibrils may in many cases display dispersion in cross-section dimension. Cross-section distribution functions have then to be considered which modifies the scattering intensity and results in a dumping of the oscillations generated by the Bessel functions.

Guenet has proposed a specific type of cross-section distribution while investigating the structure of poly vinyl chloride gels [16]. A distribution function of the type $w(r) \sim r^{-\lambda}$ (also considered in so-called *scale free* networks [17]) is considered with two cut-off radii $r_{\min}$ and $r_{\max}$. In the "*transitional*" range defined by $r_{\max} > q^{-1} > r_{\min}$ the intensity reads:

$$I(q) \sim \frac{4\pi^2}{q^4}\left(A(\lambda)q^{\lambda} - \frac{1}{\lambda\, r_{\max}^{\lambda}}\right)\Big/\int_{r_{\min}}^{r_{\max}} w(r)dr \tag{4.13}$$

with:

$$A(\lambda) = \Gamma(\lambda)\Gamma(3-\lambda/2)/2^{\lambda}\Gamma^2(\lambda+1/2)\Gamma(3+\lambda/2) \tag{4.14}$$

Γ being the gamma function.

For $qr_{\min} > 1$ the intensity reaches the Porod regime and can be written:

$$I(q) \sim \frac{4\pi}{q^4}\int_{r_{\min}}^{r_{\max}}\left[1+\frac{3}{8q^2r^2}\right]w(r)dr \tag{4.15}$$

The case $\lambda = 1$, observed for PVC gels, is particularly interesting. A plot of the type $q^4I(q)$ versus q yields a linear variation in the transitional range whose intercept q_o at $q^4I(q) = 0$ gives $r_{\max}$ through $r_{\max} = 2/\pi\ q_o$. In the same representation the intersect q^* with the plateau in the Porod range yields $r_{\min}$ through $r_{\min} = 2/\pi\ q^*$.

A similar approach was considered for polydispersed ribbons (laths) by Morin et al. [18] for which the width of the lath is much larger than the thickness. Considering also two cut-off thicknesses $\delta_{\max}$ and $\delta_{\min}$ and a distribution function of the type $w(\delta) \sim 1/\delta$ they obtained for $\delta_{\max} > q^{-1} > \delta_{\min}$:

$$q^4 I(q) \sim q\pi - \frac{2}{\delta_{\max}} \tag{4.16}$$

And for $\delta_{\min} > q^{-1}$

$$q^4 I(q) \sim \frac{4\pi}{\delta_n} \tag{4.17}$$

where δ_n is the first momentum of the distribution that reads

$$\frac{1}{\delta_n} = \left[\frac{1}{\delta_{\min}} - \frac{1}{\delta_{\max}}\right] \frac{1}{\mathrm{Log}\delta_{\max}/\delta_{\min}} \tag{4.18}$$

Again for $q^4 I(q) = 0$ one has $q_o = 2/\pi\delta_{\max}$ and the intercept between the transitional regime and the Porod regime is $q^* = 2/\pi\delta_{\min}$.

One has to keep in mind that the scattered intensity takes into account both the fibrils cross-section but equally the junctions, which are generally made up with fibrils interacting in a parallel fashion. This analysis was carried out for organogels by Terech and coworkers [19], but earlier for poly[methyl methacrylate] gels by Saiani and Guenet [20]. In some cases, a fit with two radii is sufficient, one related to the fibrils and the other to the junctions [21].

In the case of cylindrical system, for which the intensity is very rarely expressed by only one term, it is customary to plot the data either by using a Kratky plot ($q^2 I(q)$ vs q) or a $q^4 I(q)$ versus q representation. These representations usually convey more information rather than a double logarithmic scale such as a better highlighting of the oscillations arising from the Bessel functions.

Terech and coworkers [19] have used the small-angle neutron scattering technique for characterizing the fibrils cross-section of 12-hydroxystearic acid, HSA (Fig. 4.8). Depending on the solvent, HSA produces "cylindrical" fibrils of

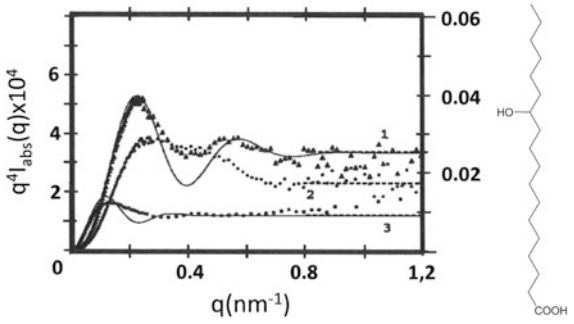

Fig. 4.8 SANS curves for HSA organogels in a $q^4 I(q)$ versus q representation: 1 (▲) benzene-d, C = 0.014 g/cm^3; 2 (●) cyclohexane-d, C = 0.013 g/cm^3; 3 (■) nitrobenzene-d, C = 0.0115 g/cm^3. *Dotted lines* indicate the asymptotic large q limit. *Full lines* are adjustments (see text for details. Scale for nitrobenzene gel is the *right* ordinate axis. *Right* the HSA chemical structure. From Terech et al. [19]

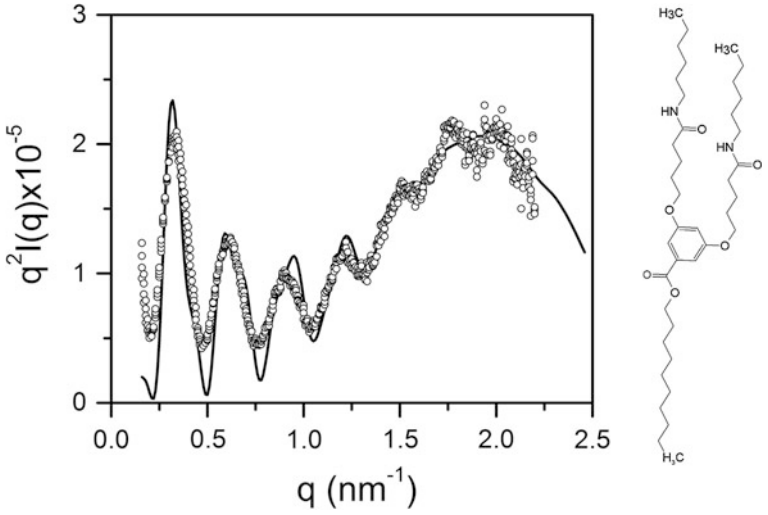

Fig. 4.9 *Left* SAXS data ($q^2I(q)$ vs q) for BHPB-10/*trans*-decahydronaphthalene organogel (C = 0.01 g cm^3). *Solid line* stands for a fit with relation 4.7 with r = 12.75 nm and γ = 0.74, and introducing a term $q^2I(q) \sim \exp a(q\text{-}1.92)^2$ for the diffraction by the arrangement of the molecules in the nanotube. *Right* the molecule. From Dasgupta et al. [24]

cross-sectional radius r = 18 nm in toluene while in nitrobenzene ribbons are obtained of square cross-sectional dimensions b = 30 nm and a = 150 nm.

Another interesting system, which can be considered a case study, consists of an array of nanotubes prepared from 3,5-Bis-(5-hexylcarbamoyl-pentyloxy)-benzoic acid decyl ester (see Fig. 4.9) and other ester derivatives, first synthesized by Mésini and coworkers [22, 23]. These systems produce nanotubes whose occurrence is ascertained from electron microscopy [22], SAXS, and SANS [22–24] and AFM [24]. Typical scattering curves in *trans*-decahydronaphthalene are shown in Fig. 4.9 and a TEM image in Fig. 4.10 [25]. The outer and inner radii of these nanotubes are 12.7 and 9 nm, respectively, so that they can house rather large molecules [25].

As said above, it is a case of study since it is rather rare to observe experimentally so many oscillations by SAXS or SANS in cylindrical systems. Usually, cross-section dispersion entails a rapid vanishing of these oscillations.

If the type of interactions between molecules is altered without drastically modifying their shape, then the nanotube structure vanishes. Khan et al. [26] have shown that partly fluorinated molecules do not form nanotubes any longer but twisted helical objects instead (Fig. 4.10 right). By toying with the contrast factor in SANS studies, they conclude that the fluorinated moiety is in the core of the helical objects, and that the molecules stack as shown in Fig. 4.11.

This conclusion is reached by studying the objects either in a hydrogenous solvent or in a deuterated solvent. The scattering curves are conspicuously different and stand as an example described by relation 3.8 and 3.10 (Fig. 4.11). The Porod

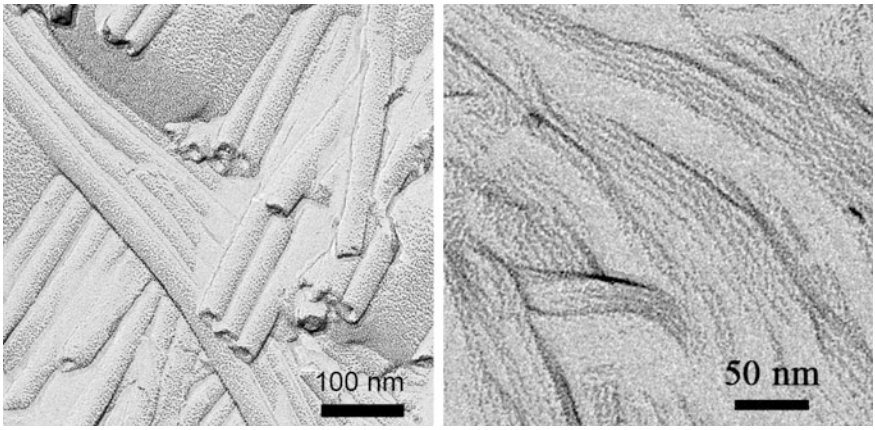

Fig. 4.10 *Left* TEM image of a BHPB-10 gel in cyclohexane by freeze fracture. *Right* TEM image of BHPBF/o-xylene obtained by freeze fracturing. Schmutz, Guenet and Mésini unpublished data (see Ref. [23] and [26])

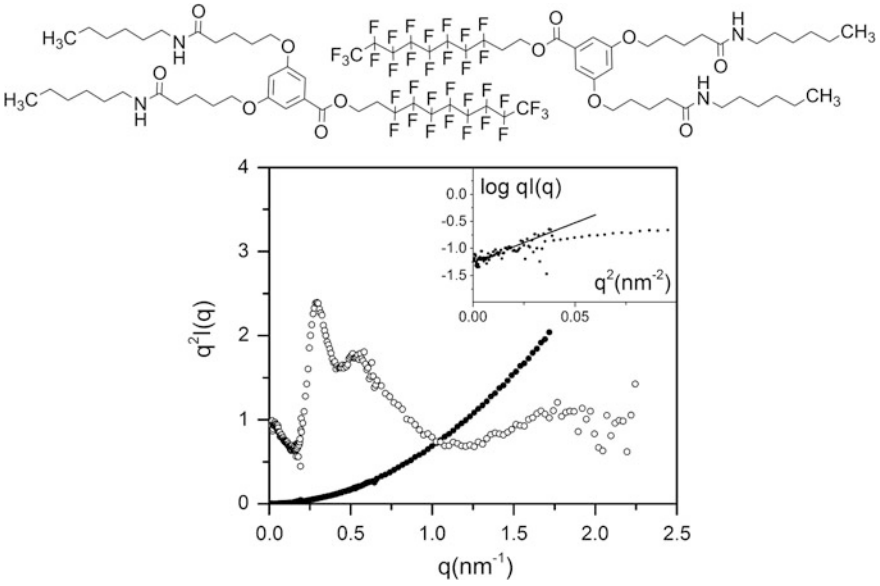

Fig. 4.11 *Top* two BHPBF molecules and the way they are said to stack. *Bottom* SANS *curve* plotted by means of a Kratky plot ($q2I(q)$ versus q). (●) BHPBF/*o*-xylene$_H$ (C = 0.02 w/w). (Inset) Same data plotted by means of a Porod plot, log $qI(q)$ versus $q2$. The *solid line* shows the linear part of this plot, allowing one to determine the cross-sectional radius. (O) BHPBF/*o*-xylene$_D$ (C = 0.02 w/w). Data replotted from Kahn et al. [26]

plot representation in the inset of Fig. 4.11 provides one with a value for the cross-sectional radius that can only be accounted for by the particular stacking shown in the same figure.

Another system producing nanotubes is made up with hydrogels prepared under physiological conditions from a synthetic peptide, namely fluorenylmethoxycarbonyl diphenylalanine (Fmoc-FF) [27]. Peptides are known to self-assemble and produce hierarchical structures such as fibrillar gels [28]. Peptides can be used as building blocks for creating new molecules with various and differing self-assembling properties.

In the case of Fmoc-FF Smith and coworkers have shown the stacking of the molecules creates a hollow tubular structure with outer radius of 1.5 nm and an inner radius of about 0.76 nm (Fig. 4.12).

Further interaction between these nanotubes generates ribbons of width somewhere between 14 and 70 nm. The thickness of these ribbons is of the order of a few nanometers, which suggests a side-by-side flat packing of the molecules. This may seem rather strange for nanotube aggregation.

Another type of hydrogel made up with N-Methyl-N-(pentacosa-10,12-diyn)-propargylamine exhibit an unusual array of laths in water [18] (see Fig. 4.13). The laths possess a large width in the micrometer range with thicknesses in the nanometer range. A neutron scattering study (Fig. 4.14) shows that the average thickness is a few nanometers. Applying Eqs. 4.16 and 4.17 allows one to conclude that the thickness distribution is of the type $w(\delta) \sim 1/\delta$ with $\delta_{\max} \approx 6.5$ nm and $\delta_{\min} = 1$ nm and $\delta_n \approx 2.2$ nm.

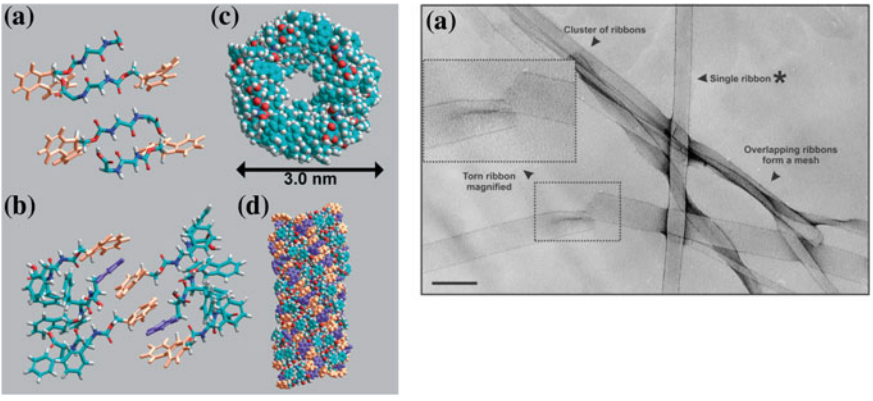

Fig. 4.12 *Left* molecular structure for Fmoc-FF peptides arranged in an anti-parallel β-sheet pattern (**a**), interlocking of Fmoc groups from alternate β-sheets to create π-stacked pairs with interleaved phenyl rings (**b**). Due to the twist of β-sheets, the second sheet must be rotated in relation to the first to maintain the interaction between the fluorenyl groups creating a cylindrical structure; *top* view (**c**) of the structure and side view (**d**) the structure was energy minimized using the Amber force field. In **a**, **b** and **d** fluorenyl groups are colored orange and the phenyl groups are colored purple to illustrate the paired π-stacked nature of the fluorenyl groups. *Right* transmission electron microscopy of Fmoc-FF negatively stained with 2 % uranyl acetate with indications. Scale bar = 50 nm. From Smith et al. [28]

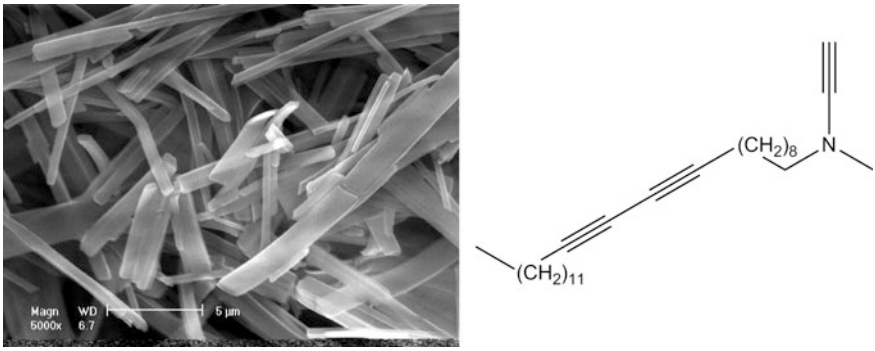

Fig. 4.13 *Left* laths composing N-Methyl-N-(pentacosa-10,12-diyn)-propargylamine hydrogels. *Right* the chemical structure. From Morin et al. [18]

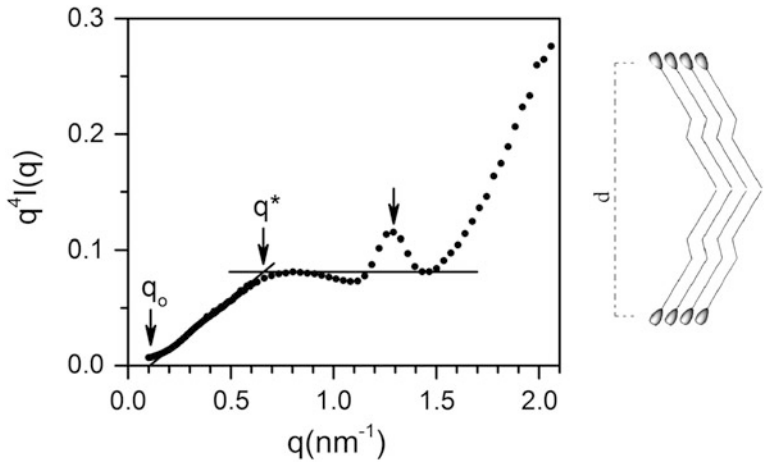

Fig. 4.14 SANS data from N-Methyl-N-(pentacosa-10,12-diyn)-propargylamine hydrogels, $C = 0.01$ g/cm^3. q_o and q^* allow calculation of δ_{min} and δ_{max} through relations (4.16) and (4.18) The *arrow* highlights the position of the peak that corresponds to the molecular arrangement. *Left* the chevron-like arrangement of the molecules. From Morin et al. [18]

The diffraction peak corresponding to the molecular arrangement within the laths can be seen in the small-q range. Its value $q = 1.28$ nm^{-1} which corresponds to a distance of 4.9 nm. The only way to accommodate this distance with the length of the molecule is to consider a chevron-like structure [18]. One may wonder why outcomes from neutron scattering suggest the existence of laths of 1 nm while the size of the molecules is larger (about 3.5 nm). This is only possible if the entire molecule lies within the plane defined by the width and the length of the laths. If they were perpendicular to this plane, much larger thicknesses would be observed. A microdiffraction study by TEM would certainly confirm or discard this assumption.

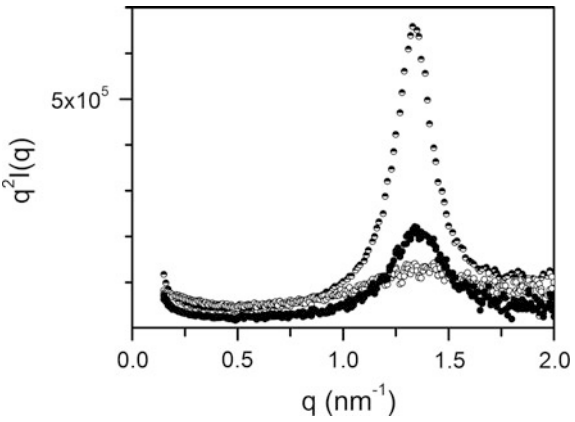

Fig. 4.15 SAXS data plotted by means of $q^2I(q)$ versus q for OPV16 organogels prepared from *cis*-decalin solutions at different concentrations and temperatures (O) C_{OPV} = 0.004 g/cm^3, $T_{formation}$ = 0 °C; (●) C_{OPV} = 0.004 g/cm^3, $T_{formation}$ = 20 °C; (◓) C_{OPV} = 0.017 g/cm^3, $T_{formation}$ = 0 °C. Data replotted from Dasgupta et al. [29]

It is worth stressing that SANS or SAXS investigations may be difficult to be interpreted when one is dealing with monotonously decreasing scattering intensities. In this case, the help of "*destructive*" techniques such as TEM or AFM can be decisive in pointing out to the scattering models that are the most relevant. Again, a feedback between these techniques is more than welcome.

The formation or quenching temperature affects the fibrils' cross-sectional dimension. This has been evidenced by SAXS experiments by Dasgupta et al. [29] for OPV organogels prepared in *cis*-decahydronaphthalene (Fig. 4.15). They have determined the full-width at half maximum Δq (FWHM) of the peak at low-angles, q = 1.33 nm^{-1} related to the packing of the OPV molecules (d = 4.7 nm) as a function of the formation temperature. Data in Fig. 4.15 show a significant effect whether the samples are prepared at 20 or 0 °C. The FWHM, Δq, varies from 0.26 to 0.51 nm^{-1}, which suggests a difference in cross-sectional section by about 2 as estimated through the Scherrer relation. Increasing concentration also increases the fibrils cross-section as Δq = 0.14 for C_{OPV} = 0.017 g/cm^3.

Despite a noticeable change in cross-section size, Dasgupta et al. have not reported any significant change in the melting temperature of these organogels. This is probably so because the corrective term in relation (3.5) is rapidly negligible.

4.2.2 About the "Critical" Gelation Concentration

At this point, a discussion about the gelation concentration, C_{gel}, is worth tackling. C_{gel} is the organogelator concentration where the aggregates size diverges to infinity. The simplest way to tackle the calculation of C_{gel} is to consider the approach used by Guenet for deriving this parameter for polymer thermoreversible gels [30]. It is assumed that C_{gel} is reached when fibrils of *end-to-end distance* of the long axis S_F can make contact with one another, or in other words when spheres of diameter S_F are in contact. This entails the following relation:

$$C_{\text{gel}} = \frac{6M}{\pi S_F^3} \tag{4.19}$$

where M is the fibril molecular weight.

That the end-to-end distance is introduced instead of the contour length of the fibrils axis, L_F allows one to consider a more general problem where fibrils are not necessarily straight (for straight fibrils $L_F = S_F$). Equation (4.19) can be further expressed by introducing the fibrils cross-sectional dimension through:

$$S_F^2 \sim L_F^{2/D_f} \tag{4.20}$$

and

$$M = \pi \rho \, r^2 L_F \tag{4.21}$$

where D_f is the fractal dimension of the fibrils' long axis ($D_f = 1$ for straight fibrils), r the cross-sectional radius, and ρ the fibrils' density. One ends up with the following expression:

$$C_{\text{gel}} \sim \frac{6\rho r^2}{L_F^{\left(3/D_f - 1\right)}} \tag{4.22}$$

Relation (4.22) indicates that C_{gel} depends essentially upon the fibrils' cross-sectional dimensions: a small cross-section yields low gelation concentration and vice versa. Since the cross-section dimensions depends upon temperature, C_{gel} *is temperature-dependent, and also undercooling-dependent.*

In the case of branching C_{gel} will be increased. In the case of cross-section dispersity, it will depend largely on the type of distribution. If one assumes that the polydispersity in length and that in cross-section are uncorrelated, then one obtains:

$$C_{\text{gel}} \sim \frac{6\rho < r^2 >_n}{< L_F^{\left(3/D_f - 1\right)} >_w} \tag{4.23}$$

where brackets indicate an average value, with n standing for the first moment and w the second moment of the distribution function.

A scale-free type, as described in relation (4.13) is therefore likely to decrease C_{gel} as thin fibrils dominate.

The cross-sectional dimension of the fibrils may change with concentration but equally with aging. Banerjee et al. have recently reported a case where gels prepared from a dipeptide-based organogelator show considerable change on aging. The gel is first transparent but evolves to a turbid gel after 10 h aging [31]. Comparison of the gel as-prepared and after aging by transmission electron microscopy reveals a change in the fibrils aspect together with the cross-section

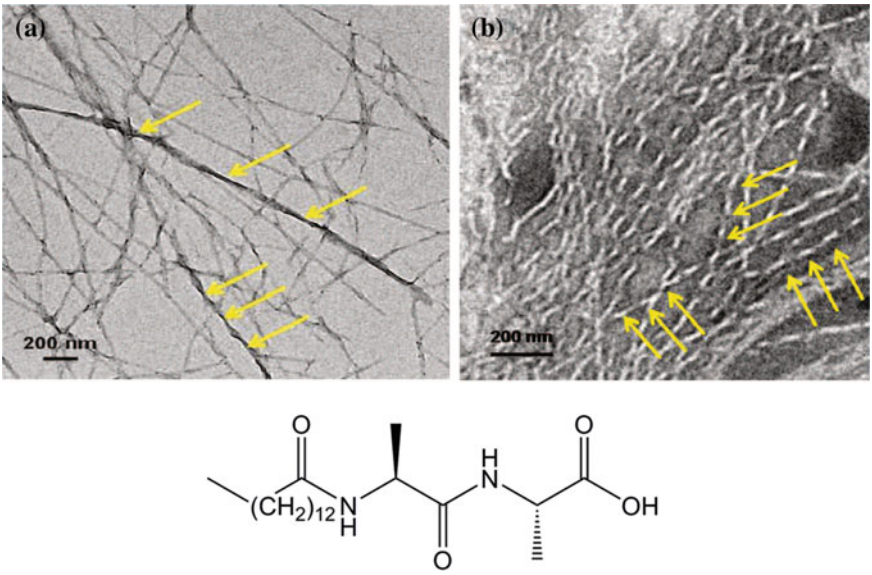

Fig. 4.16 *Top* TEM images of the gel as-prepared (*left*) and after subsequent aging (*right*). The equidistant arrows highlight the regularity of the twisting pitch in the aged gel. *Bottom* the organogelator. From Baral et al. [31]

distribution (Fig. 4.16). In the as-prepared gel there is a large cross-section distribution which is drastically reduced after subsequent aging. Basically, the fibrils of lowest cross-section have disappeared. Although fibrils in as-prepared gels and aged gels are twisted, the twist is far more regular in the latter case.

The rearrangement also occurs at the molecular level. X-ray diffraction patterns display the appearance of a new peak at $d = 4.05$ nm in addition to the peak observed for the as-prepared gel at 3.28 nm. Effect is also observed on the mechanical properties where the storage modulus is seen to increase of about twofold. Equations developed in the Chap. 6 can account for this effect.

To be sure, C_{gel} depends upon too many factors so that it cannot stand neither as a characteristic nor a critical parameter of an organogelator/solvent system. This concentration should rather be designated as "***onset gelation concentration***".

4.2.3 The Junctions

As was discussed in Chap. 2 devoted to the definition of a gel, the fibrillar objects must be connected in some way or another. In what follows will be presented some examples on how this connection is achieved or not.

Ajayaghosh and coworkers have investigated in details the junctions on gels and on rather diluted systems by TEM and AFM. [7]. The samples are prepared by drop

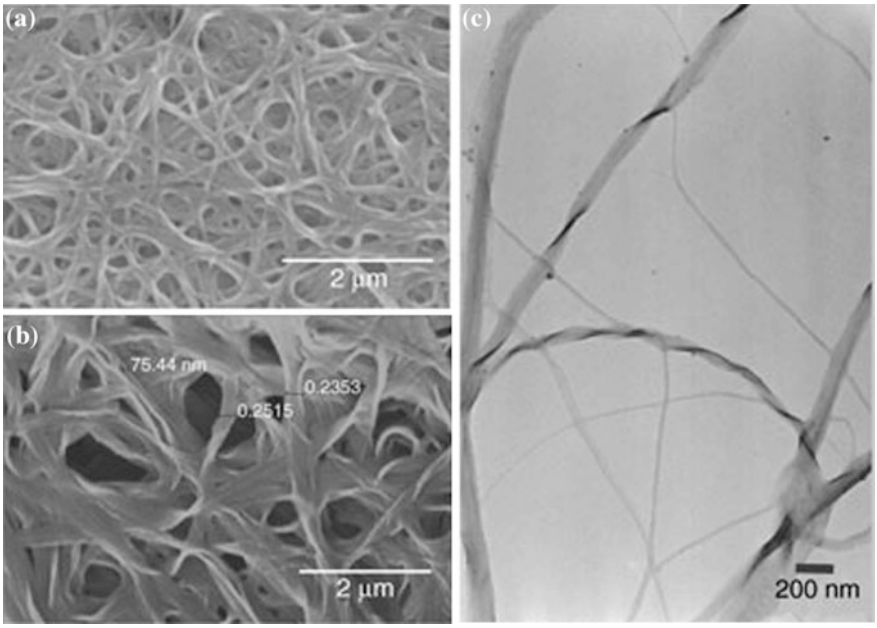

Fig. 4.17 *Left* AFM pictures detailing the different types of junctions in a gel of an OPV/toluene (chemical structure of the OPV molecule shown in Fig. 4.3); *right* TEM picture of a dilute solution of this organogel. From Ajayaghosh and Praveen [7]

casting of these solutions. In Fig. 4.17, a minimum of three different junction types can be identified: branching type, crossing type, and parallelization type (side-wise alignment) with possible intertwining.

These authors have also examined the effect of using mixture of chiral and nonchiral molecules. The chiral molecule is obtained by introducing a chiral group in their OPV molecules (Fig. 4.18). AFM investigations shown in Fig. 4.18 show interesting features. While fibrils display a rope-like structure, left-handed twists (P) and right-handed twists (M), the junction does not (Fig. 4.18a). This is further evidenced by a measure of the height of the different moieties: fibrils do exhibit oscillations unlike the junctions (Fig. 4.18b).

Ajayaghosh et al. assign these outcomes to a chirality transfer and amplification in the co-assembly. One may, however, wonder whether some local phase separation between chiral and achiral molecules would occur with the achiral molecules phase forming the junctions.

Surprisingly, while only left-handed structures are seen for the pure OPV, right-handed structures appear in the presence of achiral OPV.

The chemical structure has also a strong impact on the junctions. A striking example is given by Ajayaghosh and coworkers [7] on OPV molecules that possess heavy terminal groups as shown in Fig. 4.19. The organization of the resulting fibrils differs markedly whether a group is attached to one or the two ends of the

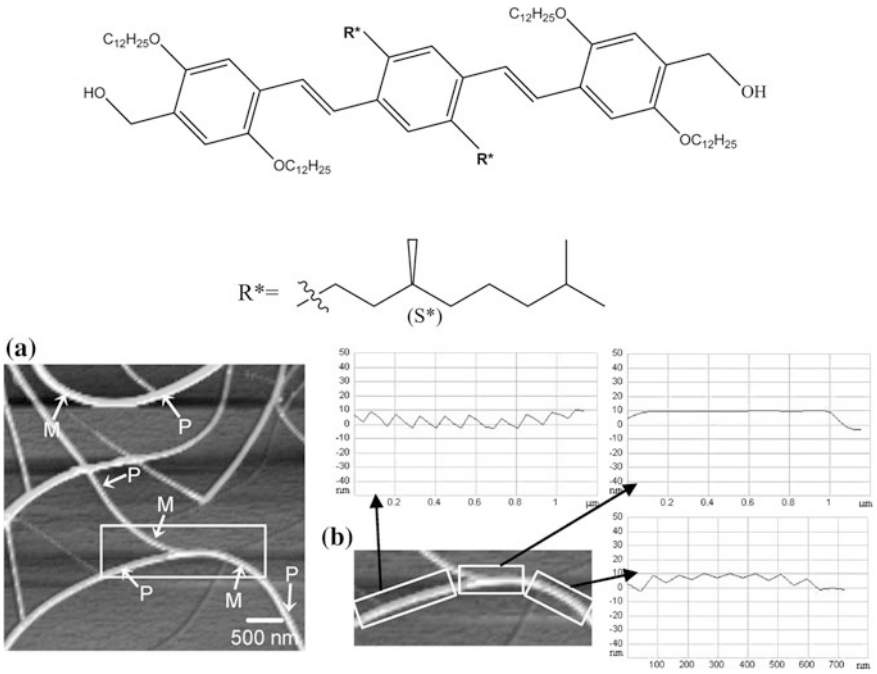

Fig. 4.18 *Top* chiral molecule noted OPV3 together with its chiral group R*. *Bottom* **a** AFM picture of junctions for a gel made up with OPV3 and OPVOH. **b** The different profile as determined by AFM. From Ajayaghosh et al. [7]

central core. In the case where only one heavy group is present, the system does not exhibit the usual aspect of a gel. The fibrils never cross but remain "parallel" to one another. This system resembles much more to a liquid crystal than to a gel, yet, this system is still composed of crystalline fibrils.

Conversely, once two identical heavy groups are attached to the ends of the central core, one retrieves the usual network architecture with fibrils intermingled and junctions made through fibrils parallelization, and/or branching.

The examples discussed so far deals with networks made up with various types of junctions (branching, crossing, parallelization,..). Recently, Dasgupta et al. [32] have reported on a system where branching chiefly occurs thus producing a *hub-like network* (Fig. 4.20). This corresponds to the system, OPVOH/benzyl alcohol, for which it is assumed that a molecular compound is formed [8, 32]. This system consists essentially in very large ribbons. They further conclude that the organogelation process is triggered by homogeneous nucleation not only on the basis of the thermodynamic investigation, that show a large hysteresis between formation and melting temperature (see Fig. 3.10), but also from confocal microscopy investigations. Indeed, the pictures obtained through this technique clearly highlight the absence of any impurity at the junction from which the fibrils radiate.

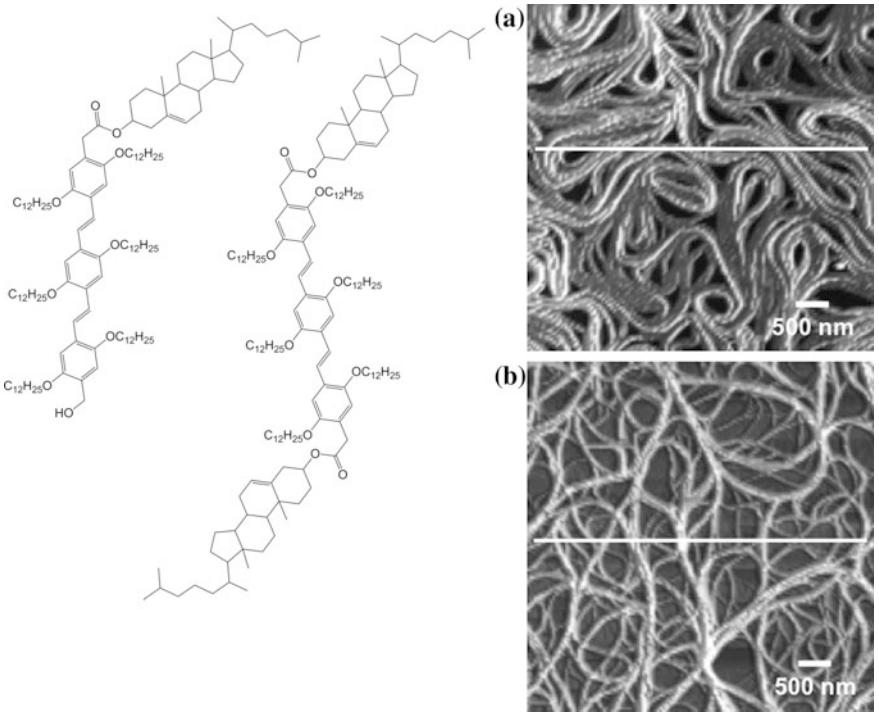

Fig. 4.19 *Left* chemical structure of OPV4 (*left*) and OPV5 (*right*). *Right* AFM pictures of systems produced by OPV4/decane (**a**) and OPV5/decane (**b**). From Ajayaghosh et al. [7]

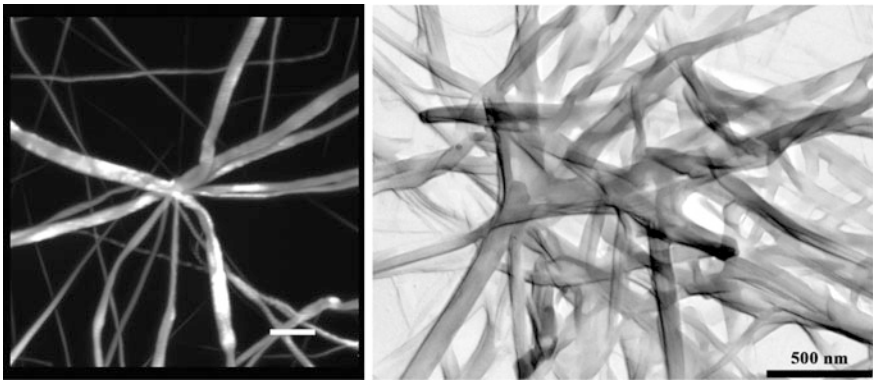

Fig. 4.20 *Left* Confocal laser scanning micrographs of OPVOH/benzyl alcohol organogels (C_{OPVOH} = 0.004 g/cm^3). Scale bar = 5 µm. From Dasgupta et al. [32]. *Right* TEM image of the same system for C_{OPVOH} = 0.00004 g/cm^3 (Schmutz, Guenet, unpublished results)

This conclusion is further supported by TEM experiments on aggregates prepared from dilute solutions and deposited onto a microscopy grid. Although the aspect of the aggregates is altered due to the collapse from 3D to 2D, the absence of any nucleating impurity is conspicuous.

This again emphasizes that the study of aggregates instead of the infinite network is easier in TEM and can bring the same or nearly the same pieces of information.

Another typical system has been reported by Sarazin and coworkers on complementary molecules that form organogels after they have assembled the way shown in Fig. 4.21 right [33]. Each partner is linked to the other by means of hydrogen bonds mimicking the same type of interactions occurring in the double helical DNA. This complex is supposed to form a supramolecular polymer by a 1D stacking process. Electron microscopy investigation reveals that they form twisted ribbons with a pitch of about 25 nm and a cross-sectional radius of about 5 nm while the junctions are built up through their intertwining.

A complementary neutron scattering study (Fig. 4.22) of these JANUS-II systems at a higher concentration ($C_{\text{JANUS-II}} = 0.55 \times 10^{-3}\text{g/cm}^3$) has revealed that the scattered intensity can be theoretically reproduced by considering relation (4.5) with two radii, which gives relation (4.24):

$$q^2 I(q) \sim X r_1^2 \times \frac{4J_1^2(qr_1)}{q^2 r_1^2} + (1 - X) r_2^2 \times \frac{4J_1^2(qr_2)}{q^2 r_2^2} \tag{4.24}$$

The best fit gives the following values $r_1 = 4.86$ nm with $X = 0.46$, and $r_2 = 1.84$ nm with $1\text{-}X = 0.54$. The value $2r_2$ corresponds to the length of the two

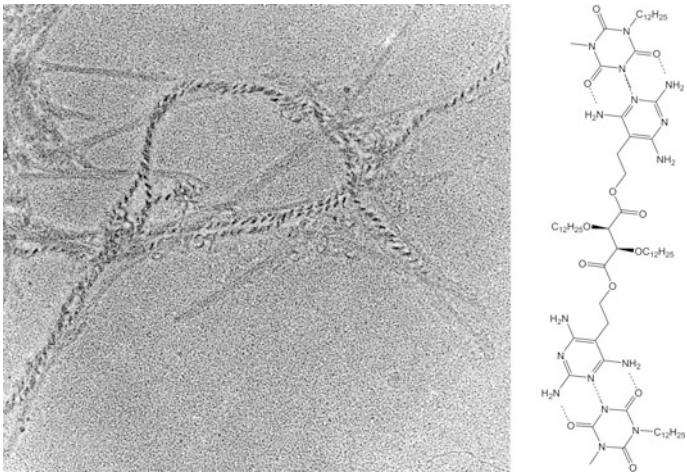

Fig. 4.21 *Left* TEM micrographs of JANUS-II/toluene systems obtained by deposition of a drop of a dilute solution onto a grid, and Pt/W shadowing at a 15° angle. *Right* the molecules and the way they interact trough hydrogen bonds. From Sarazin et al. [33]

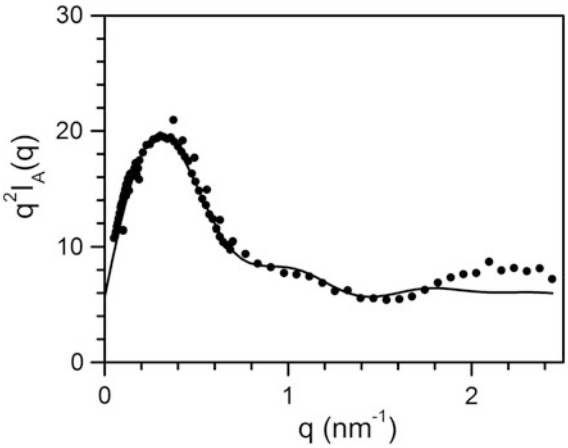

Fig. 4.22 Neutron scattering data obtained on JANUS-II/toluene systems at $C_{\text{JANUS-II}} = 0.55 \times 10^{-3}$ g/cm^3. The *solid* stands for the best fit with Eq. (4.24). From Sarazin et al. [33]

assembled elements, which means a large amount of the fibrils are in fact the supramolecular polymers described above. The value or r_1 may correspond to fibrils made up by bunching these supramolecular polymers over long distances but can equally be related to the gel junctions. This would therefore suggest that junctions are essentially made up with about seven filaments, something which was not necessarily clear from the TEM pictures.

Here, one faces the case where the supramolecular polymer may form first, and then later aggregate to produce fibrils and eventually the network.

While in many cases small-angle X-ray or neutron are only sensitive to the structure of the fibrils composing the network, in other cases these techniques also reveal intermolecular terms that are related to the mesh size of the gel. In this respect, studies by Saiani et al. on oligopeptides deserve certainly to be presented and discussed [34]. These oligopepetides are based on the alternation of a charged and noncharged peptide in order to keep the overall charge neutral (Fig. 4.23). They form hydrogels in water for pH between 6 and 7 at relatively low concentrations ($C_{\text{gel}} \approx 0.8 \times 10^{-2}$ g/cm^3).

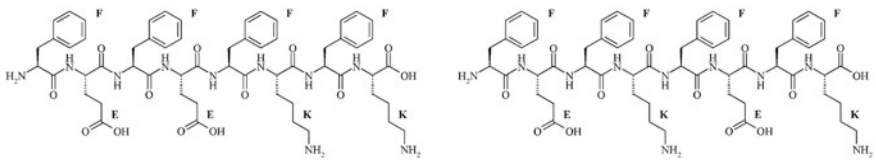

Fig. 4.23 Oligopeptides that organize in β-sheets. These are designated as FEFEFKFK (*left*) and FEFKFEFK (*right*). From Saiani et al. [34]

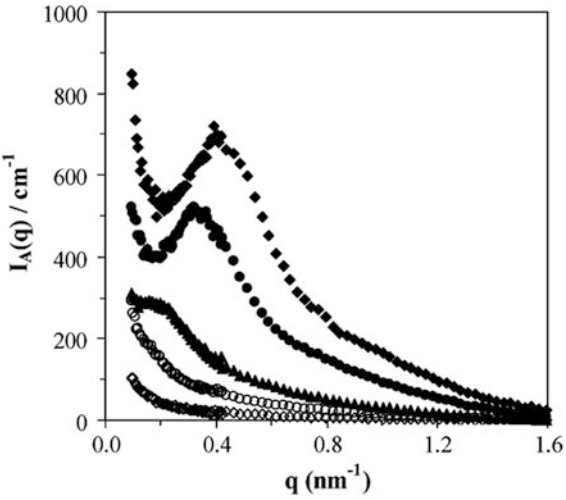

Fig. 4.24 Neutron scattering data for FEFEFKFK (see Fig. 4.23) for different concentrations. From *bottom* to *top* 0.2×10^{-2} g/cm^3, 0.5×10^{-2} g/cm^3, 1.0×10^{-2} g/cm^3, 3.0×10^{-2} g/cm^3, 4.0×10^{-2} g/cm^3. From Saiani et al. [34]

Neutron scattering curves obtained from these hydrogels exhibit peaks that appear just above the onset gelation concentration (Fig. 4.24). For rather random structure, as are organogel networks, it is always difficult to assign a distance related to such a peak. One can simply use the Bragg relation, namely $d_{net} = 2\pi/q^*$, although the relation used for liquids would probably do better, i.e. $d_{net} = 2 \times 1.23\pi/q^*$. Typical distances between 37 and 45 nm for $C \approx 1.0 \times 10^{-2}$ g/cm^3 down to 15–19 nm for $C \approx 4.0 \times 10^{-2}$ g/cm^3 are found depending on the relation used. What is worth evaluating is the variation of the distance as a function of concentration, which should be of the power law type, and so derive an exponent. In the case of a network, for which only the mesh size changes when the concentration is varied, this distance should vary as $d_{net} \sim C^{-1/3}$. Here, although only three points are available, the variation is rather of the type $d_{net} \sim C^{-0.62}$. This means that the mesh size decreases more rapidly with concentration than it should. A possible explanation for this discrepancy consists in considering that the average fibrils cross-sectional radius is not constant while increasing concentration but decreases instead. As a result, the number of fibrils per unit volume increases more rapidly, and their average spacing decreases accordingly.

4.3 The Macroscopic Structure(s). Gel Morphology

As already emphasized, the macroscopic structure, namely the organogel morphology, depends largely upon the microscopic and mesoscopic structures. The crystallization habit of the organogelator in solutions has an impact on the "objects" that compose the gel, and eventually on the macroscopic structure.

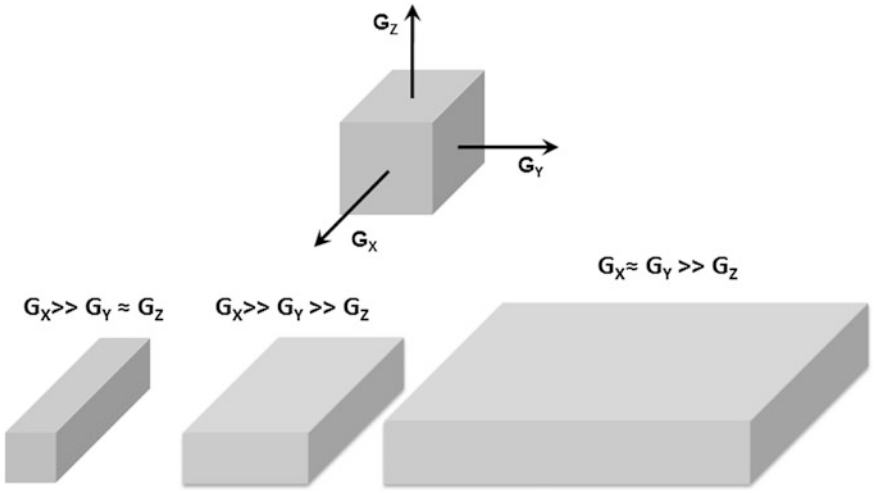

Fig. 4.25 Sketch of a crystal with growth faces characterized by differing growth rates. The three cases discussed in the text are shown [6]

Dasgupta et al. have discussed this aspect by means of simple considerations on the crystal growth in the aim of accounting for observations on OPV organogelators [6]. These considerations can be extended to other systems displaying similarities with OPV molecules.

The sketch drawn in Fig. 4.25 displays the three different growth faces in the three directions of space, namely G_X, G_Y, and G_Z. Depending on the relative ratio between these growth rates,the shape of the "objects" will markedly differ. Three cases are worth mentioning as they describe many systems studied so far.

Case 1: $G_X \gg G_Y$ and $G_X \gg G_Z$ with $G_Y \approx G_Z$ then very long fibrils will be produced either with a square or circular cross-section. This is what is seen in OPVOH/*cis*-decahydronaphthalene; for example, [8] and in many other cases reported in the literature [32, 34–38].

Case 2: $G_X \gg G_Y$ and $G_X \gg G_Z$ while $G_Y \gg G_Z$. Under these conditions, ribbons are to be produced. Again this type of fibrils is often observed [8]. Note that twisted ribbons may form, an effect usually due to the unbalanced surface stresses as was shown for polymer lamellae [39].

Case 3: $G_X \approx G_Y$ and $G_X \gg G_Z$ and $G_Y \gg G_Z$. Here platelets will be formed. This type of structure is likely to produce a spherulitic morphology. Referring back to the definition discussed in Chap. 2, no gel is therefore produced under these growth rates conditions.

A striking example of a slight chemical modification has been reported by Dasgupta et al. on OPV derivatives. A shown in Fig. 4.26 the morphology differs drastically whether the terminal group is OH or OCH_3. For OPVOH/benzyl alcohol gels, fibrillary ribbons radiate from one center and connect to other centers. As was

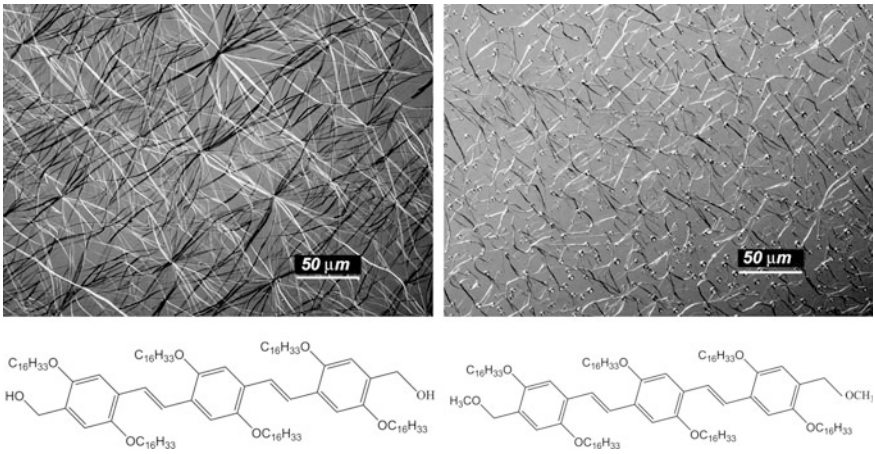

Fig. 4.26 *Top* optical micrographs of organogels prepared with OPVOH (*left*) and OPVMe (*right*) in benzyl alcohol. The OPVs corresponding chemical structures are given below. From Dasgupta et al. [8]

suggested by Dasgupta et al. [8], the network is of the *hub-type* as opposed to the usual *randomly-dispersed* type. Note that a similar type of morphology was also reported for a surfactant (sodium laurate) in various alcohols [40].

As was mentioned in Chap. 3, Dasgupta et al. have suspected the formation of a molecular compound of OPVOH with benzyl alcohol due to the similarity of the solvent and the end-group, and the occurrence of hydrogen bonds, a situation which is likely to be excluded with OPVMe. As a result, the growth faces containing the terminal groups may display different growth rates. The network morphology is rather reminiscent of the *randomly-dispersed* type.

Another gel system worth quoting consists in N-lauroyl-L-glutamic acid di-n-butylamide in propylene glycol [41]. Depending on the formation temperature and concentration, a drastic change of morphology is observed (Fig. 4.27). Quenching at a temperature above 55 °C gives a fibrillary network, while quenching below 55 °C produces a spherulitic morphology.

According to Wang et al. [41], the change of morphology arises from a gradual branching at lower temperature of the fibrils that form at high temperature. That branching occurs is not questionable, but the morphology below 55 °C is most probably not due to this process but rather to the formation of large lamellae instead as is usually the case for spherulitic objects. Indeed, the network above $T = 55$ °C is of the *randomly-dispersed type* without any nucleation center. This is totally at variance with the case of OPVOH/benzyl alcohol for which a *hub-like* architecture is seen (Fig. 4.26). Below $T = 55$ °C, a drastic change occurs with well-defined nucleation centers. This is more reminiscent of a phase transition of the solid-solid type rather than gradual branching. Unfortunately, no investigations on the molecular structure are available in order to find out whether the system may take on two different crystalline structures.

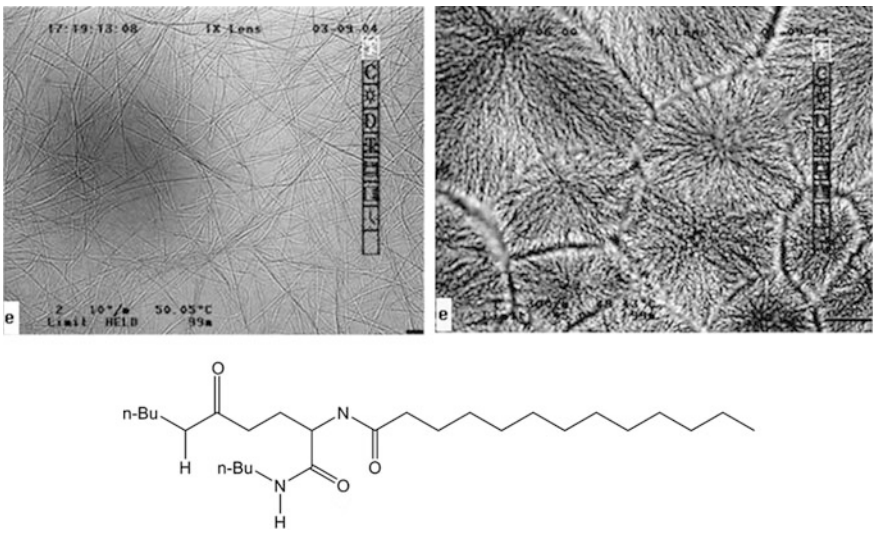

Fig. 4.27 Optical micrographs of N-lauroyl-L-glutamic acid di-*n*-butylamide in propylene glycol. *Left* morphology observed when cooling above 55 °C; *right* for the same system cooled at 50 °C. *Below* the organogelator chemical structure. From Wang et al. [41]

As discussed above (Fig. 4.25) a change in the growth rates of the different crystal faces may be at play. While at high temperature one face grows much faster than the other two, at low temperature two faces may grow at the same or nearly the same pace. If this interpretation makes sense, the origin of the effect remains unknown. Possibly, the occurrence of a molecular compound should be contemplated as propylene glycol (propane-1,2-diol) is liable to establish hydrogen bonds, and so form a complex with the organogelator. In any case, it is clear that below 55 °C, the system cannot be considered a gel if one refers to the discussion in Chap. 2 devoted to the gel definition.

An unusual morphology has been observed by Morin et al. [18] with the hydrogel prepared from N-Methyl-N-(pentacosa-10,12-diyn)-propargylamine. Figure 4.28 shows an array of laths assembled in such a way as to produce a morphology reminiscent of a drapery of nonwoven fibers [18]. Similar morphologies were reported by Fang and coworkers for a glucose-based gelator [42]. Whether there are strong interactions between these laths or not is difficult to conclude. Unfortunately, no studies on the mechanical properties of these systems are available. According to Morin et al. these systems are self-supporting [18]. It is, however, likely that they will display high relaxation rates similar to that reported by Collin et al. [43].

Another interesting effect on the gel morphology has been reported by Wan and coworkers while studying the effect of the length of the aliphatic moiety for sugar-appended organogelators (see Fig. 4.29), namely 4-(40-alkoxyphenyl) phenyl-β-O-D-glucoside [44]. Using water/dioxane mixtures (60/40) as a gelling medium, they have recorded SEM pictures displayed in Fig. 4.29.

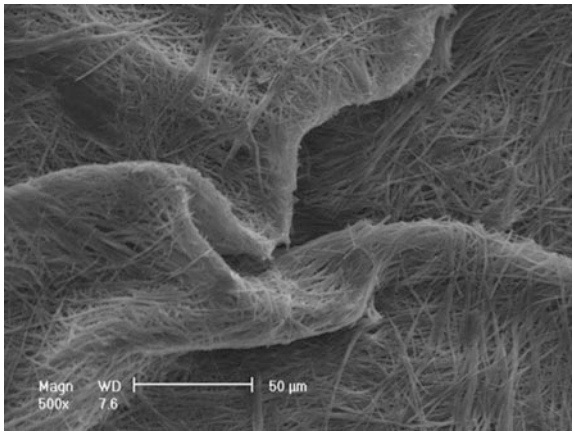

Fig. 4.28 SEM picture of N-Methyl-N-(pentacosa-10,12-diyn)-propargylamine hydrogel [17]. A. Wagner unpublished results

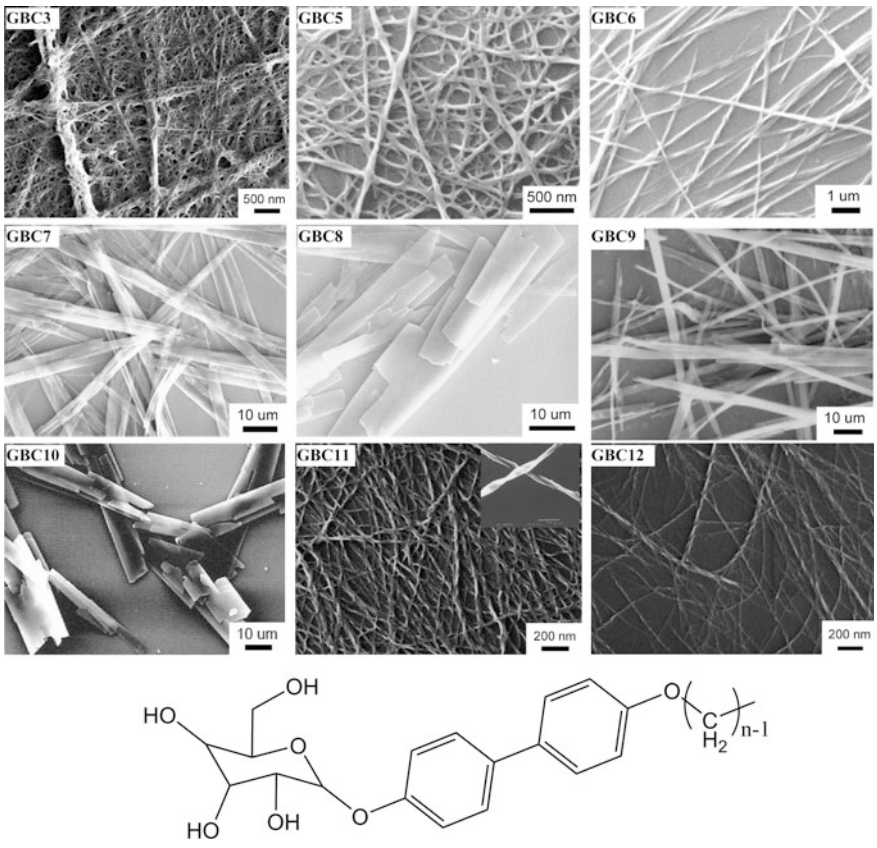

Fig. 4.29 SEM micrographs of sugar-appended organogelators (GBC) with n = 3, 5 to 12 in H2O/1,4-dioxane (60/40 v/v) at 0.005 g/cm^3. From Wan et al. [44]

For a short aliphatic moiety ($n < 6$) the gel is fibrillary and of the randomly dispersed type. Increasing the length of the aliphatic moiety ($n = 7$ to 9) entails a drastic change of morphology. Assemblies of laths as those observed by Morin et al. [18] are seen whose assembly is reminiscent of a Mikado game (Fig. 4.13). For $n = 10$, only platelets are formed similar to single crystals. Increasing further the length of the aliphatic moiety gives the fibrillary morphology back, yet with highly twisted fibrils ($n = 11$ and 12).

The cases for $n = 7, 8, 9$ are systems with seemingly little physical cross-linking between the laths so that the mechanical behavior is probably characterized by a strong relaxation under compressive stress.

4.4 Summary

The succinct survey in this chapter focused on the structures occurring in organogels highlights the high crystallinity of the fibrils constituting the gel scaffold. As a general rule, fibrils are produced through a *near 1-D crystallization* as opposed to a *two-step mechanism*, where the building of long supramolecular polymers would be first formed through a self-assembling process, and then followed by the formation of fibrils through parallel bunching. This two-step mechanism cannot be, however, totally discarded. A few systems, such as the Janus supramolecular polymers shown in Fig. 4.21, rather obey this mechanism as ascertained by SANS experiments that reveal the presence of long supramolecular polymers along with fibrils [Fig. 4.22]. The possible origin may stem from the need of the complementary molecules to interact first before any further fibrillar growth can take place. This also suggests that their co-crystallization is not the driving process.

At the mesoscopic level, fibrils may be more or less connected in basically two different ways forming either *a randomly-dispersed network* or a *hub-like network*. In the former, fibrils grow more or less independently and connect at random either through branching created by crystallization defects or through side-wise alignment. In the latter, fibrils radiate from nucleation centers. Fibrils cross-sections can be rounded, square-shaped, or ribbons. In any case, the cross-sectional dimensions are usually larger than those observed in polymer thermoreversible gels by a minimum of one order of magnitude.

As was mentioned in the introduction section, the "*chimera*" aspect of the molecules, namely the presence of different moieties of unlikely bonding characteristics, appears most certainly responsible for the different growth rates of the crystal faces. Therefore, one should be capable of predicting the formation of fibrils from a given molecule, and correspondingly of an organogel, provided that the crystal structure and the growth face kinetics are known. Unfortunately, this seems to be out of reach presently, although one may anticipate that simulation calculations may in future give access to these pieces of information.

References

1. Rouquerol, J., Avnir, D., Fairbridge, C.W., Everett, D.H., Haynes, J.M., Pernicone, N., Ramsay, J.D.F., Sing, K.S.W., Unger, K.K.: Recommendations for the characterization of porous solids. Pure Appl. Chem. **66**, 1739 (1994)
2. Placin, F., Desvergne, J.P., Belin, C., Buffeteau, T., Desbat, B., Ducasse, L., Lassègues, J.C.: molecular arrangement in the gel fibers of 2,3-didecyloxyanthracene (ddoa): a spectroscopic and theoretical approach. Langmuir **19**, 4563 (2003)
3. Nonappa, Lahtinen, M., Behera, B., Kolehmainen, E., Maitra, U.: Unraveling the packing pattern to gelation using SS NMR and X-ray diffration : direct observation of the evolution of self-assemble fibres. Soft Matter **6**, 1748 (2010)
4. Ostuni, E., Kamaras, P., Weiss, R.G.: Novel X-ray method for in situ determination of gelator strand structure: polymorphism of cholesryl anthraquinone-2-carboxylate. Angew. Chem. Int. Ed. **35**, 1324 (1996)
5. Terech, P., Aymonier, C., Loppinet-Serani, A., Bhat, S., Banerjee, S., Das, R., Maitra, U., Del Guerzo, A., Desvergne, J.P.: Structural relationships in 2,3-bis-n-decyloxyanthracene and 12-hydrostearic acid molecular gels and aerogels processed in supercritical CO_2. J. Phys. Chem. B **114**, 11409 (2010)
6. Dasgupta, D., Thierry, A., Rochas, C., Ajayaghosh, A., Guenet, J.M.: Key role of solvent type in organogelation. Soft Matter **8**, 8714 (2012)
7. Ajayaghosh, A., George, S.S.: First phenylenevinylene based organogels: self-assembled nanostructures via cooperative hydrogen bonding and ð-stacking J. Am. Chem. Soc. **123**, 5148 (2001); George, S.J., Ajayaghosh, A.: Self-Assembled nanotapes of oligo(p-phenylene vinylene)s: sol-gel-controlled optical properties in fluorescent π-electronic gels. Chem.—Eur. J. **11**, 3217 (2005); Ajayaghosh, A., Praveen, V.K.: π-organogels of self-assembled p-phenylenevinylenes: soft materials with distinct size, shape, and functions. Acc. Chem. Res. **40**, 644 (2007)
8. Dasgupta, D., Srinivasan, S.A., Rochas, C., Ajayaghosh, A., Guenet, J.M.: Solvent-mediated fiber growth in organogels. Soft Matter **7**, 9311 (2011)
9. Cui, J., Shen, Z., Wan, X.: Study on the gel to crystal transition of a novel sugar-appended gelator. Langmuir **26**, 97 (2010)
10. Wang, R., Geiger, C., Chen, L., Swanson, B., Whitten, D.G.: Direct observation of sol-gel conversion: the role of the solvent in organogel formation. J. Am. Chem. Soc. **122**, 2399 (2000)
11. Fournet, G.: Fonctions de diffusion pour des formes géométriques Bull. Soc. Franç. Minéral. Crist. **74**, 39 (1951)
12. Schmidt, P.W.: Small angle X-ray scattering from helical filaments. J. Appl. Cryst. **3**, 257 (1970); Pringle, O.A., Schmidt, P.W.: Small-angle X-ray scattering from helical macromolecules. J. Appl. Cryst. **4**, 290 (1971)
13. Mittelbach, P.: Zur Röntgenkleinwinkelstreuung Verdunnter Kolloider Systeme. Acta Phys. Austr. **19**, 53 (1964); Mittelbach, P., Porod, G.: Zur Röntgenkleinwinkelstreuung verdünnter kolloiden Systeme. Acta Phys. Austr. **14**, 185 (1961)
14. Guenet, J.M., Fazel, N., Rochas, C.: Similarities between thermoreversible gels of synthetic polymers and biopolymers: case of poly methyl methacrylate and κ-carrageenan. Trends Macromol. Res. **1**, 345 (1994)
15. Oster, G., Riley, D.P.: Scattering from cylindrically symmetric systems. Acta Cryst. **5**, 272 (1952)
16. Guenet, J.M.: Scattering by prolate, cross-section polydispersed cylinders applicable to fibrillar thermoreversible gels. J. Phys. II **1994**, 4 (1077)
17. Barabási, A.L., Albert, R.: Emergence of scaling in random networks. Science **286**, 509 (1999)
18. Morin, E., Guenet, J.M., Dıaz, D.D., Remy, J.S., Wagner, A.: Fine-tuning the morphology of self-assembled nanostructures of propargyl ammonium-based amphiphiles. J. Phys. Chem. B **114**, 12495 (2010)

19. Terech, P., Pasquier, D., Bordas, V., Rossat, C.: Rheological properties and structural correlations in molecular organogels. Langmuir **16**, 4485 (2000)
20. Saiani, A., Guenet, J.M.: Nanostructure and helicity in syndiotactic poly(methyl methacrylate) thermoreversible gels. Macromolecules **32**, 657 (1999)
21. Saiani, A., Guenet, J.M.: On the helical form in syndiotactic poly(methyl methacrylate) thermoreversible gels as revealed by small-angle neutron scattering. Macromolecules **30**, 966 (1997)
22. Diaz, N., Simon, F.-X., Schmutz, M., Rawiso, M., Decher, G., Jestin, J., Mesini, P.J.: Self-assembled diamide nanotubes in organic solvents. Angew. Chem. Int. Ed. **44**, 3260 (2005)
23. Simon, F.X., Nguyen, T.T.T., Diaz, N., Schmutz, M., Deme, B., Jestin, J., Combet, J., Mesini, P.J.: Self-assembling properties of a series of homologous ester-diamides - from ribbons to nanotubes. Soft Matter **9**, 8483 (2013)
24. Dasgupta, D., Kamar, Z.A., Rochas, C., Dahamani, M., Mésini, P.J., Guenet, J.M.: Design of hybrid networks by sheathing polymer fibrils with self-assembled nanotubules. Soft Matter **6**, 3573 (2010)
25. Nguyen, T.T.T., Simon, F.X., Khan, N.A., Schmutz, M., Mesini, P.J.: Formation of reactive aerogels and their reactivity in aqueous media. Wettability induces hydrophobic vs. hydrophilic selectivity. J. Mat. Chem. **22**, 7712 (2012)
26. Khan, A.N., Nguyen, T.T.T., Dobircau, L., Schmutz, M., Mesini, P.J., Guenet, J.M.: Investigation of the interactions involved in the formation of nanotubes from organogelators. Langmuir **29**, 16127 (2013)
27. Zhang, S.G., Holmes, T., Lockshin, C., Rich, A.: Spontaneous assembly of a self-complementary oligopeptide to form a stable macroscopic membrane. Proc. Natl. Acad. Sci. USA **90**, 3334 (1993)
28. Smith, A.M., Williams, R.J., Tang, C., Coppo, P., Collins, R.F., Turner, M.L., Saiani, A., Ulijn, R.V.: Fmoc-diphenylalanine self assembles to a hydrogel via a novel architecture based on p–p interlocked b-sheets. Adv. Mater. **20**, 37 (2008)
29. Dasgupta, D., Srinivasan, S., Rochas, C., Ajayaghosh, A., Guenet, J.M.: Hybrid thermoreversible gels from covalent polymers and organogels. Langmuir **25**, 8593 (2009)
30. Guenet, J.M.: Polymer-Solvent Molecular Compounds. Elsevier, London (2008)
31. Baral, A., Basak, S., Basu, K., Dehsorkhi, A., Hamley, I.W., Banerjee, A.: Time-dependent gel to gel transformation of a peptide based supramolecular gelator. Soft Matter **11**, 4944 (2015)
32. Dasgupta, D., Srinivasan, S., Rochas, C., Thierry, A., Schröder, A., Ajayaghosh, A., Guenet, J. M.: Insight into the gelation habit of oligo(para-phenylene vinylene) derivatives: effect of end-groups. Soft Matter **7**, 2797 (2011)
33. Sarazin, D., Schmutz, M., Petitjean, A., Lehn, J.M., Guenet, J.M.: Structure of supramolecular polymers generated via self-assembly through hydrogen bonds. Mol. Cryst. Liq. Cryst. **468**, 539 (2007)
34. Saiani, A., Mohammed, A., Frielinghaus, H., Collins, R., Hodson, N., Kielty, C.M., Sherratt, J., Miller, A.F.: Self-assembly and gelation properties of a-helix versus b-sheet forming peptides. Soft Matter **5**, 193 (2009)
35. Babu, S.S., Praveen, V.K., Ajayaghosh, A.: Functional π-gelators and their applications. Chem. Rev. **114**, 1973–2129 (2014)
36. Weiss, R.G.: The past, present and future of molecular gels. What is the status of the field, and where is it going? J. Am. Chem. Soc. **136**, 7519–7530 (2014)
37. Terech, P., Weiss, R.G. (eds.): Molecular Gels: Materials with Self-Assembled Fibrillar Networks, Springer, Berlin (2006)
38. Liu, X.L., Li, J.L. (eds.): Soft Fibrillar Materials: Fabrication and Applications. Wiley-VCH, New York (2013)
39. Keith, D., Padden, F.: Twisting orientation and the role of transient states in polymer crystallization. Polymer **25**, 28 (1984); Lotz, B.A., Cheng, S.Z.D.: A critical assessment of surface stresses as the mechanical origin of lameller twist and scroll. Polymer **46**, 577 (2005);

Ye, H.M., Xu, J., Guo, B.H., Iwata, T.: Left- or right-handed lamellar twists in poly[(r)-3-hydroxyvalerate] banded spherulite: dependence on growth axis. Macromolecules, **42**, 694 (2009)
40. Wang, D., Hao, J.: Self-assembly fibrillar network gels of simple surfactants in organic solvents. Langmuir **27**, 1713 (2011)
41. Wang, R., Liu, X.Y., Xiong, J., Li, J.: Real-time observation of fiber network formation in molecular organogel:supersaturation-dependent microstructure and its related rheological property. J. Phys. Chem. B **110**, 7275 (2006)
42. He, N.Y.G., Zhang, H., Ding, L., Fang, Y.: Glucose-based fluorescent low-molecular mass compounds: creation of simple and versatile supramolecular gelators. Langmuir **26**, 5909 (2010)
43. Collin, D., Covis, R., Allix, F., Jamart-Grégoire, B., Martinoty, P.: Jamming transition in solutions containing organogelator molecules of amino-acid type: rheological and calorimetry experiments. Soft Matter **9**, 2947 (2013)
44. Cui, J., Zheng, Z., Shen, Z., Wan, X.: Alkoxy tail length dependence of gelation ability and supramolecular chirality of sugar-appended organogelators. Langmuir **26**, 15508 (2010)

Chapter 5
Solvent Role, Current Approaches

The major concern of scientists for preparing organogels lies in the choice of the solvent. Predictions about the solubility of a given molecule together with its propensity of producing the desired organogel are expected and much welcomed. Attempts to predict gel formation are well described in a recent review by Rogers et al.[1].

It should be, however, emphasized that ***predicting the solubility and the temperature at which the system crystallizes does not allow one to conclude that a gel will be formed***. One should be also able to predict the formation of fibrils if one sticks to the definition discussed in Chap. 2 and in the summary of Chap. 4.

There is an important point which must be always fulfilled when studying crystalline systems: ***the mixture must be heated to a temperature where the history of the sample is totally erased, so as to obtain a true solution***. A sample may not dissolve at room temperature but will do after increasing the temperature. This is something common with semicrystalline polymers and routinely performed prior to anything. Curiously enough, it seems that such a protocol is not always applied in the case of organogels which may result in nonreproducible data. Note that sonication, a method often used, may not destroy totally the organogel structure and so may still leave "remnants" that may act as self-seeding nuclei.

5.1 Binary Systems

A binary system consists of an organogelator and the solvent. The simplest approach is to suppose that the system is *close to ideality* so that one can express the melting temperature of the system by means of relation 3.8. By knowing the melting temperature and the melting enthalpy of the pure component, one should be able to find out whether the system is a solution or a condensed crystalline phase at a given temperature and concentration, namely above or below the melting

J.-M. Guenet, *Organogels*, SpringerBriefs in Materials,
DOI 10.1007/978-3-319-33178-2_5

temperature $T(X)$ of the system at concentration X, through the equation derived from 3.8:

$$\frac{1}{T_m(X)} = -\frac{RLogX}{\Delta H_m} + \frac{1}{T_m} \tag{5.1}$$

Obviously, this only holds if the crystalline structure grown at a concentration X is the same as that in the pure state.

As was pointed out by Feng and Cavicchi [2] and Guenet and coworkers [3, 4], this approach is irrelevant because ideality generally infers close molar volumes and no specific interactions. In view of the chemical structures and the large molar volumes of the organogelators compared with the solvents used, these assumptions are not fulfilled. In addition, this does not tell anything as to the initial solubility of the organogelator in the solvent. ***In other words this approach, which is all too often used, must be systematically discarded for describing organogels.*** The best example of the irrelevancy of this equation for the organogelators is given by the set of data collected by Shinkai and coworkers [5] where they systematically observe a large discrepancy between the values derived from relation 5.1 and those measured by DSC experiments. It should be made clear again that, only calorimetric experiments are relevant for measuring latent heats.

As was mentioned above, Feng and Cavicchi derived an equation for the liquidus by considering an interaction parameter χ [relation 3.10], which finally yields the melting temperature:

$$\frac{1}{T_m(X)} = \frac{1}{T_m^o} - R\left[\frac{LnX + (1-X)^2\chi}{\Delta H_m}\right] \tag{5.2}$$

For expressing the interaction parameter, Feng and Cavicchi used the following relation which involves the so-called solubility parameters of the solvent and the organogelator:

$$\chi = \frac{V}{RT}\left[\left(\frac{\sum F_i^{\text{org}}}{\sum V_i^{\text{org}}}\right)^{0.5} - \left(\frac{\sum F_i^{\text{solv}}}{\sum V_i^{\text{solv}}}\right)^{0.5}\right]^2 \tag{5.3}$$

where F_i^{org} and V_i^{org} are the contribution from each chemical unit of the organogelator to the cohesive energy density and their molar volume, and F_i^{solv} and V_i^{solv} are the equivalent parameters for the solvent. Actually, F_i's are the vaporization energies at a given temperature, something not directly accessible for most organogelator, nor for polymers, and therefore need to be estimated. For calculating these parameters, Feng and Cavicchi rely on a method devised by Fedors 40 years ago [6] that consists in summing the solubility parameters of the different identified groups of the molecule. Incidentally, solubility parameters are not commonly used in polymer solutions. An experimental determination of χ is preferred as it is more reliable.

Another rather popular option for determining the solubility parameter makes use of the so-called Hansen parameter [7–9]. Hansen has suggested to consider three different terms for calculating δ, namely a dispersive term, δ_d, a polar term, δ_p, and a hydrogen bonding term, δ_h, so that:

$$\delta = \sqrt{\delta_d^2 + \delta_p^2 + \delta_h^2} \tag{5.4}$$

The present approach developed by Bouteiller and coworkers [10, 11] rather favors the use of this relation:

$$R = \sqrt{4(\delta_d - \delta_d^s)^2 + (\delta_p - \delta_p^s)^2 + (\delta_h - \delta_h^s)^2} \tag{5.5}$$

where $\delta_i's$ stands for the organogelator and $\delta_i^{s\prime}s$ for the solvent.

R is simply the radius of a sphere centered on the coordinates δ_d, δ_p, δ_h in the Hansen space defined by the three axes $\delta_d^s, \delta_p^s, \delta_h^s$. If R is smaller than an empirical value R_{sol}, then the system is totally soluble. Outside this sphere, the molecule may still be soluble but its propensity to become insoluble increases gradually.

Raynal and Bouteiller have compiled the data for several organogelators and several solvents to find out to which extent there is a correlation between the gelation propensity and the Hansen parameter. An example is given in Fig. 5.1 where the behavior of a sugar-based molecule bearing a para-nitrophenyl chromophore is reported for a series of solvents [12].

Before commenting further Fig. 5.1, it should be clearly stated that the abscissae convey not a special meaning. Raynal and Bouteiller have simply regrouped the solvents as *soluble*, *insoluble*, and *gelating*. Only the position of the solvent with respect to the radius of the solubility sphere or the gelation sphere is meaningful.

These results indicate, as expected, that all the Hansen coordinates of all soluble molecules stand inside the solubility sphere (Fig. 5.1a), while those insoluble molecules or gelating molecules stand above. It is to be noted that there is not much difference between the gelating and the insoluble molecules. Also, many soluble molecules stand just near the outskirt of the solubility sphere.

The radius of the gelation sphere (Fig. 5.1b) is determined by taking the center of gravity of all the data gathered from the gelating solvents. Here, the gelating solvents are therefore within this sphere, which does not come as a surprise. The insoluble molecules are just outside while a majority of the soluble molecules are outside.

The Hansen parameter is an interesting but limited approach for selecting gelation solvents. Indeed, several factors are not taken into account:

(1) Tests are carried out, and therefore restricted to room temperature although solvents may trigger gelation below. Also, the concentration range is limited: gelation may then appear on increasing the gelator concentration.

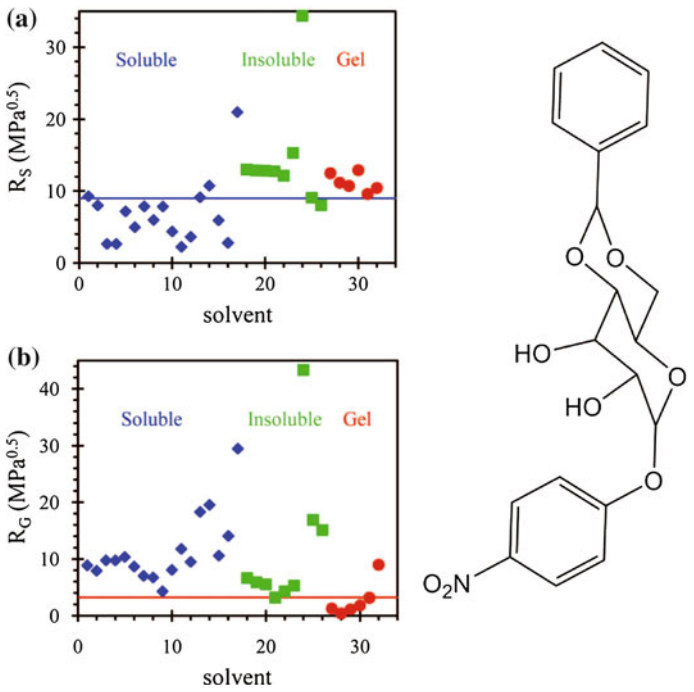

Fig. 5.1 *Left* distances in Hansen space: **a** to the center of the solubility sphere [δ_d = 16.0; δ_p = 9.4; δ_h = 8.7; RSol = 9.0 MPa0.5]; **b** to the center of the gelation sphere [δ_d = 18.0; δ_p = 1.0; δ_h = 2.0; R_{Gel} = 3.2 MPa0.5]. The *line* represents the radius of the solubility sphere (**a**) and the gelation sphere (**b**). The solvents are grouped by type, so that the abscissae do not convey any other information than the solvent numbering. *Right* the molecule studied by Shinkai and coworkers [12]. *Left figures* from Raynal and Bouteiller [10]

(2) The cooling rate is important as reported for BHPB gels. In this case, a slow cooling rate will give a precipitate while a high cooling rate will give a gel. This is not strictly speaking a kinetic effect, but is due to the fact that the system is brought into another domain of the phase diagram. The liquid–liquid phase separation is then bypassed (see Chap. 3).

(3) The morphology is not deduced from the Hansen parameter. A striking example is provided by the work of Bhattacharya and coworkers [13] who have observed two different morphologies for a system made up of a fatty acid amide of amino acid, of which only one morphology can be regarded as a gel, while the other most probably consists of an assembly of spherulites (see Fig. 5.2).

(4) The occurrence of a molecular compound may totally modify the prediction. As was seen in polymer thermoreversible gels , compounds were often formed with good solvents [14]. In this case, the driving parameter was the shape of the helical structure taken on by the polymer chains with respect to the solvent's. As will be seen below, this effect seems to occur in organogels.

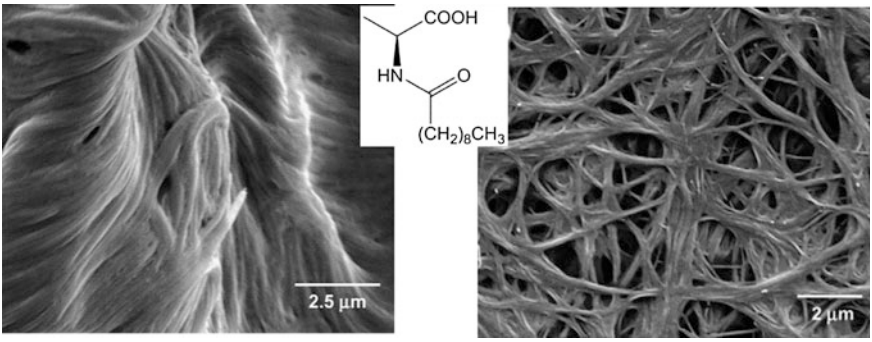

Fig. 5.2 SEM pictures from gels prepared from a fatty acid amide of amino acid (molecule in insert) in toluene (*left*) and in heptane (*right*). From Pal et al. [13]

(5) Some molecules may behave as block copolymers do. A given solvent may interact strongly with one moiety of the molecule but not with the other. For instance the OPV molecules synthesized by Ajayaghosh and coworkers are likely to pertain to this category. Recent results by Dasgupta et al. [4] have shown strikingly different results for OPVR (Figs. 4.2 and 4.3), whether benzyl alcohol or *trans*-decahydronaphthalene is used. The molecular structure differs drastically as shown in Chap. 4 (see Fig. 4.2) but also the morphology (see Fig. 5.3). This arises from the fact that *trans*-decahydronaphthalene is a good solvent to the aliphatic arms unlike benzyl alcohol. As a result a kind of *solid solution*, using the customary nomenclature for phase diagrams, is formed where *trans*-decahydronaphthalene molecules are occluded within the aliphatic moiety of the OPVR crystal. This disrupts the long-range order with obvious consequences on the resulting morphology.

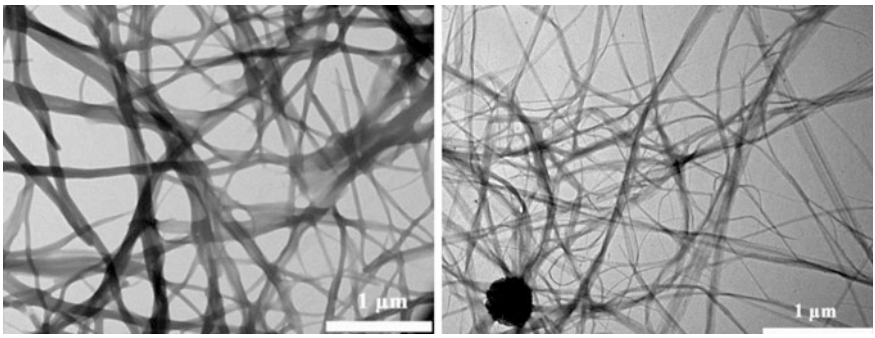

Fig. 5.3 *Left* TEM micrograph of aggregates of OPVR (Fig. 3.2) formed in benzyl alcohol; *right* OPVR aggregates in *trans*-decahydronaphthalene. OPVR/benzyl fibrils are better defined, namely displaying higher long-range molecular order, and essentially thicker than those prepared in *trans*-decahydronaphthalene. Scale is the same in both pictures. From Dasgupta et al. [4]

As emphasized above, the approach developed by Bouteiller and coworkers [10] is of the mean-field type which may not apply in numerous cases.

5.2 Ternary Systems

Organogelation in a mixture of solvent is an interesting and fascinating topic. This has been recently studied by Weiss and coworkers for glucono-appended 1-pyrenesulfonyl derivatives with α, ω diaminoalkane spacers in water/THF systems [15] and Wan et al. [16] for sugar-appended organogelators in water/dioxane mixtures.

The glucono-appended 1-pyrenesulfonyl derivatives studied by Weiss and coworkers are neither soluble in water nor in THF [15]. Yet, in a certain range of composition of the mixture water-THF, typically 10–90 % dissolution can take place while increasing the water content further from 55 to 90 % gives a gel according to Weiss et al. although the fibrillary structure seems to appear only for compositions above 70–30.

Weiss et al. approach the question by considering Hansen solubility factors by means of Eqs. 5.4 and 5.5 and calculating the resulting Hansen factor for the mixture through:

$$\delta_i^{\text{mix}} = \varphi_{\text{THF}}\delta_i^{\text{THF}} + \varphi_{\text{water}}\delta_i^{\text{water}} \tag{5.6}$$

where δ_i s are the Hansen parameters calculated with Eq. 5.4 and φ with the appropriate subscripts the volume fraction of the solvents.

They obtain a series of results which show that the compositions where gelation occurs are well located within the gelation sphere (Fig. 5.4).

To infer that the behavior of the solvent mixture is a simple linear combination of the solution properties of either solvent is clearly an approximation that may not hold at all compositions. It is known that similar type of aqueous mixtures, such as water/DMSO, water/DMF, produces molecular compounds with water in the solid state that persist in the liquid state [17–19]. The interaction between water and its cosolvent is established through hydrogen bonds [17]. As a result, the mixture behaves as a new solvent with unusual properties.

Similar studies for water/THF are available. For instance, the temperature–concentration phase diagram (Fig. 5.5) reveals the occurrence of an incongruently melting compound whose stoichiometry is 1/17 [20, 21]. To be sure, the molecular structure in the solid state consists of a cage of water molecules surrounding a THF molecule [22]. Yet, Myerson and coworkers have found a maximum in the viscosity of various mixtures (Fig. 5.5) although this maximum would rather give a ratio 1/5. That the ratio changes from the solid state to the liquid state is not surprising. In the solid state, geometrical constraints predominate over only hydrogen bonds interactions.

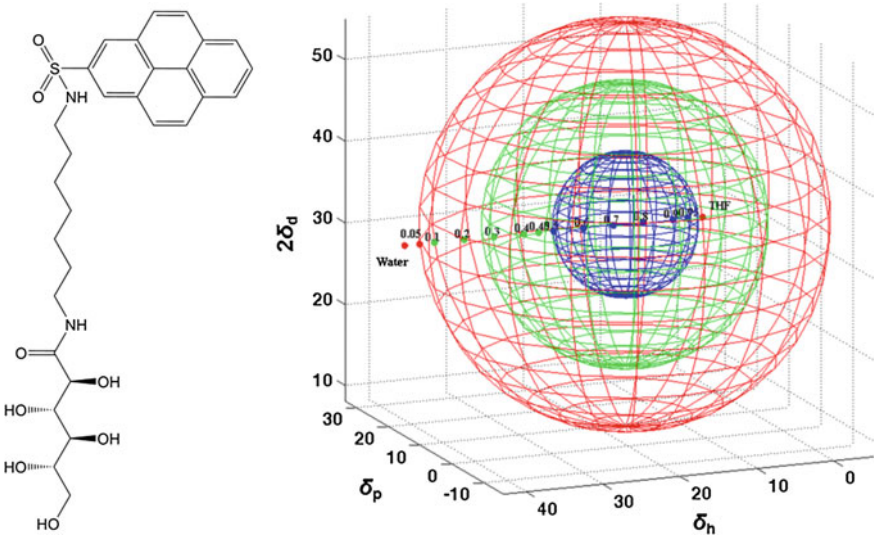

Fig. 5.4 Solubility data for 2 % concentration of the molecule on the left (P7 in Weiss'paper) in liquid mixtures represented in Hansen space with sphere/shells: *blue* = soluble; *green* = gel; *red* = insoluble. From Weiss et al. [15]

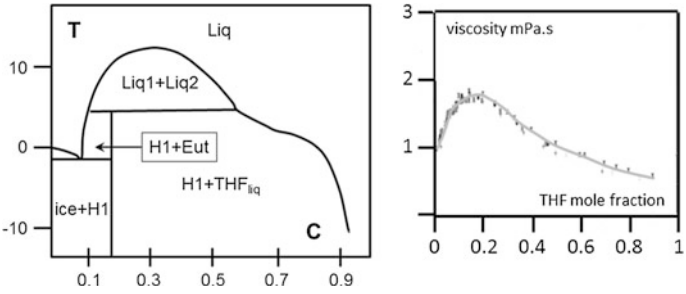

Fig. 5.5 *Left* temperature–concentration phase diagram water/THF (THF concentration in w/w). H1 is a compound of stoichiometry 1/17. From Carbonnel and Rosso [20]. *Right* viscosity of water/THF mixtures at 25 °C. From Devarakonda et al. [21]

At the stoichiometric composition, the solvent properties are therefore not a linear association of the properties of each solvent as the complex behaves as a new solvent. Conversely on either side of the stoichiometric composition, the properties might be a linear combination of the properties of the "liquid complex" and the properties of water (excess of water) or of THF (excess of THF).

It is interesting to mention that a small miscibility gap is observed just after the incongruent melting of the compound, a very rare situation which highlights the peculiarity of this aqueous mixture.

5.3 Molecular Compound

Molecular compounds are known to play an important role in the thermoreversible gelation of stereoregular polymers [23]. So far, only a few reports mention the occurrence of organogelator/solvent compounds [24–26].

As was discussed in Chap. 3, the molecular structure of OPVOH/benzyl alcohol organogels is thought to be made up with a molecular compound. This assumption relies heavily on circumstantial evidence, particularly on the variation of the melting enthalpy with concentration [24]. Extrapolation of this parameter to 100 % OPVOH gives a value significantly higher than that of the pure OPVOH. Another set of evidence deals with SEM pictures taken on vacuum-dried sample. As can be seen in Fig. 5.6, the morphology of OPVOH/benzyl alcohol xerogels is hardly distinguishable unlike that of OPVR/benzyl alcohol xerogels. This effect is known to take place when desolvation of the compound occurs, which entails a collapse of the structure and the loss of the original morphology. Conversely, as no compound is said to be formed with OPVR organogelators (see Chap. 3 and Fig. 4.2), the structure remains unaltered after drying.

Recently Meier and coworkers have reported the effect of chiral tartaric acid molecules on the piling of non-chiral OPV molecules [25, 26]. In methylcyclohexane, these OPV molecules form a racemic mixture of M and P helices (Fig. 5.7). Introducing a chiral tartaric acid molecule in the solution prior to cooling to room temperature, favors the formation of either P or M helices depending upon the chirality of the tartaric acid. Clearly, formation of a molecular compound occurs between OPV molecules and tartaric acid in the way shown in Fig. 5.8.

Another set of experiments that indicate the possible occurrence of molecular compound involve di-o-benzylidene-D-sorbitol (DBS) in a series of alcohol [26]. Itagaki et al. studied DBS in ethylene glycol, diethylene glycol, triethylene glycol,

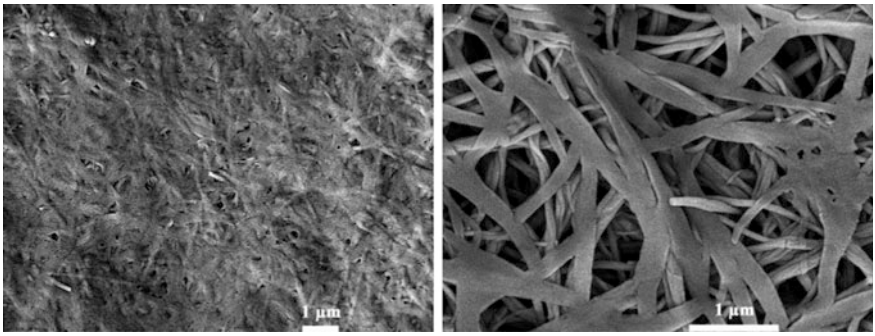

Fig. 5.6 SEM pictures: *left* OPVOH/benzyl alcohol organogel (C_{OPVOH} = 0.004 g/cm^3) after vacuum drying. *Right* OPVR/benzyl alcohol organogel (C_{OPVR} = 0.004 g/cm^3) after vacuum drying. It can be seen in the picture on the *left* that the fibrillary morphology is hardly distinguishable as opposed to the picture on the *right*. Desolvation of the molecular compound can produce such a morphology collapse. From Dasgupta et al. [24]

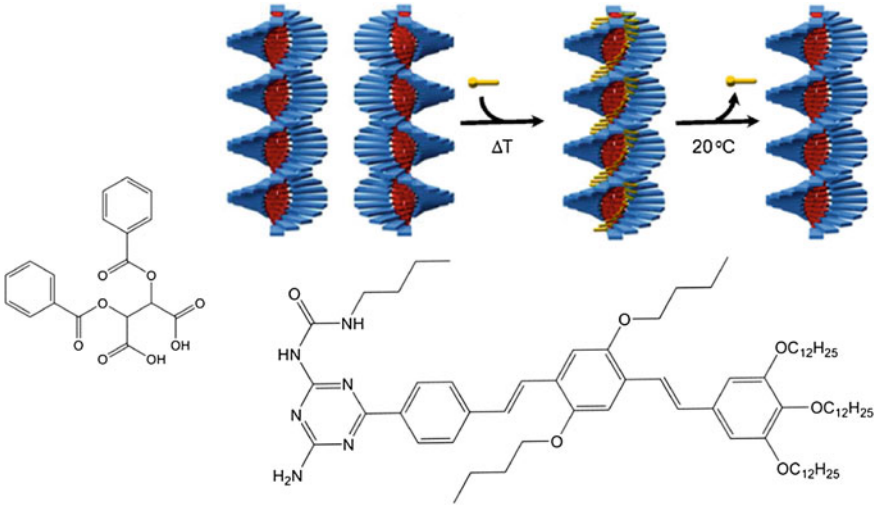

Fig. 5.7 *Top* non-chiral OPV molecules form M and P helical structure in MCH. *Red* stands for the N-rich part of the molecule. Preparing a solution OPV/methylcyclohexane in the presence of D-tartaric acid or L-tartaric acid (*yellow*) yields either M or P helices. *Left* D-tartaric acid, *bottom right* the OPV molecule under study. From George et al. [26]

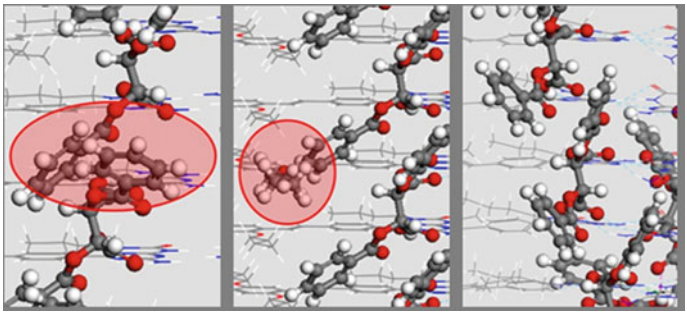

Fig. 5.8 Geometries of right-handed (*left*) cofacial (*middle*) and left-handed (*right*) AOPV3 assemblies in the presence of the L-TA molecules. The AOPV3 stack is shown with thin lines while the L-TA molecules are in a "ball-and-stick" representation. Note that in the central structure one side group of one AOPV3 molecule is also represented in "ball-and-stick" to visualize better its interaction with the L-TA molecule. From George et al. [25]

tetraethylene glycol, and glycerol. They found that the melting enthalpy of the organogels depended upon the solvent, and particularly on the "density" of hydroxyl group of the alcohol (Fig. 5.9). If one were dealing with non-solvated crystals, ***the melting enthalpy would be independent of the solvent*** as this is an intrinsic property of the crystal. In this case, the existence of a compound is clearly pointed out, although the authors suggested only interactions at the "crystal"

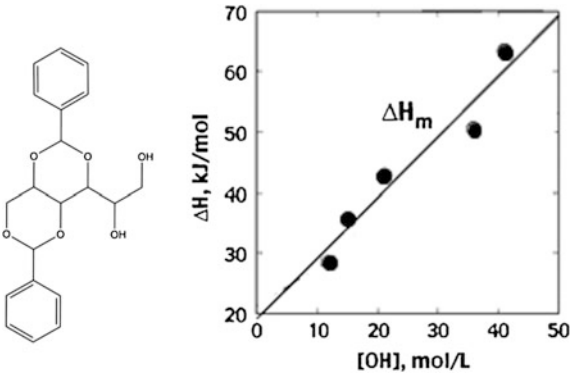

Fig. 5.9 *Left* di-o-benzylidene-D-sorbitol molecule; *right* variation of the gel melting enthalpy as a function of the hydroxyl content of the solvent [OH]. Only the melting enthalpies have been shown here unlike the original figure where formation enthalpies were also given. From Watase et al. [27]

surface. If this were the case, only the melting temperature would be affected. Further, the enthalpy increases with increasing the hydroxyl content therefore suggests a strong hydrogen bonding between DBS and the solvent molecules.

Another interesting system prone to produce compound of the clathrate type has been reported by Ajayaghosh and coworkers [28, 29]. The OPV molecules they studied possess terminal fluorine groups (Fig. 5.10 top). This confers to the molecule an unusual way of packing compared to "classical" OPVs in the sense that a brick-wall-type arrangement is obtained (Fig. 5.10 bottom). OPV molecules are thus shifted with respect to its neighbors and this creates a rather large nanocavity.

Owing to this cavity, clathrates can be formed. Kartha et al. do report that this structure is capable of encapsulating guests such as N, N-dimethylaniline. As will be commented in Chap. 8, advantage is taken from this peculiar property for devising materials possessing the capability of detecting nitroaromatic explosives.

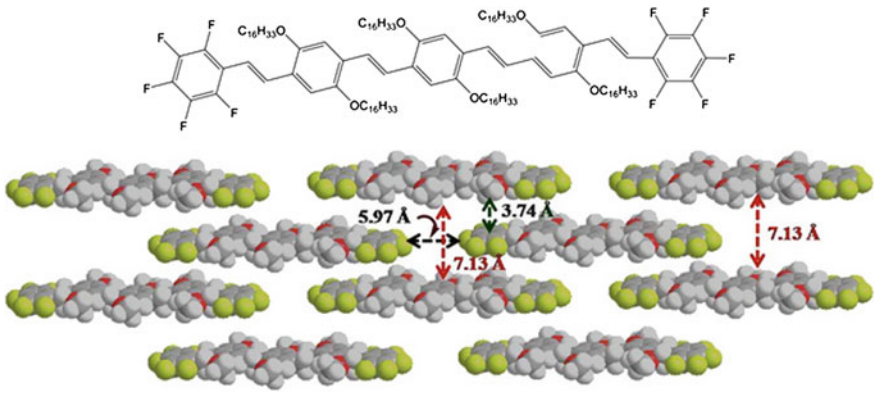

Fig. 5.10 *Top* chemical structure of a fluorinated OPV (nomenclature OPV 20); *bottom* the molecular arrangement of the molecules leaving a nanocavity capable of housing large molecules such as aromatic derivatives. From Kartha et al. [28, 29]

It must be emphasized that the formation of a compound does not necessarily occur in the gel formation process. The cavity is only resulting from the properties of this fluorinated OPV. That it may house or not a solvent molecule depends upon the size of the latter: too large a size it will not be occluded and too small a size possibly not retained.

5.4 Liquid Crystalline Solvents

Some examples of organogels prepared in solvents possessing liquid crystalline properties can be found in the literature [30, 31], particularly in the case of nematogene systems.

The temperature–concentration phase diagram of such a system is given in Fig. 5.11. The liquidus line is quite similar to those observed in many organogels. The transition from the liquid solvent to the nematic phase is temperature non-variant, which complies with Gibbs' phase rule. Basically at the transition liquid nematic for the solvent (5CB), the gel does not undergo any morphological change. Whether the liquid possesses nematogene properties or not does not alter the gel architecture provided its forms when the solvent is still liquid.

Another case is observed when the solvent undergoes the *liquid → nematic transition* prior to the organogelation [32]. The organogel scaffold is then highly oriented as the gelation occurs in a highly anisotropic medium. This confers interesting properties to the gel which is originally transparent in the homeotropic state. Applying an electric field entails disorientation of the nematic liquid, with formation of uncorrelated domains. This results in a loss of transparency due to strong light scattering.

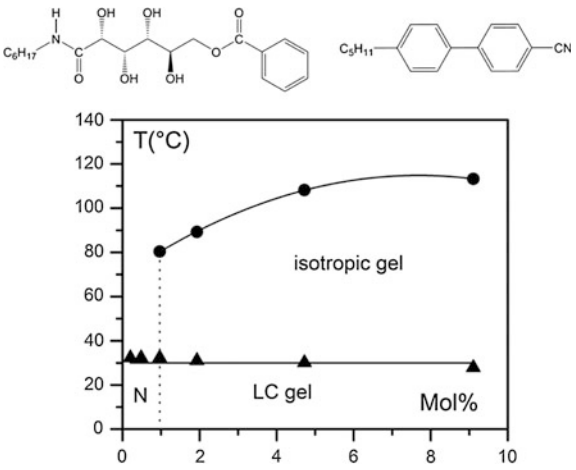

Fig. 5.11 Temperature–concentration phase diagram for GA8 (chemical structure above, *left*) in 5CB (chemical structure above, *right*). Redrawn from Yabuuchi et al. [31]

5.5 Summary

The use of solubility parameters can be helpful in guessing whether a molecule possesses the propensity to form a gel in a given solvent. Yet, this can only be an approximation in view of the complex structure of the organogelators. To some extent, this is reminiscent of a mean-field approach. While the solubility parameter can give some hint as to whether the molecule will crystallize but in no case can predict whether a gel or an assembly of spherolites will be produced. For a given pair molecule/solvent, one has to estimate concurrently the capability for crystallization and for 1D growth so as to obtain fibrillary morphologies. Admittedly, the approach through the solubility parameter cannot unveil all the subtleties of the organogelator/solvent interactions. Possibly, computer simulations may be the best way for throwing some light on the organogelation phenomenon in the coming years.

So far, very few reports are available on the occurrence of organogelator/solvent molecular compound. In view of the specific interactions that can be established between solvents and parts of the molecules, these compounds should be more abundant. Again, such compounds might be discovered in investigations to come.

References

1. Lan, Y., Corradini, M.G., Weiss, R.G., Raghavan, S.R., Rogers, M.A.: To gel or not to gel: correlating molecular gelation with solvent parameters. Chem. Soc. Rev. **44**, 6035 (2015)
2. Feng, L., Cavicchi, K.A.: Investigation of the relationships between the thermodynamic phase behavior and gelation behavior of a series of tripodal trisamide compounds. Soft Matter **8**, 6483 (2012)
3. This question was already raised concerning the gelatin gels by Guenet, J.M. Thermoreversible Gelation of Polymers and Biopolymers. Academic Press, London (1992)
4. Dasgupta, D., Thierry, A., Rochas, C., Ajayaghosh, A., Guenet, J.M.: Key role of solvent type in organogelation. Soft Matter **8**, 8714 (2012)
5. Murata, K., Aoki, M., Suzuki, T., Harada, T., Kawabata, H., Komri, T., Ohrseto, F., Ueda, K., Shinkai, S.: Thermal and light control of the Sol-Gel phase transition in cholesterol-based organic gels. Novel helical aggregation modes as detected by circular dichroism and electron microscopic observation. J. Am. Chem. Soc. **116**, 6664 (1994)
6. Fedors, R.F.: A method for estimating both the solubility parameters and the molar volume of liquids. Polym. Eng. Sci. **14**, 147 (1974)
7. Hansen, C.M.: The three dimensional solubility parameter and solvent diffusion coefficient and their importance in surface coating formulation. Danish Technical Press, Copenhagen (1967)
8. Hansen, C.M.: Hansen solubility parameters: a user's handbook, 2nd edn. CRC Press LLC, Boca Raton (2007)
9. Hansen, C.M.: Prog. Org. Coat. **51**, 77 (2004)
10. Raynal, M., Bouteiller, L.: Organogel formation rationalized by Hansen solubility parameters Chem. Commun. **47**, 8271 (2011)
11. Bonnet, J., Suissa, G., Raynal, M., Bouteiller, L.: Organogel formation rationalized by Hansen solubility parameters: dos and don'ts. Soft Matter **10**, 3154 (2014)
12. Amanokura, N., Yoza, K., Shinmori, H., Shinkai, S., Reinhoudt, D.N.: New sugar-based gelators bearing a p-nitrophenyl chromophore: remarkably large influence of a sugar structure on the gelation ability. J. Chem. Soc. Perkin Trans. **2**, 2585 (1998)

13. Pal, A., Ghosh, Y.K., Bhattacharya, S.: Molecular mechanism of physical gelation of hydrocarbons by fatty acid amides of natural amino acids. Tetrahedron **63**, 7334 (2007)
14. Daniel, C., De Luca, M.D., Brulet, A., Menelle, A., Guenet, J.M.: Thermoreversible gelation of syndiotactic polystyrene in benzene. Polymer **37**, 1273 (1996)
15. Yan, N., Xu, Z., Diehn, K.K., Raghavan, S.R., Fang, Y., Weiss, R.G.: How do liquid mixtures solubilize insoluble gelators? Self-assembly porperties of pyrenyl-glucono gelators in tetrahydrofuran-water mixtures. JACS **135**, 8989 (2013)
16. Cui, J., Zheng, Z., Shen, Z., Wan, X.: Alkoxy tail length dependence of gelation ability and supramolecular chirality of sugar-appended organogelators. Langmuir **26**, 15508 (2010)
17. Cowie, J.M.G., Toporowski, P.M.: Association in the binary liquid system dimethyl sulphoxide/water Can. J. Chem. **39**, 2240 (1961)
18. Rasmussen, D.H., MacKenzie, A.P.: Phase diagram for the system water-dimethyl sulphoxide. Nature **220**, 1316 (1968)
19. Ramzi, M., Rochas, C., Guenet, J.M.: Phase behavior of agarose in binary solvents. Macromolecules **29**, 4668 (1996)
20. Carbonnel, L., Rosso, J.C.: Les clathrates des ethers cycliques: leur stoichiométrie déduite des diagrammes de phases eau-éthers cycliques. J. Solid State Chem. **8**, 304 (1973)
21. Devarakonda, S., Groysman, A., Myerson, A.S.: THF-water hydrate crystallization: an experimental investigation. J. Cryst. Growth **204**, 525 (1999)
22. Gough, S.R., Davidson, D.W.: Composition of Tetrahydrofuran Hydrate and the Effect of Pressure on the Decomposition. Can. J. Chem. **49**, 2691 (1971)
23. Guenet, J.M.: Polymer-solvent molecular compounds. Elsevier, London (2008)
24. Dasgupta, D., Srinivasan, S., Rochas, C., Thierry, A., Schröder, A., Ajayaghosh, A., Guenet, J. M.: Insight into the gelation habit of oligo(para-phenylene vinylene) derivatives: effect of end-groups. Soft Matter **7**, 2797 (2011)
25. George, S.J., Tomovic, Z., Schenning, A.P.H.J., Meijer, E.W.: Insight into the Chiral Induction in Supramolecular Stacks through Preferential Chiral Solvation. Chem. Commun. **47**, 3451 (2011)
26. George, S.J., de Bruijn, R., Tomović, Z., Van Averbeke, B., Beljonne, D., Lazzaroni, R., Schenning, A.P., Meijer, E.W.: Asymmetric noncovalent synthesis of self-assembled one-dimensional stacks by a chiral supramolecular auxiliary approach. J. Am. Chem. Soc. **134**, 17789 (2012)
27. Watase, M., Nakatani, Y., Itagaki, H.: On the origin of the formation and stability of physical gels of di-O-benzylidene-D-sorbitol. J. Phys. Chem. B **103**, 2366 (1999)
28. Kartha, K.K., Babu, S.S., Srinivasan, S., Ajayaghosh, A.: Attogram sensing of trinitrotoluene with a self-assembled molecular gelator. J. Am. Chem. Soc. **134**, 4834 (2012)
29. Kartha, K.K., Sandeep, A., Praveen, V.K., Ajayaghosh, A.: Detection of nitroaromatic explosives with fluorescent molecular assemblies and π-gels. Chem. Rec. **15**, 252 (2015)
30. Kato, T.: Self-assembly of phase-segregated liquid crystal structures science **295**, 2414 (2002)
31. Yabuuchi, K., Rowan, A.E., Nolte, R.J.M., Kato, T.: Liquid-crystalline physical gels: self-aggregation of a gluconamide derivative in mesogenic molecules for the formation of anisotropic functional composites. Chem. Mater. **12**, 440 (2000)
32. Suzuki, Y., Mizoshita, N., Hanabusa, K., Kato, T.: Homeotropically oriented nematic physical gels for electrooptical materials. J. Mater. Chem. **13**, 2870 (2003)

Chapter 6
Rheological Aspects

When a solution turns into a gel, namely a solid-like material, determination of its mechanical properties is among the first investigations to be performed. Since the gel contains a large amount of solvent, the science dealing with these systems is rheology which encompasses several properties such as elasticity, viscosity, plasticity, thixotropy, and the like.

The rheology of polymers solutions and polymer gel has been abundantly studied by means of several techniques. The same techniques can be and are actually used with organogels as well as the theories they rely on. Some theoretical bases will be accordingly given in order to have a better understanding of the domain dealing with gel systems. Data gathered on organogels will then be presented and discussed in the light of these theories.

6.1 Some Theoretical and Practical Bases

Rheological experiments consist usually in determining the dynamic properties under stress or deformation of systems that depart from a pure elastic behavior. In this aim, oscillatory experiments are carried out to determine the modulus which contains a real part, G', and an imaginary part, G''. The former represents the elastic behavior and is called the storage modulus, G', and the latter stands for the viscous behavior and is named the loss modulus, G''.

In viscous solutions, polymer or dynamic polymer solutions, the experimental results are usually well accounted for with the Maxwell model [1, 2]. This model consists of a spring and a dash-pot in series with one characteristic time τ. The equations as a function of frequency ω then read (Fig. 6.1)

$$G' = G\frac{\omega^2\tau^2}{(1+\omega^2\tau^2)} \text{ and } G'' = G\frac{\omega\tau}{(1+\omega^2\tau^2)} \tag{6.1}$$

J.-M. Guenet, *Organogels*, SpringerBriefs in Materials,
DOI 10.1007/978-3-319-33178-2_6

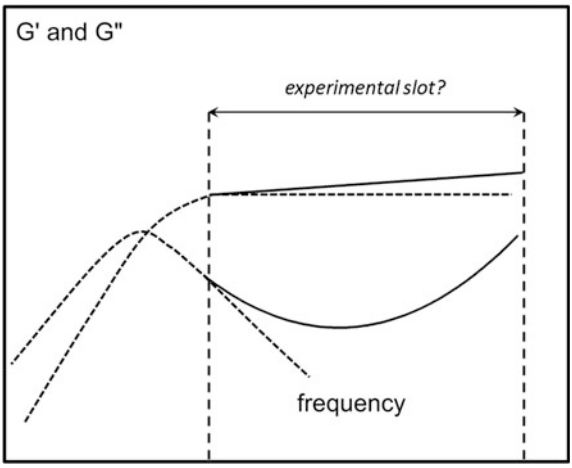

Fig. 6.1 Theoretical Log–Log plot of the storage modulus G' and the loss modulus G″ versus oscillatory frequency. The dotted lines stand for the Maxwell model; the full line for the expectations for a gel. The "experimental slot" is discussed in the text

A typical plot is shown in Fig. 6.1. At low frequency $G'' > G'$ while at high frequency the reverse situation occurs, $G' > G''$, while G' reaches a plateau (the plateau modulus). At low frequency the Maxwell model gives $G' = G\omega^2\tau^2$ and $G'' = G\omega\tau$ so that slopes are in the ratio 2/1 in a double logarithmic plot.

For a gel the relation $G' > G''$ should always be fulfilled as one expects the relaxation process to be controlled by elasticity. In practice G' is larger by one to two orders of magnitude.

This depends largely on the accessible range of frequency. In most experimental setup, the accessible slot may not be large enough, particularly at very low frequency. That G'' can increase at low frequency, in a way shown in Fig. 6.1, it may eventually suggest a behavior reminiscent of viscoelastic solutions at much lower frequencies. This implies a much higher characteristic time, which denotes very slow relaxation processes as has been reported in some polymer thermoreversible gels. These processes are thought to arise from the lability of the chains within the junctions under stress.[1] In other words, junctions destroy under stress and reform [3]. A similar type of behavior as that portrayed in Fig. 6.1 has been observed by Lescane et al. [4] for 2,3-di-n-decyloxy-anthracene/propylene carbonate organogels (see Fig. 6.2). This shows similar effect what was reported for polymer thermoreversible gels. Similarly, results reported by Collin et al. (see Fig. 2.1) further highlight such a long relaxation time arising from junctions lability [5].

The understanding of the rheological behavior of organogels would certainly benefit from compressive relaxation experiments. The advantages are twofold: (i) it requires no adhesion at all to the plates but total slippery instead, whereas in plate–plate or cone–plate oscillatory rheometers proper gel anchoring is crucial but sometimes difficult to achieve, and (ii) it gives access to slow relaxation processes, and correspondingly to long characteristic times.

[1]Effect similar to the fusion-recrystallization of water under stress.

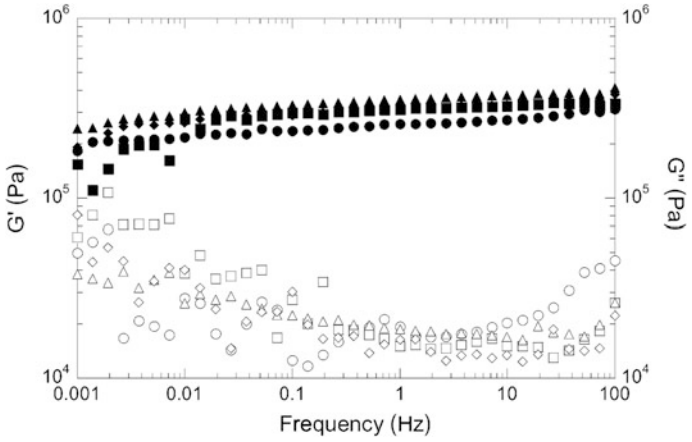

Fig. 6.2 Four different measurements of the evolution of G' (filled symbols) and G'' (open symbols) as a function of the frequency. The applied shear stress is equal to 20 Pa. The experiment is performed in the linear regime. The sample is a gel of DDOA in propylene carbonate ($C_{DDOA} = 2.5 \times 10^{-2}$ M). The cooling rate is 20 °C/min, and the experiment is performed at 20 °C. From Lescanne et al. [4]

6.2 Percolation Model Versus Fibrillar Model

The mechanism of gel formation determines its molecular structure, and correspondingly its morphology. This has a direct bearing upon the rheological behavior, particularly during the gel formation. Here we discussed two models that are often used in the realm of gelation.

In the 1980s a theoretical breakthrough was achieved for describing the phenomenon of chemical gelation thanks to the use of the *percolation model*. This model was primarily developed mathematically by Hamersley [6], and extended to the case of chemically cross-linked gels by Stauffer [7, 9], and de Gennes [8].

The percolation model is a critical phenomenon of connectivity. If p is the fraction of connected objects, then a *percolation threshold* p_c can be defined; below p_c the system consists only of clusters of finite size, while above p_c an infinite network is formed (see Fig. 6.3).

An important aspect of the theory states that on either side of, and close to the gelation threshold the system consists of *fractal objects* of fractal dimension D_f, displaying a large molecular weight polydispersity. Note that D_f is here always larger than 1 as clusters are connected objects. Also, this fractal dimension must not be confused with the fractal dimension of the fibril's long axis (see below). As a result, on either side of the gelation threshold the molecular structure does not differ markedly so that scattering experiments should give essentially the same scattering pattern. For $p > p_c$ the scattered intensity reads [10, 11]:

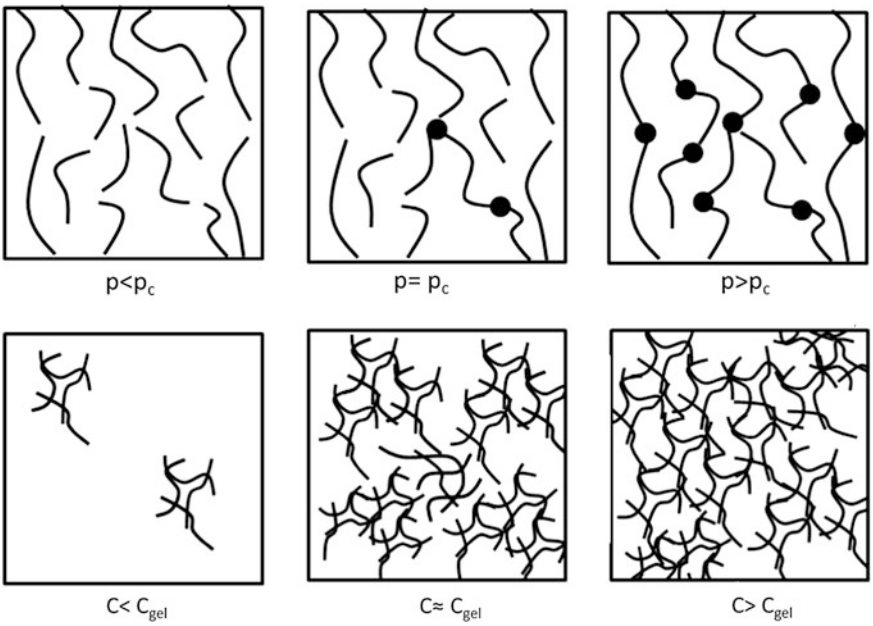

Fig. 6.3 Schematic representation of the percolation model (*top*) and the fibrillary model (*bottom*). See text for details. In the percolation model the concentration of materials remains unchanged, only the degree of cross-linking, p, increases (shown by *dots*). In the fibrillary model the concentration of materials has to increase up to a concentration C_{gel}, onset gelation concentration, in order to make a gel

$$I(q) \sim \frac{1}{q^{(3-\tau)D_f}} \tag{6.2}$$

where τ is an exponent related to the polydispersity of the cluster below p_c [10].

Conversely, far from p_c the scattering pattern differs is written [12]:

$$I(q) \sim \frac{1}{q^2 + \xi^{-2}} \tag{6.3}$$

where ξ is the gel average mesh size.

The storage modulus G' is written above the gelation threshold

$$G' \sim \left(\frac{p - p_c}{p_c}\right)^t \tag{6.4}$$

in which the exponent t takes a value around 2 depending upon the models (see Ref. [12] for example).

Two important points must be emphasized: (i) in the percolation theory the amount of species is set at an appropriate concentration for making a gel, and so remains unchanged. The process consists only in connecting the species. No further addition of matter is needed: (ii) the value of p_c is independent of the size of the sample.

The *fibrillary model* portrayed in Fig. 6.3 is simply derived from observations [13]. It states in the case of polymer thermoreversible systems that the microgels formed below a concentration named gelation concentration, $C_{gel,}$ possess a structure virtually identical to the structure of the gel at the same scale [14]. In other words, microgels prepared well below C_{gel}, in particular do not differ drastically with gels obtained well above C_{gel} as far as their scattering intensities are concerned (see Fig. 6.3) [14].

Investigations into the morphology of organogels by optical microscopy and aggregates by electron microscopy [15] show also their close resemblance (see Fig. 6.4). This can be expressed in other terms: ***a gel is a microgel of infinite size***. The fibrillary model can therefore pertain to organogels as well. The approach developed by Jones and Marquès for rigid gels, presented in the next section, is therefore relevant.

Two important points deserve also to be emphasized against the percolation model: (i) ***the value of C_{gel} depends on the sample size***. If the rheological measurements are carried out in the devices such as a piezorheometer where submicron distances between plates are employed, then microgels of comparable size to the plate–plate distance will display a gel response. (ii) as a result the same conclusion is expressed in 4.2.2 ***C_{gel} is not a critical parameter unlike p_c***. Studying rheological properties as a function of the parameter $(C\text{-}C_{gel})/C_{gel}$ is therefore irrelevant.

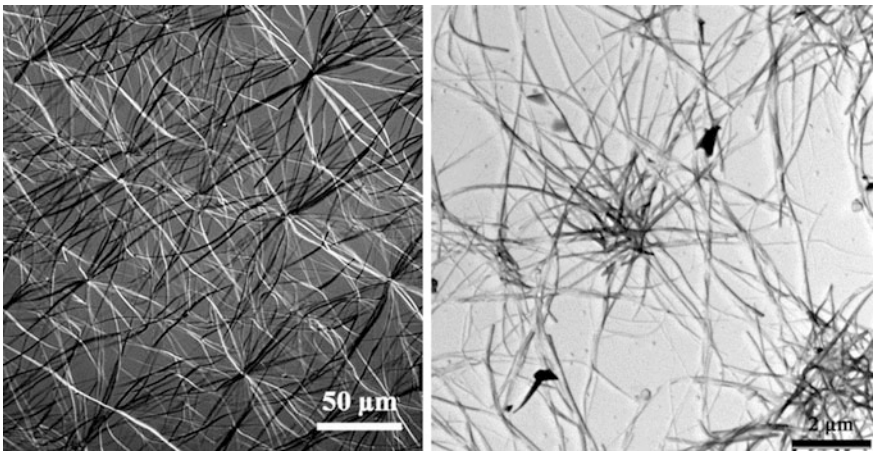

Fig. 6.4 *Left* optical micrograph of a gel prepared at an OPVOH concentration C_{OPVOH} = 0.01 g/cm^3 in benzyl alcohol. *Right*, a TEM micrograph of aggregates in benzyl alcohol at a concentration C_{OPVOH} = 0.0004 g/cm^3. From Dasgupta et al. [15]

6.3 Modulus Versus Concentration

The study of the variation of the elastic modulus a function of concentration can bring useful information about the gel architecture. The theory developed by Jones and Marquès for rigid systems is quite appropriate for polymer thermoreversible gels and organogels that are made up in most cases with rigid elements [16]. This theory relies upon the notion of *enthalpic elasticity* as opposed to *entropic elasticity*. Enthalpic elasticity implies that deformation proceeds only through the bending of the objects making the gel scaffold, while entropic elasticity is related to conformational change as it occurs in polymer chemical gels made up with flexible chains. Freely-rotating junctions, should they exist in organogels, would entail entropic elasticity.

The theory relies upon the fractal dimension, D_f, of very long objects with circular symmetry connecting at the junctions (see Fig. 6.5). For straight object the fractal dimension is 1. If we extend the concept to fibrils [17], the modulus can be written:

$$G \sim \frac{e r_\sigma^4 n}{N^{(3+D_f)/D_f} a^4} \tag{6.5}$$

where r_σ is the object cross-sectional radius, n the number of objects, N the number of "monomers" composing the object and a the size of these "monomers",[2] Na being the contour length of the fibril long axis, and e the intrinsic Young's modulus. Evidently, this relation is only valid for $Na >> r_\sigma$.

Introducing the volume fraction of the network

$$\varphi \sim \frac{nNar_\sigma^2}{S^3} \tag{6.6}$$

where n is the number of objects, and S the end-to-end distance of the object. In the case of fibrils, S is the end-to-end distance of the long axis. In any case S reads

$$S \sim N^{\frac{1}{D_f}} a \tag{6.7}$$

The modulus is eventually written

$$G \sim \frac{e r_\sigma^4 n}{a^4} \left(\frac{\varphi a^2}{r_\sigma^2 n} \right)^{3+D_f/3-D_f} \tag{6.8}$$

For straight fibrils, one obtains

$$G \sim \frac{e\varphi^2}{n} \tag{6.9}$$

[2] "Monomers" are basic bricks that can be defined as wished.

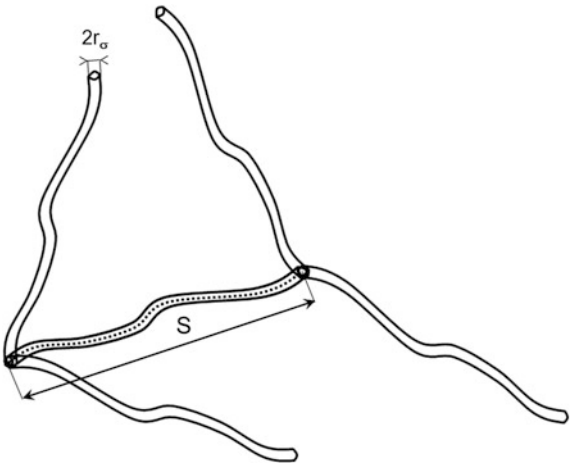

Fig. 6.5 Schematic representation of fibrils connecting at a junction. The *dotted line* shows the fibril's long axis. S is the end-to-end distance of this axis and amounts to $N^{1/Df}a$ where D_f is the fractal dimension of the fibril's long axis, r_σ is the fibrils'cross-sectional radius

Here, the modulus is independent of the fibrils' cross-section but depends inversely upon the number of objects. Since this number of fibrils is inversely proportional to r_σ^2 it turns out that G is proportional to r_σ^2. Therefore, relation [6.9] implies, the thicker the fibrils, the higher the modulus.

Terech and coworkers have investigated a series of gels as a function of polymer concentration [18] and obtained the parameter listed in Table 6.1. As can be seen, the exponents measured for the variation of the storage modulus as a function of concentration are close to $\beta = 2$, and therefore in good agreement with Jones and Marquès predictions. The prefactors are, however, conspicuously different between dodecane and toluene on the one hand, and nitrobenzene on the other hand. Since the crystal structure is supposed to be the same (actually there is no clear indication about this point in their paper) the intrinsic modulus, e, should also be the same. As a result, this discrepancy may arise from the fibrils cross-section or shape. From their neutron scattering study they indeed observe much larger ribbons in nitrobenzene of rectangular cross-section with a = 30 nm and b = 150 nm, than in toluene of circular cross-section 18 nm (see Chap. 4, Fig. 4.8). This agrees well with relation 6.9 which states, the thicker the fibrils, the higher the modulus.

Now, for fractal dimensions of the objects higher than 1, 6.5 reads

$$G \sim e\left[\frac{r_\sigma^{6-6D_f} a^{6D_f-6}}{n^{D_f}}\right]^{1/(3-D_f)} \tag{6.10}$$

Table 6.1 Values of G' at two different concentrations (w/w), and $\beta = (3 + D_f)/(3 - D_f)$ for three different solvents

Solvent	G′(Pa) 1 %w/w	G′(Pa) 7 %w/w	$\beta = 3 + D_f/3 - D_f$
Nitrobenzene	40190	1790000	1.89
Dodecane	9010	580000	2.22
Toluene	8390	423000	2.04

From Terech and coworkers [18]

This shows a more complex relation involving both the fibril cross-section and the number of fibrils. If one still assumes that $n \sim r_\sigma^{-2}$, then the modulus becomes proportional to

$$G \sim e r_\sigma^{6-4D_f/(3-D_f)} \tag{6.11}$$

For $D_f = 1.5$ the modulus should become independent of the cross-sectional radius. The long axis of askew fibrils may be characterized by such a fractal dimension. Not enough data are currently available on this topic for testing in depth the validity of this statement.

There is little prospect to encounter organogels for which junction are of the freely-hinged type, namely for which entropic elasticity would dominate. Still, it seems of interest to give the relation established by the same authors for this case. Again, using the fractal dimension of the objects, Jones and Marquès obtained

$$G \sim kT \times \varphi^{3/\left(3-D_f\right)} \tag{6.12}$$

where k is the Boltzmann constant and T the temperature. For a fractal dimension $D_f = 1$, the exponent is 1.5 instead of 2 for enthalpic elasticity. Such an exponent has been observed in agarose thermoreversible gels [19], possibly due to the fact that the junctions arise from the crossing of fibrils, so that they can be chiefly amorphous and therefore flexible. Under these conditions, the modulus has been seen to increase with increasing temperature as shown in relation 6.12 provided that no melting process occurs in the meantime. Again, this situation is rather unlikely with organogels unless flexible moieties would be purposefully introduced at the junctions.

Another case worth mentioning corresponds to the situation where the functionality of the junctions, namely the number of objects connecting at the same junction changes with concentration, while the mesh size remains constant or nearly constant. Although no specific information on this case is seemingly available for organogels, it may be of interest to provide the reader with the equation derived by Jones and Marquès [16]:

$$G' \sim \frac{e r_\sigma^2 \varphi}{N^2 a^2} \tag{6.13}$$

In this case, the storage modulus G' varies like the organogel fraction, and is independent of the fractal dimension of the objects connecting at the junctions.

It ought to be emphasized, irrespective of the different models, that *the organogelator concentration does not necessarily correspond to the concentration of elastic material*. For instance, "pendant" fibrils, namely those fibrils for which one tip is not connected to any other fibril, do not participate in the elastic properties. This situation has already been reported for agarose gels [19], and is also equivalent to the presence of pendant chains in chemical gels [20]. Similarly, the molecules in the *organogelator-poor* phase do not participate in the gel scaffold as

will be further discussed below. If this fraction is important, then the gel fraction will differ markedly from the organogelator concentration. In most cases, the exponent can be far larger than 2 [19], from which a wrong fibril's fractal dimension may be derived. Structural investigations are often required to confirm rheological outcomes. Clearly, the value of the exponent in the modulus-concentration relation does not allow one to conclude definitely about the fractal dimension of the objects.

6.4 Storage Modulus Versus Temperature

Some studies on the evolution of the storage modulus as a function of temperature are available [5]. This variation is prone to depend upon the shape of the liquidus in the phase diagram and the temperature at which the system is studied. It depends therefore upon the fraction of the solid phase.

An example to illustrate this point can be taken from the phase diagram mapped out by Feng and Cavicchi shown in Fig. 3.8 [21]. At $T = 420$ K, the system will phase separate into an *organogelator-poor phase* of fraction φ_{poor} and an *organogelator-rich phase* of fraction φ_{rich}. The concentration of the poor phase is not negligible so that the real fraction of material participating in the elastic properties of the organogel, φ_{net} can be simply derived from the lever rule [22]:

$$\varphi_{net} = \frac{\varphi_{org} - \varphi_{poor}}{\varphi_{rich} - \varphi_{poor}} \tag{6.14}$$

The concentration of the poor phase becomes negligible only once the temperature is lowered to $T = 370$ K.

Theoretical examples can be shown by considering the phase diagrams in Fig. 6.6. The phase diagram on the left, which involves only a *liquid-solid phase separation* can be represented by a function of the type

$$T = f(\varphi) = \left[\mathrm{Log}(10^5 \varphi_{org})\right]^{1/2} \tag{6.15}$$

Here, the function chosen is just to mimic the typical shape of experimental phase diagrams, but does rely on any theoretical basis. The concentration can be then expressed through the inverse function

$$\varphi_{org} = f^{-1}(T) = 10^{-5}\exp(T^2) \tag{6.16}$$

Applying 6.14 allows one to calculate the fraction of gel by assuming it to be directly related to the fraction of solid material. Considering that $\varphi_{rich} = 1$, one obtains

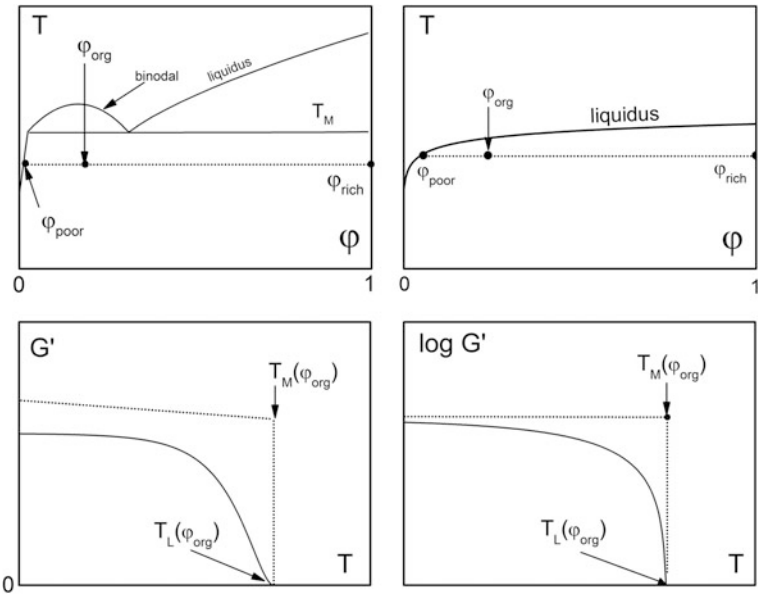

Fig. 6.6 *Upper figure right* schematic *T-C* phase diagram for a *liquid–solid* phase separation. The liquidus *line* is calculated with $T = [\mathrm{Log}(10^5 \varphi_{org})]^{1/2}$ in order to mimic common *liquidus lines* observed in organogel systems [11]. *Upper figure left* system displaying a miscibility gap. The *liquidus line* for $\varphi < \varphi_{poor}$ is approximated to a *straight line*. Lower figures: theoretical evolution of the storage modulus G' as a function of temperature for the two cases (*left* G' vs. T, *right* log G' vs. T): full line = case for the *liquid-solid* phase transition, $T_L(\varphi_{org})$ is the position of the liquidus at $\varphi = \varphi_{org}$; dotted line = case for the *liquid–liquid* phase separation arrested in the early stage by *liquid-solid* phase transition, $T_M(\varphi_{org})$ is the monotectic temperature (for details on the phase diagrams see Chap. 3, Sect. 3.2.1)

$$\varphi_{gel} = \frac{\varphi_{org} - f^{-1}(T)}{1 - f^{-1}(T)} \tag{6.17}$$

Assuming that the modulus varies as $G' \sim \varphi_{net}^2$ and using Eq. 6.17, one obtains a nearly-sigmoidal shape for the variation of G' with T (lower Fig. 6.6, full line). This agrees with recent findings by Collin et al. [5] reported in Fig. 6.7.

The other case considers the existence of a miscibility gap. The behavior of the modulus will depend upon the cooling rate used for preparing the organogel. If the system is cooled very rapidly so as to by-pass the *liquid–liquid* phase separation and to enter the domain below T_M virtually unaltered, then the onset of organogel formation will always be at the same temperature, namely T_M. Also, the rich phase will always have the same concentration, only the poor phase/rich phase ratio will vary. As a result, a sharp increase of the modulus will be observed (see Fig. 6.6, bottom). The modulus may increase very slowly while cooling further, depending

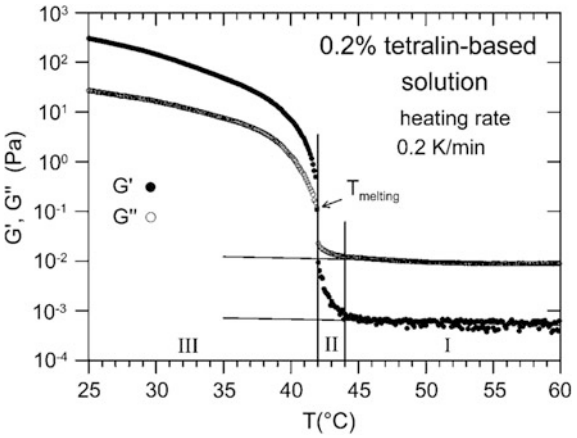

Fig. 6.7 Variation of G' and G'' for a heating rate of 0.2 K/min for 0.2 % peptide type organogelator/tetraline. $T_{melting}$ does not correspond to the total disappearance of organized structures but to the loss of the infinite network by using the usual criterion $G' = G''$. From Collin et al. [5]

upon the shape of the liquidus line in the low-concentration domain. Here a linear variation for the liquidus has been considered for the sake of illustration.

Knowledge of the phase diagram is beyond doubt essential to account for the behavior of the storage modulus as a function of temperature.

6.5 Summary

Rheology investigations are certainly of prime importance to determine the mechanical properties and behavior of organogels. It is not, however, a technique that can bring much information about the molecular structure. A combination of structural investigations and rheology is therefore much needed. Also, the percolation model, although very popular, does not necessarily pertain to the realm thermoreversible gels, and particularly organogels. The fibrillar model is likely to be more relevant for these systems. Finally, the temperature-concentration phase diagram is essential and is definitely required if one wants to account for the behavior as a function of temperature.

References

1. Doi, M.; Edwards, S.F. *The Theory of Polymer Dynamics*, **1986**, Oxford University Press, Oxford
2. Dammer, C., Maldivi, P., Terech, P., Guenet, J.M.: Rheological Study of a Bicopper Tetracarboxylate/Decalin Jelly. Langmuir **11**, 1500 (1995)
3. McKenna, G.B., Guenet, J.M.: The effects of the solvent type on the concentration dependence of the compression modulus of thermoreversible isotactic polystyrene gels. J. Polym. Sci. Polym. Phys. Ed. **26**, 267 (1988)

4. Lescanne, M., Colin, A., Mondain-Monval, O., Fages, F., Pozzo, J.L.: Structural Aspects of the Gelation Process Observed with Low Molecular Mass Organogelators. Langmuir **2003**, 19 (2013)
5. Collin, D., Covis, R., Allix, F., Jamart-Grégoire, B., Martinoty, P.: Jamming transition in solutions containing organogelator molecules of amino-acid type: rheological and calorimetry experiments. Soft Matter **9**, 2947 (2013)
6. Hammersley, J.M.: Percolation processes: lower bounds for the critical probability Ann. Math. Stat. **28**, 790 (1957)
7. Stauffer, D.: 'Gelation in concentrated critically branched polymer solutions. J. Chem. Soc., Faraday Trans. 2 **72**, 1354 (1976)
8. de Gennes, P.G.: On a relation between percolation theory and the elasticity of gels. J. Phys. France Lett. **37**, 1 (1976)
9. Stauffer, D.: *Introduction to Percolation Theory*. Taylor and Francis, London (1985)
10. Daoud, M., Family, F., Jannink, G.: Dilution and polydispersity in branched polymers. J. Phys. France Lett. **45**, 199 (1984)
11. Martin, J., Ackerson, B.J.: Static and dynamic scattering from fractals Phys. Rev. A **31**, 1180 (1985)
12. Adam, M.; Lairez, D. *Sol-gel transition*, in *The Physical Properties of Polymeric Gels*, **1996**, 84, ed. J. P. Cohen-Addad, Wiley, New York
13. Guenet, J.M.: Structure versus rheological properties in fibrillary thermoreversible gels from polymers and biopolymers. J. Rheol. **44**, 947 (2000)
14. Abied, H., Brulet, A., Guenet, J.M.: Physical gels from PVC: molecular structure of pregels and gels by low-angle neutron scattering Colloid Polym. Sci. **268**, 403 (1990)
15. Dasgupta, D., Srinivasan, S.A., Rochas, C., Ajayaghosh, A., Guenet, J.M.: Solvent-mediated Fiber Growth Organog. Soft Matter **7** 9311 (2011); Dasgupta, D., Srinivasan, S.A., Rochas, C., Thierry, A., Schröder, A., Ajayaghosh, A., Guenet, J.M.: Insight into the gelation habit of oligo(para-phenylene vinylene) derivatives: effect of end-groups. Soft Matter **7,** 2797 (2011)
16. Jones, J.L., Marques, C.M.J.: Phys. (les Ulis) **51**, 1113 (1990)
17. Guenet, J.M.: Thermoreversible gels from Polymers and Biopolymers. Academic Press, London (1992)
18. Terech, P., Pasquier, D., Bordas, V., Rossat, C.: Rheological Properties and Structural Correlations in Molecular Organogels. Langmuir **16**, 4485 (2000)
19. Ramzi, M., Rochas, C., Guenet, J.M.: Structure-Properties Relation for Agarose Thermoreversible Gels in Binary Solvents. Macromolecules **31**, 6106 (1998)
20. Bastide, J., Picot, C., Candau, S.: *Influence of pendent chains on the thermodynamic and viscoelastic properties of swollen networks*. J. Pol. Sci. B **17**, 1441 (1979)
21. Feng, L., Cavicchi, K.A.: Investigation of the relationships between the thermodynamic phase behavior and gelation behavior of a series of tripodal trisamide compounds. Soft Matter **8**, 6483 (2012)
22. Guenet, J.M.: Polymer-solvent Molecular Compounds. Elsevier, London (2008)

Chapter 7
Hybrid Gels

Until recently, organogels and polymer thermoreversible gels were worlds apart. Possibly, because the former were chiefly studied by organist chemists while the latter were investigated by polymer physical chemists. The making of hybrid networks from these two types of gels seemed obvious the more so as polymer chains and organogelators are in most cases compatible in the solution state. Dasgupta et al. were probably the first to try and succeed in preparing these hybrid systems with isotactic polystyrene (iPS) thermoreversible gels and OPV organogels in 2009 [1]. They called these systems "*intermingled gels*" in order to avoid confusion with the expression *interpenetrated networks* already in use for chemical networks. Guenet and coworkers also studied another type of hybrid gels: "*sheathed fibrils gels*" where the self-assembled system sheathes the polymer gel fibrils [2, 3]. In all these systems, once the basic components have been synthesized, hybrid materials are produced by means of physical processes only at relatively low temperature.

A short chapter deserves to be devoted to this particular field that may develop rapidly in the near future, particularly for the making of functional materials with specific properties.

7.1 Intermingled Gels

In the case of blends of covalent polymers, the main issue deals with compatibility problems. As a matter of fact, homogeneously mixing two polymers in most cases is impossible due to a mixing entropy effect [4]. Two conditions are required for homogeneous mixing to occur:

$$\Delta G_m = \Delta H_m - T\Delta S_m < 0 \text{ and } \frac{\partial^2 \Delta G_m}{\partial \varphi^2} > 0 \tag{7.1}$$

J.-M. Guenet, *Organogels*, SpringerBriefs in Materials,
DOI 10.1007/978-3-319-33178-2_7

where ΔG_m, ΔH_m, and ΔS_m, are the free energy, the enthalpy , and the entropy of mixing, and φ the mixture composition.

For solutions of polymer mixtures, the entropy of mixing is greatly reduced compared to that of simple solutions so that the condition $\Delta G_m < 0$ is rarely fulfilled. As a result, obtaining homogeneous solutions turns out to be impossible in most systems.

In the case of ternary solutions, polymer/organogelator/solvent compatibility in the molten state is more likely to be achieved as the mixing entropy problem differs since organogelators are smaller molecules. Therefore, the first concern of Dasgupta et al. [1] was to evaluate the degree of compatibility prior to attempting the making of hybrid gels. Dasgupta et al. have first tackled this basic question by checking whether OPV gel can grow with the same characteristics, thermodynamic, and morphology, in the presence of atactic polystyrene (aPS), a non-gelling polymer. AFM pictures basically reveal the same fibrillar structure with cross-sectional diameters nearly identical to those in the pure OPV organogels (Fig. 7.1 left). By DSC , they found out no significant change of the formation and melting

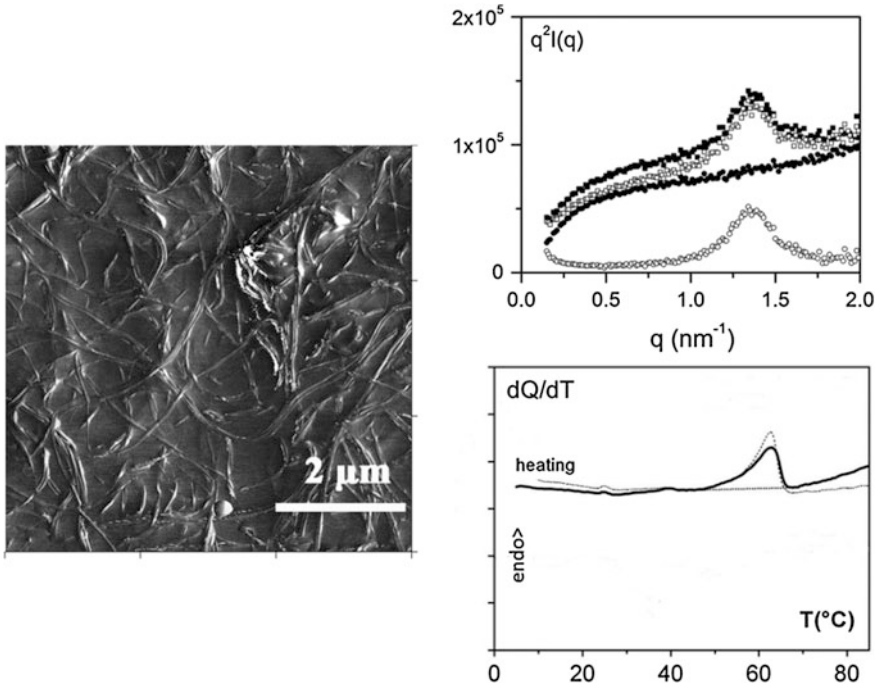

Fig. 7.1 *Left* AFM picture from the ternary system OPV/aPS/*cis*-decahydronaphthalene; *top right* SAXS intensities for O = OPV/*cis*-decahydronaphthalene (C_{OPV} = 0.004 g/cm^3), ● = aPS/*cis*-decahydronaphthalene (C_{aPS} = 0.025 g/cm^3), ■ = sum of the scattered intensities by the binary systems, □ = actual intensity of the ternary system. *Bottom right* DSC traces obtained at 2.5 °C/min, full line OPV/*cis*-decahydronaphthalene gel, dotted line OPV/*cis*-decahydronaphthalene/aPS. From Dasgupta et al. [1]

temperature (Fig. 7.1 bottom right). In SAXS experiments, it is seen that the scattered intensity for the ternary system OPV/aPS/benzene is simply the sum of the intensities recorded for the binary systems (Fig. 7.1 top right). These sets of experiments clearly demonstrate that ***a covalent polymer can be compatible with an organogelator***, but also that this polymer does not impede nor modify the organogelation process.

When aPS is replaced by iPS, a gelling polymer, AFM images exhibit distinctly both networks that appear intimately intermingled (Fig. 7.2 top left). DSC investigations highlight that the formation temperature together with the melting temperature of either gel is not affected by the presence of the other system (Fig. 7.2 top right). This means that after the growth of the OPV network, the iPS network can grow unperturbed by its presence. It ought to be stressed that this is probably so because the mesh size of the OPV network is large enough to leave space for the

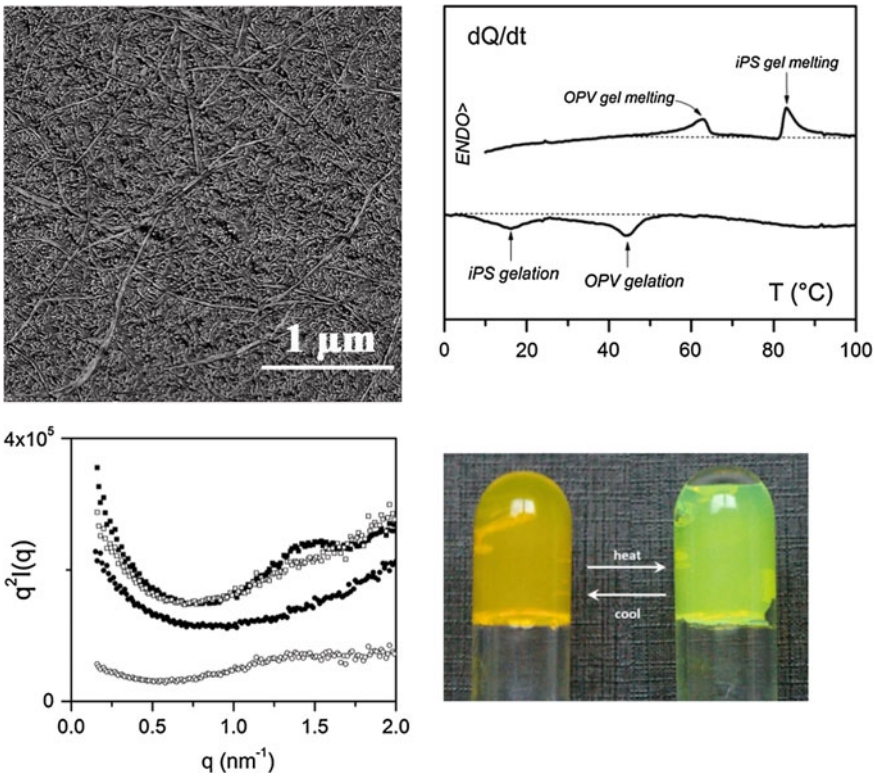

Fig. 7.2 *Top left* AFM picture of an OPV/iPS hybrid gel formed in *trans*-decahydro-naphthalene. *Top right* DSC traces for the hybrid gel with indications of the formation and melting temperature of the gels. *Bottom left* SAXS intensities for O = OPV/*trans*-decahydronaphthalene (C_{OPV} = 0.004 g/cm^3), ● = iPS/*trans*-decahydronaphthalene (C_{iPS} = 0.025 g/cm^3), □ = sum of the scattered intensities by the binary systems, ■ = experimentally measured intensity of the ternary system. *Right* Melting the OPV network entails a colour change while preserving the macroscopic gel state as the iPS network remains unaltered. From Dasgupta et al. [1]

iPS network to pervade it. Finally, SAXS experiments show that the scattering intensity of the intermingled gel is simply the sum of the scattered intensity by the OPV gel and the iPS gel of same concentrations (Fig. 7.2 bottom left). An interesting property arises from the intrication of both networks: on heating slightly above the melting temperature of the OPV network, a change of color occurs while keeping the macroscopic gel state as the iPS network remains unaltered (Fig. 7.2 bottom right). This process is perfectly reversible, which shows that the OPV gel can equally grow within the iPS network, a situation reverse to that occurring when starting from the homogeneous solution.

The fabrication of an intermingled hybrid gel is possible because the mesh size of either network is large enough, typically in the micrometer range, so as to allow the growth of one network into the other. Seemingly, this may not be possible any longer at higher concentrations.

Rheological investigations reveal that the hybrid gel possesses a storage modulus virtually identical to that of the iPS gel, something expected in view of the structural and thermodynamic studies [5].

7.2 Sheathed Fibrils Gels

Hollow nanotubes as those obtained by Mesini and coworkers [6, 7] display an inner cavity of diameter in the range of the cross-sectional diameter of polymer fibrils observed in thermoreversible gels (see Chap. 4). On this basis, Dasgupta et al. [2] contemplated the possibility of sheathing polymer fibrils by these nanotubes by means of a heterogeneous nucleation process. The polymer fibrils were expected to nucleate the growth of the nanotubes. They focused their studies to isotactic polystyrene (iPS).

As with OPVs, BHPB-10 molecules are compatible at high temperature with isotactic polystyrene since, a homogeneous solution is obtained in *trans*-decahydronaphthalene. Micro-DSC experiments were carried out on a system where $C_{\text{BHPB-10}} = 0.001$ g/cm^3 and $C_{\text{iPS}} = 0.07$ g/cm^3 (namely a ratio1/70). In the case of the binary solutions, the BHPB-10 system gels at higher temperature than iPS solutions. Yet, in the ternary system, the gelation exotherm of BHPB-10 has vanished (Fig. 7.3). Seemingly, the presence of iPS improves the solvation quality towards BHPB-10.

AFM pictures do not show nanotube structures, but the fibrils cross-sectional diameter has increased significantly (Fig. 7.3 left). Increasing by ten times, the BHPB-10 concentration ($C_{\text{BHPB-10}} = 0.01$ g/cm^3 and $C_{\text{iPS}} = 0.07$ g/cm^3) entails the reappearance of long nanotube structures (Fig. 7.3 right). Dasgupta et al. were aware that these data and experiments, although consistent with a sheathing process, were not sufficient to nail the case. They performed small-angle neutron scattering making use of the contrast matching method in order to collect more information as to the structures present in the ternary system for $C_{\text{BHPB-10}} = 0.001$ g/cm^3 and

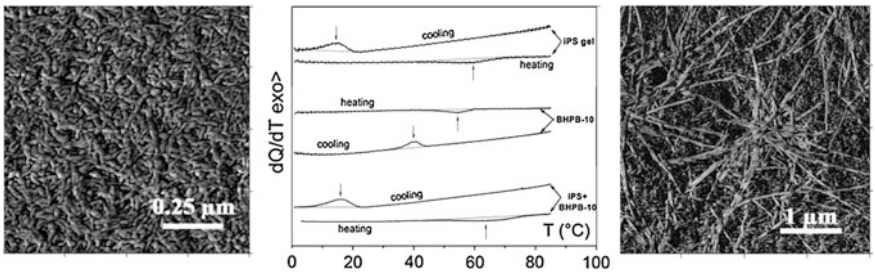

Fig. 7.3 *Left* AFM picture of an iPS/BHPB-10 hybrid gel obtained for $C_{\text{BHPB-10}}$ = 0.001 g/cm3 and C_{iPS} = 0.07 g/cm3. *Middle* µDSC for the binary and the ternary systems for $C_{\text{BHPB-10}}$ = 0.001 g/cm^3 and C_{iPS} = 0.07 g/cm^3. Right: AFM picture of an iPS/BHPB-10 hybrid gel obtained for $C_{\text{BHPB-10}}$ = 0.01 g/cm^3 and C_{iPS} = 0.07 g/cm^3. From Dasgupta et al. [2]

C_{iPS} = 0.07 g/cm^3. When dealing with a ternary system the scattered intensity, $I(q)$, is written:

$$I(q) \sim (A_{\text{p}} - A_{\text{s}})^2 S_{\text{p}}(q) + (A_{\text{o}} - A_{\text{s}})^2 S_{\text{o}}(q) + 2(A_{\text{p}} - A_{\text{s}})(A_{\text{o}} - A_{\text{s}}) S_{\text{po}}(q) \quad (7.2)$$

where A with appropriate subscripts stands for the scattering amplitudes of the polymer (p) and the organogel (o), $S(q)$ with appropriate subscripts are the scattering factor for the polymer (p), the organogel (o), and the cross term (po).

If a solvent is chosen so as to have $A_{\text{p}} \approx 0$, then the structure of the BHPB-10 molecules can be revealed as the terms related to the polymer and the cross term are zero (contrast matching, see Fig. 7.4 top right).

In the system iPSD/BHPB-10/*trans*-decahydronaphthalene$_{\text{D18}}$,[1], the polymer contrast is close to zero. The observation of the oscillations typical of the nanotube structure (see Chap. 4 Fig. 4.9) do indicate their presence in the ternary system (Fig. 7.4 top left). In addition, the vanishing of the oscillations in the system iPSH/BHPB-10/*trans*-decahydronaphthalene$_{\text{D18}}$, namely for which the neutron contrast is not zero and nearly the same for both the polymer and the organogelator, is a strong point in demonstrating the sheathing of the polymer fibrils by the nanotubes (Fig. 7.4 bottom left). Indeed, if the nanotubes were independent of the iPS network, then one should have observed oscillations in both cases.

Another outcome of interest relies on the scattered intensities at very small scattering vectors, where a significant discrepancy between the scattered intensity for the binary gel and that of the ternary system is seen. The first oscillation is more intense for the binary gel than for the ternary system, and its position differs (q = 0.034 nm^{-1} for the former against q = 0.08 nm^{-1} for the latter).

In the binary gels, parallel associations of nanotubes occur (see Fig. 4.10), an effect which must be taken into account. The scattered intensity is then written [8]:

[1]D18 means that all the hydrogens of *trans*-decahydronaphthalene are replaced by deuterium atoms.

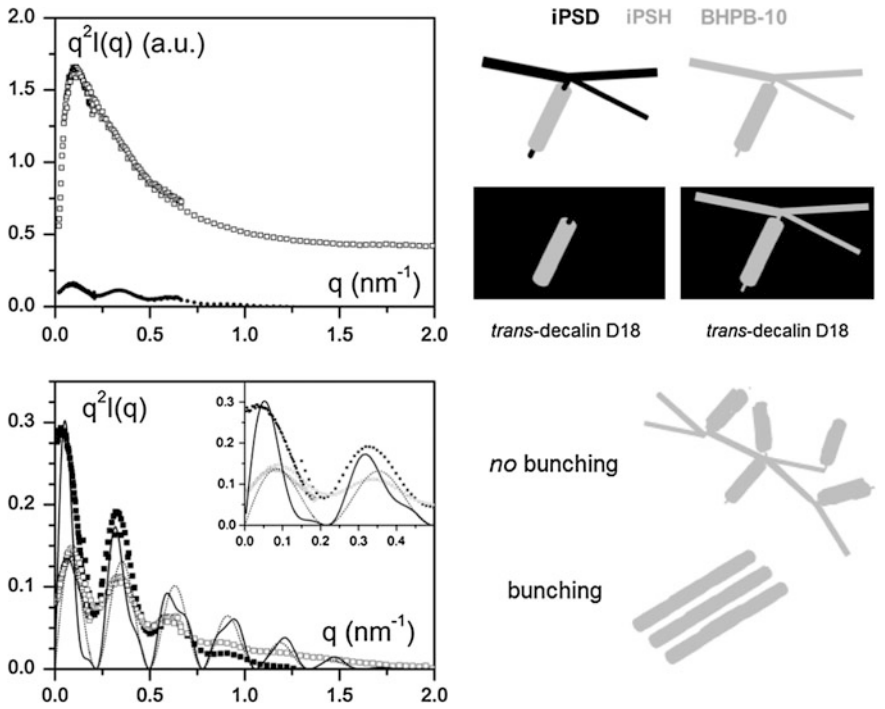

Fig. 7.4 *Top left* neutron scattering curves for O = iPSH/BHPB-10/*trans*-decahydro-naphthalene$_{D18}$; ● = iPSD/BHPB-10/*trans*-decahydronaphthalene$_{D18}$. *Top right* schematic representation of the labeling *black* stands for deuterated material while *grey* stands for hydrogenous material. When the polymer is deuterated, its contrast is close to zero in a deuterated solvent. *Bottom left* neutrons scattering intensities for $C_{BHPB\text{-}10}$ = 0.001 g/cm^3 in the binary solution (■), and in the ternary system (□). Inset close-up in the q-range 0–0.5 nm^{-1}. Full line and dotted lines are theoretical intensities calculated by means of Eq. 4.7 (*dotted line*), and Eq. 7.3 (*full line*). *Bottom right* schematic representation for the sheathed structure showing no parallel association (no bunching) and the case of BHPB-10 gels where parallel associations take place. From Dasgupta et al. [2]

$$q^2 I(q) \sim P_{hc}(q) \times \sum_{j=1}^{n} \sum_{k=1}^{n} J_o(q r_{jk}) \tag{7.3}$$

where $P_{hc}(q)$ is the scattering function for a hollow tube (see Eq. 4.7), r_{jk} is the distance between nanotubes labeled j and k, and n their number in a bunch (J_o is the Bessel function of first kind and first order).

The intensity in the binary gel is well reproduced; particularly the position of the first maximum, by considering simply bunches of 3 nanotubes (a larger number does not affect the position of the first maximum).

If the nanotubes are not bunched but are randomly oriented, as this is what is expected once they have sheathed the gel fibrils, then this intermolecular scattering term must vanish [8]. This is what is experimentally observed [2].

Another ternary system was studied by Khan et al. [3], involving syndiotactic polystyrene (sPS) and a fluorinated version of BHPB-10, BHPBF (see Chap. 4, Figs. 4.10 and 4.11). It should be again emphasized that BHPBF and sPS form homogeneous solutions at high temperature. Although BHPBF does not produce nanotubes, there are strong indications that these molecules form filaments that coil around the polymer fibrils. Again scattering techniques provide one with significant evidence for this coiling process.

Small-angle neutron scattering experiments (SANS) have been performed on ternary samples made up with deuterated syndiotactic polystyrene and hydrogenous BHPBF in deuterated *ortho*-xylene. Under these conditions, contrast matching for sPSD is achieved so that the scattered intensity is only related to the BHPBF filaments. Oscillations are seen that can be interpreted with the scattering function of a hollow cylinder according to Khan et al. This does not mean that BHPBF nanotubes are sheathing the sPS fibrils but rather that the BHPB filaments are coiling around the sPS fibrils as the theoretical function for a hollow cylinder also pertains to a helical coil in this low-resolution range (see model inserted in Fig. 7.5 left).

SAXS experiments bring further confirmation to the possible coiling of BHPBF around the polymer fibrils. For X-ray, the fluorinated organogelator scatters more strongly X-rays than polystyrene, thanks to the presence of fluorine atoms. Indeed, the contrast factor for a given compound reads

$$K_X \sim \left(Z_s - \frac{v_s}{v_o} Z_o \right)^2 \tag{7.4}$$

where Z with the appropriate subscript is the number of electrons in the molecules (s) and in the solvent (o), v are the molar volumes

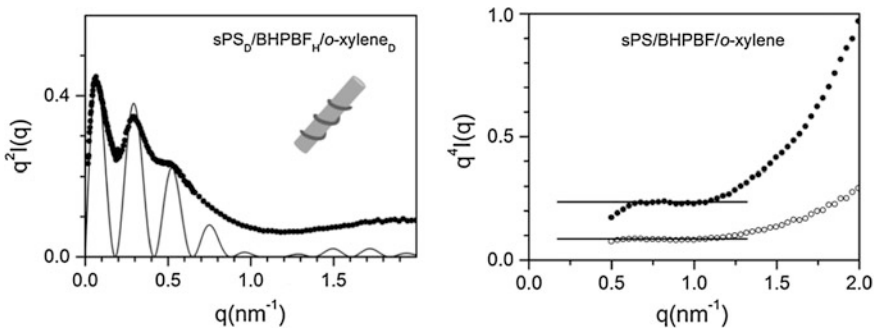

Fig. 7.5 *Left* SANS experiments plotted by means of a Kratky-plot ($q^2I(q)$ vs. q) for a sPSD/BHPBF/o-xylene$_D$ hybrid system with C_{BHPBF} = 0.01 g/cm^3 and C_{sPSD} = 0.15 g/cm^3. *Full line* obtained with the Eq. 4.7 for a hollow cylinder with r = 16 and γ = 0.65. *Inset* schematic representation of the way BHPBF filaments coil around the polymer fibrils. *Right* Normalized SAXS experiments plotted by means of a $q^4I(q)$ versus q representation; ● = sPS/BHPBF/o-xylene with C_{BHPBF} = 0.01 g/cm^3 and C_{sPS} = 0.15 g/cm^3; O = sPS/o-xylene gels with C_{sPS} = 0.15 g/cm^3. From Khan et al. [3]

The intensities scattered by the polymer gel, and by the hybrid systems can be described by a two-density model in both cases as expected for solid fibrils. The scattered intensity reads [9]

$$I(q) \sim K_X \frac{2\pi S}{Vq^4}$$

where S and V are the surface and the volume of the particle. For a cylinder $S/V = 1/r$.

The intensity scattered by the hybrid gel is about 3 times larger than that by the polymer gel (Fig. 7.5), which can only be explained by an increase of the scattering amplitude. Coiling of the BHPBF filaments around the polymer fibrils is thus liable to do the trick. Note that the increase of the cross-sectional radius related to the coiling of BHPBF filaments, which should entail a decrease of intensity, is largely compensated by the increase of the X-ray contrast factor. Khan et al. estimate that just one layer of BHPBF helices could be enough to account for this increase as K_X is $K_X \approx 10^2$ for sPS/*o*-xylene against $K_X \approx 5 \times 10^4$ for BHPBF/*o*-xylene. Further, if the BHPBF filaments were independent of the sPS network, namely not coiling around the polymer fibrils, then one should observe oscillations.

7.3 Hybrid Hydrogels with Graphene Oxide

The use of graphene or graphene oxide in gel systems is a current topic of interest in view of reaching new properties [10, 11].

Banerjee and coworkers have recently reported a study of hybrid systems made up with hydrogels of a pyrene-conjugated tryptophan-based organogelator in phosphate buffer in the pH range 7.3–8.7 and graphene oxide [11].

As can be seen in Fig. 7.6, fibrils connect at the graphene oxide nanosheets in addition to the usual parallelization/intertwining processes reported for other

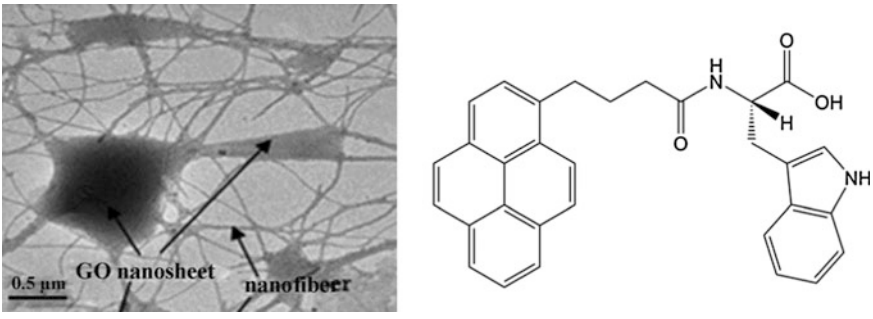

Fig. 7.6 *Left* TEM image of a dihybrid gel showing the presence of nanofibrils as well as of nanosheets. The hydrogel consists of 31 mg of the organogelator + 0.24 mg of graphene oxide. From Banerjee et al. [11]

systems. Banerjee et al. have observed a near twofold increase of the storage modulus for the dihybrid systems.

Trihybrid gels can also be prepared by incorporation of metallic particles that are stabilized in the gel scaffold.

7.4 Summary

The available studies on hybrid systems from polymers and organogels are admittedly still limited but can be promising for preparing new functional materials. Indeed, polymers are relatively cheap compared to organogelators that require many synthesis steps. Yet, organogelators may bear functional properties something that cannot necessarily be achieved in a simple way with classical polymers. The combination of both systems may therefore open new horizons. New molecular structures can be created only by physical processes.

Another interesting outcome of the above studies lies in the fact that organogelators are readily compatible with polymers as homogeneous solutions can be prepared at high temperature in these three different studies. This is clearly an advantage in the design of processes in view of obtaining new functional materials.

References

1. Dasgupta, D., Srinivasan, S., Rochas, C., Ajayaghosh, A., Guenet, J.M.: Hybrid thermoreversible gels from covalent polymers and organogels. Langmuir **25**, 8593 (2009)
2. Dasgupta, D., Kamar, Z., Rochas, C., Dahmani, M., Mesini, P., Guenet, J.M.: Design of hybrid networks by sheathing polymer fibrils with self-assembled Nanotubules. Soft Matter **6**, 3573 (2010)
3. Khan, A.N., Schmutz, M., Lacava, J., Al Ouahabi, A., Nguyen, T.T.T., Mesini, P.J., Guenet, J. M.: Design of nanohybrid systems from a partially fluorinated organogelator and syndiotactic polystyrene. Thermorevers. Gel Langmuir **31**, 7666 (2015)
4. see for instance Strobl, G.R.: The Physics of Polymers: Concepts for Understanding their Structures and Behavior. Springer, New York (1996)
5. Collin, D., Guenet, J.M.: unpublished data
6. Diaz, N., Simon, F.-X., Schmutz, M., Rawiso, M., Decher, G., Jestin, J., Mesini, P.J.: Self-assembled diamide nanotubes in organic solvents. Angew. Chem. Int. Ed. **44**, 3260 (2005)
7. Simon, F.X., Nguyen, T.T.T., Diaz, N., Schmutz, M., Deme, B., Jestin, J., Combet, J., Mesini, P.J.: Self-assembling properties of a series of homologous ester-diamides: from ribbons to nanotubes. Soft Matter **9**, 8483 (2013)
8. Oster, G., Riley, D.P.: Scattering from cylindrically symmetric systems. Acta Crystallogr. **5**, 272 (1952); Guenet, J.M., Fazel, N., Rochas, C.: Similarities between thermorever-sible gels of synthetic polymers and biopolymers: case of poly methyl methacrylate and kappa-carrageenan. Trends Macromol. Res. **1**, 345 (1994)

9. Porod, G.: Die Rontgenkleinwinkelstreuung Von Dichtgepackten Kolloiden.2. Systemen Kolloid-Zeitschrift And Zeitschrift Fur Polymere. **125**, 51 (1951)
10. Bai, H., Li, C., Wang, X., Shi, G.: On the gelation of graphene oxide. J. Phys. Chem. C **115**, 5545 (2011)
11. Nanda, J., Biswas, A., Adhikari, B., Banerjee, A.: A gel-based trihybrid system containing nanofibers, nanosheets, and nanoparticles: modulation of the rheological property and catalysis. Angew. Chem. Int. Ed. **52**, 5041 (2013)

Chapter 8
Current and Potential Applications

Not some many applications involve organogels at least on a large-scale use. Many potential applications are, however, at hand, particularly for high-tech purposes as the synthesis of organogelators is usually costly. Herein, a few typical examples are given, but again this list is far from being exhaustive. Rather, it aims at spanning a large range of domains of applications. The cases presented here differ from those published in the books and reviews mentioned in the introduction.

8.1 Nucleating Agent

Organogelators, such as 1,3:2,4-dibenzylidene sorbitol (DBS) (see Chap. 5), or dimethyl dibenzylidene sorbitol are a very efficient agents for the nucleation of polyolefins, and belongs to a specific class named *clarifying agents*. DBS forms a gel at extremely low concentrations in large variety of solvents except water. Its shows a typical fibrillar structure which is the main feature for its use for nucleation purposes [1] (see Fig. 8.1).

The propensity to nucleate polymer crystallization is highlighted by a "*decoration*" technique devised by Wittmann and Lotz which consists in "evaporating" polyethylene (PE) onto a DBS xerogel [2, 3]. Under these conditions, low molecular weight polymer chains are produced that interact in an epitaxial manner with the substrate. As can be seen in Fig. 8.2, PE crystallization does conspicuously occur on the DBS fibrils.

For a long time, the crystallization half-time for isothermal annealing was taken as a criteria, although polymer processing is usually a non-isothermal process. Nucleation capability of a given component was therefore not properly assessed. Thierry et al. and Fillon et al. tackled the question by contemplating another approach [3, 4]. It is based on the fact that the highest efficient for any nucleating agent cannot outreach that of the own crystals of a given polymer. Values obtained with self-seeding techniques,

J.-M. Guenet, *Organogels*, SpringerBriefs in Materials,
DOI 10.1007/978-3-319-33178-2_8

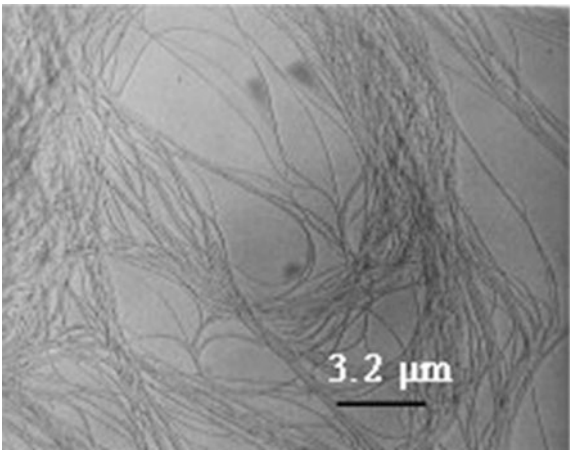

Fig. 8.1 Xerogel of DBS, prepared on the microscope grid from a tetrahydrofuran solution gelled by addition of benzene. From Thierry et al. [1]

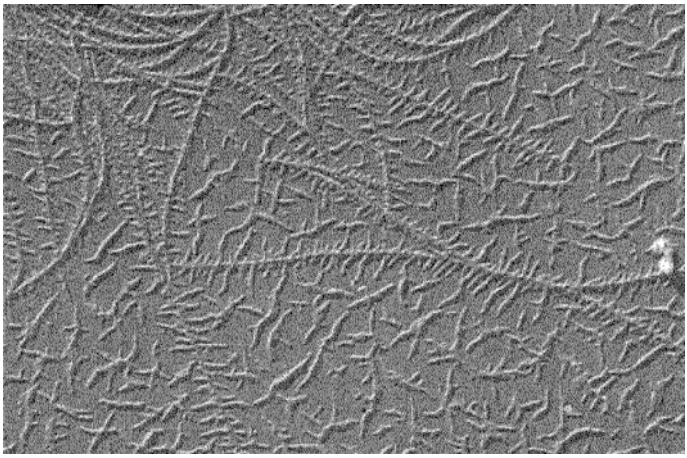

Fig. 8.2 Electron micrograph of DBS fibers "decorated" by "vaporized" PE [2]. The PE lamellae have grown onto DBS fibrils at a right angle, whereas the PE lamellae grown onto the glass substrate are randomly oriented. From Thierry et al. [1–3]

namely homogeneous nucleation triggered by the own crystals remnants of the polymer, defines the upper crystallization temperature in their efficiency scale which relies on the following equation [4]:

$$E = 100 \times \left[\frac{(T_c - T_{co})}{(T_{c\max} - T_{co})} \right] \tag{8.1}$$

where T_c is the effective crystallization temperature of the nucleated system, T_{co} the crystallization temperature in the absence of nucleating agent, and T_{cmax} the highest achievable crystallization temperature obtained by the polymer self-seeding method.

In this scale, DBS yields $E = 41$ a value well below compared to self-seeding. Yet, as said above, the essential gain is the drastic reduction of the crystal size with this compound which entails a large increase of the transparency of the processed polymer.

DSB fibrils can also be efficient with different polymers such as polypropylene, poly[ethylene oxide], and the like.

8.2 Hydrophobic Materials

Ajayaghosh and coworkers have succeeded in preparing highly hydrophobic materials [5, 6] involving OPV molecules and carbon nanotubes (CNT). These are clearly hybrid materials and could have been presented in Chap. 7. Yet, their potential application makes it that it best deserves to be detailed in the present chapter.

The nanocomposite is obtained by dispersing multiwalled nanotubes (MWNTs) in solutions of OPVs in chloroform followed by sonication. To be sure, no true solution is obtained but rather a stable suspension. A comparison of TEM images of CNTs and the hybrid system shows a conspicuous difference in surface morphology. In the hybrid system, there is a clear nanometer scale roughness generated by the coating of the CNTs by OPV molecules (Fig. 8.3). This hybrid material possesses the lotus properties: it is highly hydrophobic and also displays self-cleaning properties.

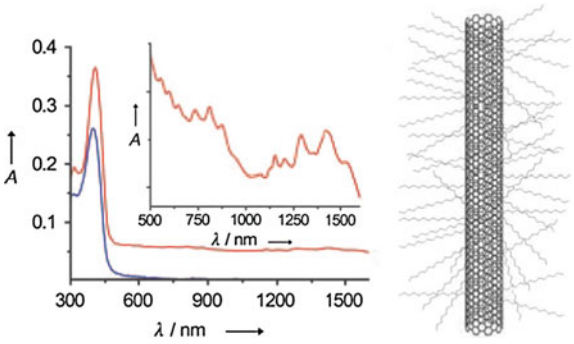

Fig. 8.3 *Left* absorption spectra of OPV (*blue*) and OPV/SWNT hybrid (*red*) in chloroform. *Inset* enlarged area between 500 and 1600 nm showing the van Hove singularities. *Right* a schematic representation of OPV molecules adsorbed on a SWNT, showing the hairy alkyl chains projecting outwards. From Srinivasan et al. [5]

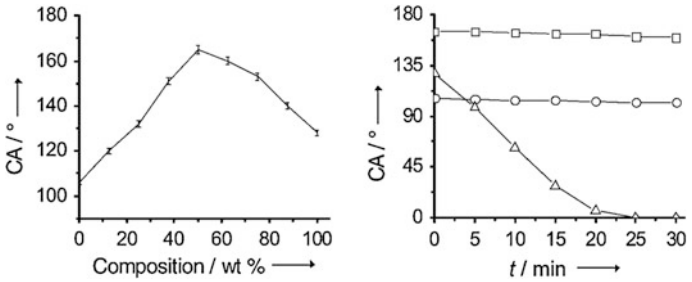

Fig. 8.4 *Left* variation of the water contact angle against the CNT content in the nanocomposite; *right* contact angle as a function of time for OPV/CNT (•), pure OPV (•) and pure CNT (•). From Srinivasan et al. [5]

According to Ajayaghosh and coworkers [5], the structure of the hybrid system consists of OPV molecules adsorbed onto the CNT where the aliphatic moieties are pointing outwards. This confers hydrophobic properties as demonstrated by measuring the water contact angle of the nanocomposite deposited onto a glass surface (Fig. 8.4). Values around 162° are reached for 50/50 mixtures. There is clearly a synergetic enhancement of the hydrophobicity, since neither pure OPV nor pure CNTs coatings reach contact angles that are high. Also, OPV molecules stabilize this hydrophobicity which otherwise gradually vanishes on pure CNTs as shown in Fig. 8.4.

The water contact angle for a hydrophobic surface is usually expressed through a modified Cassie equation [7]

$$\cos\theta_r = f_1 \cos\theta - f_2 \tag{8.2}$$

where θ_r and θ are the contact angles measured on the hybrid system and on the pure OPV coating, respectively; f_1 stands for the fraction of solid/water interface, and f_2 for that of the air/water interface.

A rough surface, as is the case for the nanohybrid is likely to trapping air, which eventually enhances the hydrophobicity. The f_2 value is estimated by means of Eq. 8.2, which yields $f_2 \approx 0.953$, namely a very high fraction of trapped air.

Also, water droplets can roll on the composite surface much more easily than on the CNT and OPV surfaces. This difference is explained by the difference in the CA hysteresis the force required to move the droplets [8]

$$F = \gamma_{LV}(\cos\theta_R - \cos\theta_A) \tag{8.3}$$

where θ_R and θ_A are the receding and advanced contact angles, γ_{LV} the surface tension of the liquid-vapor interface.

According to Ajayaghosh, it takes a force about 24–44 times larger for the water droplets to move on pure CNT and OPV coatings, respectively, than on the nanocomposite surface [5, 6]. This particular aspect accounts for the self-cleaning property of the hybrid material.

8.3 Detection of Explosives

Techniques based on fluorescence properties of specific compounds are used for detecting explosives, whose presence alters the spectrum through a decrease, an increase or a shift in the emission. Fluorescent polymers were used for this purpose until recently when fluorescent organogels are shown to be also efficient systems. Ajayaghosh have studied the detection properties of the molecule described in Fig. 5.10 whose crystalline lattice contains a nanocavity [9]. It turns out that the nanocavity possesses the propensity to house molecules of the size of aromatic derivatives such as trinitrotoluene (TNT), a well-known explosive (Fig. 8.5). In doing so, the fluorescent properties for an excitation wavelength of λ_{ex} = 450 nm are deeply altered even for very low contents of TNT as shown in Fig. 8.5.

In order to be used as a simple test for detecting explosives on hands, clothes, and the like, the gel has to be deposited onto a blotting paper. The same authors have observed that under this solvent removal procedure the xerogel still retains the original fibrillar morphology but essentially takes on an orange–red color. Exposing this coated blotting paper to TNT solutions in acetonitrile entails a strong attenuation of the fluorescence for 10^{-3} M while some attenuation is still observed for concentrations as low as 10^{-15} M (see Fig. 8.6). This is the reason why Kartha et al. define their system as "attogram sensing" device [9].

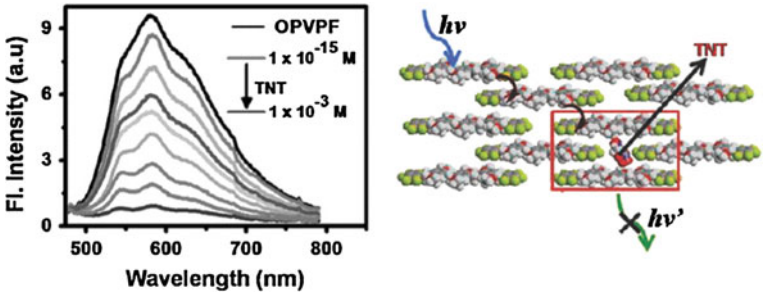

Fig. 8.5 *Left* fluorescence spectra for TNT solutions of different molar concentrations. Each curve differs from its neighbors by concentrations one order of magnitude higher or lower. *Right* the location of the TNT molecules in the lattice. From Kartha et al. [9]

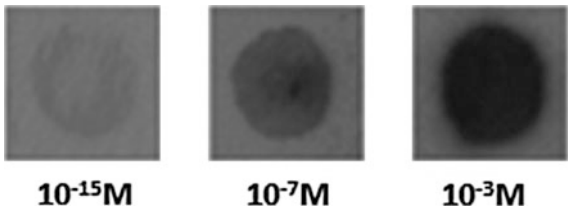

Fig. 8.6 Quenching of the fluorescence of OPV gels after deposition onto a blotting paper and viewed under 365 nm UV illumination. Molar concentrations as indicated. From Kartha et al. [9]

According to Kartha et al. [9], the nanocavity allows the formation of a tight complex between the OPV molecules and TNT as shown in Fig. 8.5. As a result, the occluded TNT molecules behave as a fluorescence trap. A faster exciton diffusion mechanism of the type described for conjugated polymers may be at play [9], which facilitates efficient fluorescence quenching by possible energy-transfer and electron-transfer mechanisms.

In any case, this technique is shrewd and very simple. It can be brought about very easily at low cost, as the concentrations for the OPV solutions that are required for preparing the gels are rather low (below 1 %) which entails a very low organogelator consumption.

8.4 Mesoporous Catalysts

The search for new type of catalytic substrate is still a topic of interest. Porous media are usually popular as they possess very large surface area in a comparatively small volume. These are in some cases prepared by making use of templates, such as surfactants, that are eliminated once the scaffold of interest has been obtained [10].

Mésini and coworkers have recently devised an original process for obtaining mesoporous materials with cylindrical pores [11]. Their approach is based on the use of nanotubes as those described in Chap. 4 (Figs. 4.9 and 4.10).

The preparation procedure consists of five steps: (1) preparing a homogeneous solution of a polymerizable monomer/solvent (ethylene glycol diacrylate) and a nanotube-forming molecule (BHPB-10); (2) cooling to make an organogel consisting of an array of nanotubes; (3) photopolymerize the monomer/solvent (with diphenyl-(2,4,6-trimethylbenzoyl)-phosphine oxide (TPO) as the photoinitiator); (4) extracting the nanotubes for leaving the porous resin only; (5) grafting onto the resin walls appropriate functional groups for catalysis purposes.

As can be seen in Fig. 8.7 the morphology of the materials consists of cylindrical pores tubes that are more or less interconnected. After exposure to a solution made up with 1 M NaOH (MeOH/H2O: 1/1 v/v) the mesopore walls are clad in COO^- groups. This chemical treatment alters the pores diameters significantly by shifting the center of the distribution from 30 to 50 nm. The specific area is not very high (50 m^2:g) but still of interest for performing catalyzed reactions.

The catalytic properties of this mesoporous material are shown in Fig. 8.7 by means of a Knoevenagel reaction. Comparison is given with a blank experiment. The turnover of the catalyst from these curves is of 705×10^{-6} $s^{-1}g^{-1}$ and the specific activity at 25 °C is of 16 mmol/hxg. For comparison with Na-MCM41 (Na substituted mesoporous silica) the activity is of 15.5 mmol/hxg but at 70 °C [12].

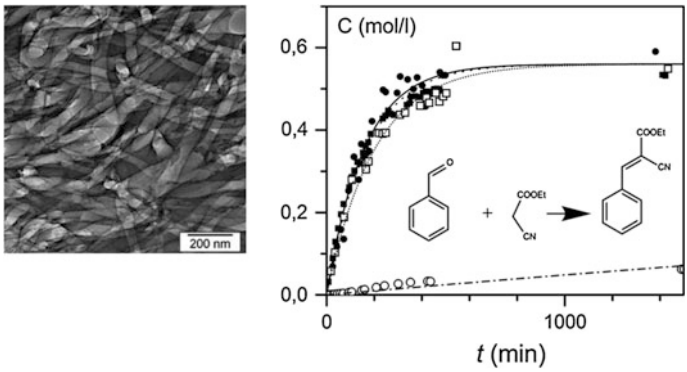

Fig. 8.7 *Left* TEM morphology of a slice of the mesoporous material. *Right* Concentration versus time in the kinetics of the catalyzed reaction of Knoevenagel (shown in *inset*).; ●: 1st cycle; ■: 2nd cycle; □: 3rd cycle; ◯: blank experiments. Fits are performed considering a first order reaction with $C = K(1\text{-}\exp(-t/\tau))$. From Nguyen et al. [11]

8.5 Highly Conducting Fibrils

Recently, a team headed by N. Giuseppone has devised organogels possessing fibrils with unusual properties such as high conductivity of the metallic type [13–16] and plasmonic interconnectors. The organogelators are derivatives from triarylamine. These organogels, prepared in chloroform or tetrachloroethane, display the usual array of randomly dispersed fibrils (Fig. 8.8).

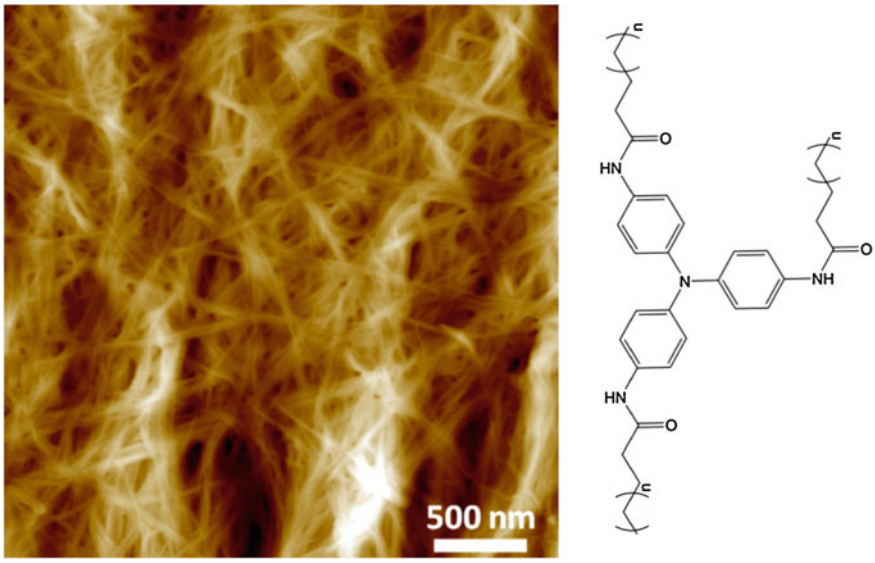

Fig. 8.8 *Left* AFM picture of an organogel prepared from right: a triarylamine derivative (here $n = 8$) in chloroform. $C_{org} = 0.015$ g/cm^3. From Armao et al. [13]

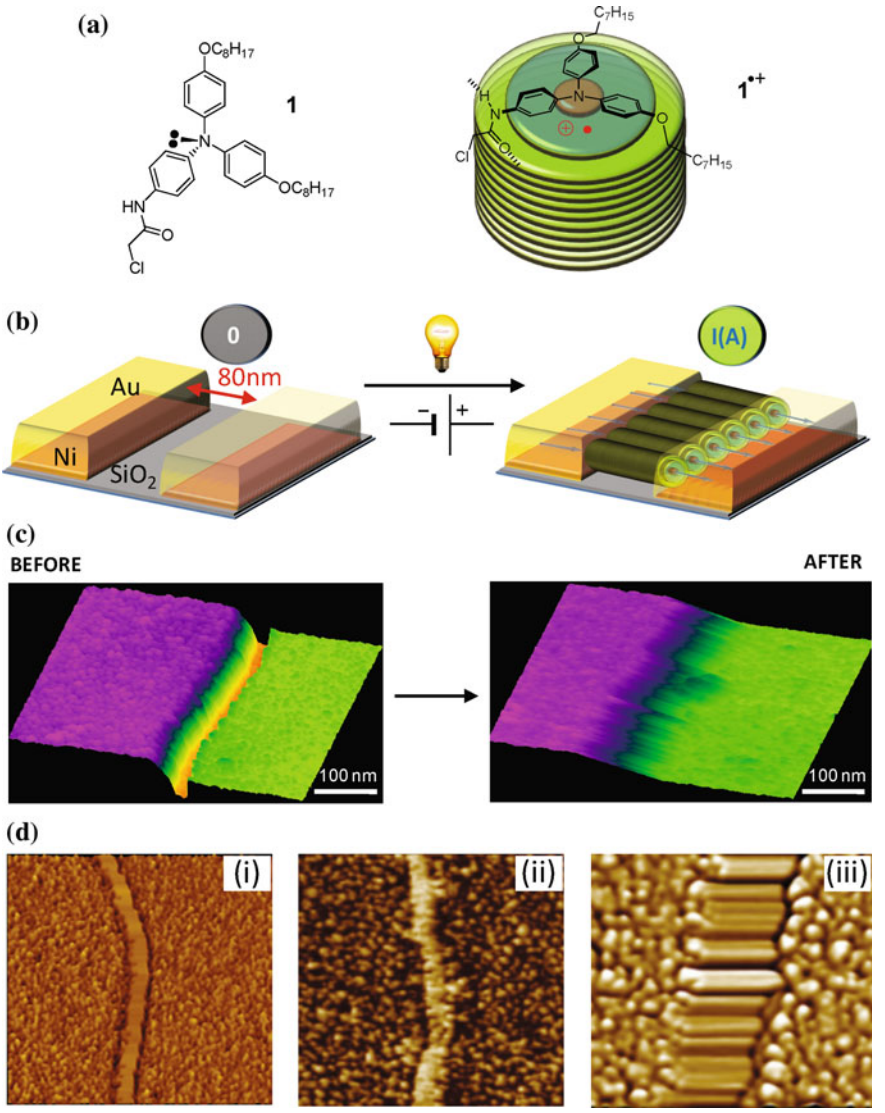

Fig. 8.9 **a** The triaryl derivative together with the way molecules stack to form fibrils; **b** self-assembly and orientation of the fibrils triggered by shining light onto the sample; **c** topographic view of the nanotrench before and after the illumination process; **d** AFM pictures: *i* the fibril-free gap, *ii* gap filled with the self-assembled molecules after light irradiation; *iii* zoom into the gap highlighting the fibrils orientation. From Faramarzi et al. [14]

The grail for many chemists would consist in synthesizing organic systems with a conductivity close to that observed in metals. Giuseppone and coworkers have succeeded in preparing such materials through the self-assembly of triarylammonium cationic radicals [14] that is triggered by visible light (Fig. 8.9). Large fibrils

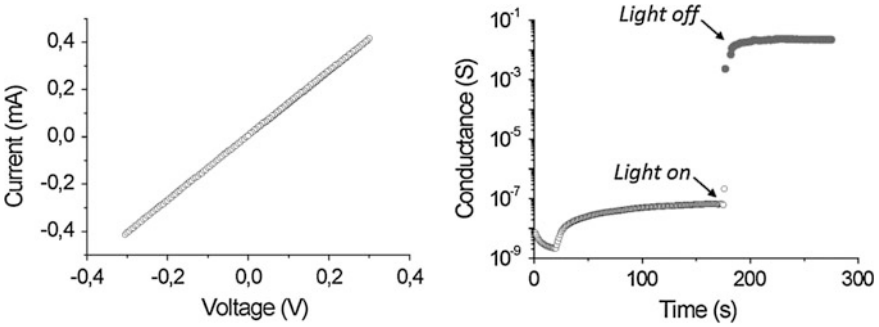

Fig. 8.10 *Left* I/V curve after self-assembly upon light irradiation of 0.001 g/cm^3 solution in tetrachloroethane. Right: variation of the conductance upon illumination. From Faramarzi et al. [14]

of diameter in the range 10–50 nm are formed. These are designated as supramolecular triarylamine nanowires (STANWs). A synergetic process stabilizes the charges of the initial radicals by electronic delocalization within the fibrils. Giuseppone et al. estimate delocalization length of 80 ± 3 nm corresponding to 1 charge every 160 triarylamines [14, 15].

These authors have studied the conductivity properties by depositing a drop of a solution in tetrachloroethane under no-light conditions between nanotrench of nano-patterned gold/nickel electrodes (Fig. 8.9). Illuminating with visible light results in the formation of cationic radicals together with strongly-oriented self-assembled fibrils.

Once properly oriented the STANWs display metallic properties as shown by a I/V study (intensity vs voltage). The variation of the intensity as a function of the voltage applied follows Ohm's law (Fig. 8.10). The conductance measured before and after illumination exhibits a jump of about six orders of magnitude, reaching values in the range 10^{-2}–10^{-1}S. The conductivity is estimated to be about 5 × 10^3 S/m, a value one order of magnitude lower than that observed with parallel metallic carbon nanotubes.

Giuseppone and coworkers have also shown that nanofibrils from triarylamines derivatives can act as plasmonic wave guides by connecting gold nanoparticles. This allows future making of optical nanocircuits that are said to be able to outdo classical electronic systems thanks to the faster information processing through light [16, 17].

8.6 Oil Extraction from Aqueous Media

The propensity of some gelator to form organogels only with the oily component in an aqueous mixture may be used for the containment of oil spills. Bhattacharya and Krishnan-Ghosh [18] were the first to report the capability of a simple amino acid derivative, N-lauroyl-L-alanine (Fig. 8.11).

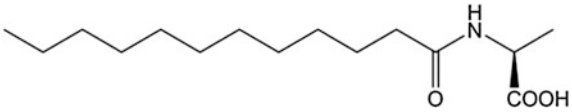

Fig. 8.11 Fatty acid derived amino acid, *N*-lauroyl-L-alanine used by Bhattacharya and Krishnan-Ghosh to gel oil-containing aqueous mixtures [18]

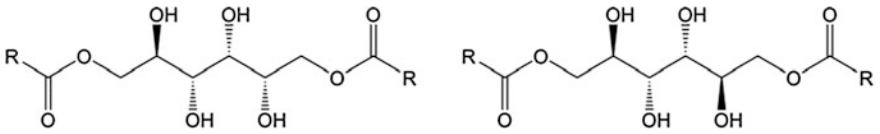

Fig. 8.12 Dialkanoate derivatives of the sugar alcohols of sorbitol (*upper left*) and mannitol (*upper right*) where *R* can be R = C_3H_7 or C_7H_{15}. From Jadhav et al. [18]

The gelators can be dissolved in aqueous systems but once room temperature is reached they gel the oily component rather than water. This is possibly due to the long aliphatic tail.

Later Jadhav et al. have observed the same effect with sugar-based organogelator shown in Fig. 8.12 [19].

8.7 Peptides Hydrogels for Medicinal Purposes

Hydrogels from peptide derivatives are of interest in biomedical applications such as cell scaffold for regenerative medicine [20] and/or injectable medium for drug release at well-defined places in human tissues and organs [21–23].

Stupp and coworkers used hydrogel prepared from a pentapeptide (isoleucine-lysine-valine-alanine-valine) incorporating an epitope known to promote neurite sprouting and to direct neurite growth. When aqueous solutions of this pentapeptide is mixed in a 1/1 ratio with a suspension of neural progenitor cells a hydrogel is produced. The underlying mechanism for the hydrogel formation is not detailed, and thus remains rather strange. Do cells trigger gelation in a heterogeneous way? This remains a pending question.

This hydrogel possesses the typical fibrillary morphology with fibrils of cross-sectional radii between 5 and 8 nm. This hydrogel, which contains 99.5 % of water acted as an excellent scaffold for the cells that remain viable for over 20 days. The formation of the hydrogel can also be obtained by injection of the peptide solution into tissues thanks to their thixotropic properties.

Thixotropic gels are particularly worth of consideration as they can be turned into a SOL, or at least a suspension of aggregates, when a threshold stress is

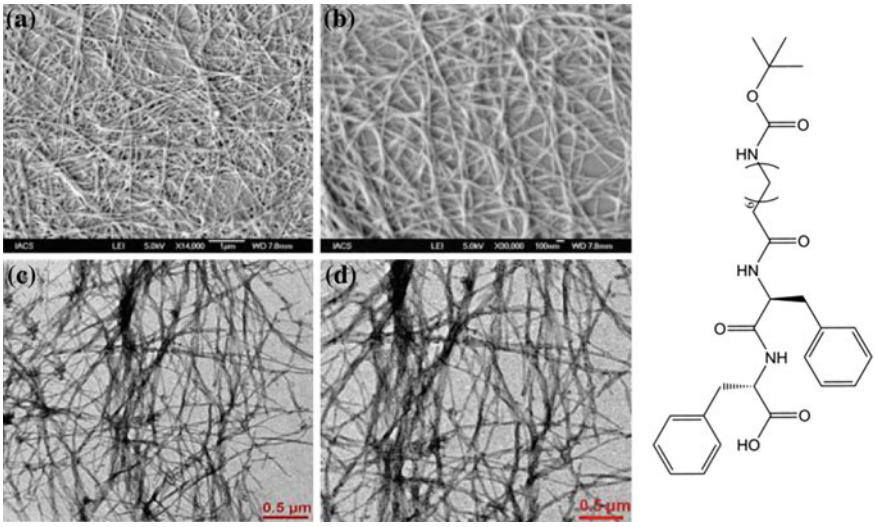

Fig. 8.13 *Left upper pictures* **a**, **b** FE-SEM images of a gel prepared at a 9.375 mM concentration; *lower pictures* **c**, **d** TEM images of hydrogels prepared at a 2.34 mM concentration. pH = 7.46. *Right* the chemical structure of the peptide-based gelator. From Baral et al. [23]

applied, but are regenerated once placed into the targeted location. The shear-thinning can be achieved when pushed through a needle by a usual syringe.

The design of the hydrogelator must be such that its melting temperature is above 37 °C as must be its formation/reformation temperature. Also, it must be formed in aqueous solutions whose pH is close to pH = 7.

A recent example of such hydrogels has been given by Banerjee and coworkers [23] on a peptide-based gelator (see Fig. 8.13). The resulting gels are of the fibrillary type with fibrils of cross-sectional section in the nanometer range (30–100 nm). These hydrogels were tested for release of cyanocobalamin, namely vitamin B12, and vancomycin, an antibiotic used against penicillin-resistant *staphylococcus aureus*. Banerjee et al. duly checked that these hydrogels did not show any cytotoxicity.

The rheological study of these hydrogels reveals that they are virtually 100 % reversible after applying a strain of 40 % (Fig. 8.14). After applying this strain, the storage modulus drops down dramatically, around a few tens of Pa, and the loss modulus becomes larger, which shows a transition to the SOL state. Note, however, that this SOL state may well be made up with finite aggregates but not at all with isolated peptide-based molecules. Recovery to the initial value of the storage modulus takes place within a few minutes, together with a loss modulus one order lower, which clearly indicates the reformation of a GEL state.

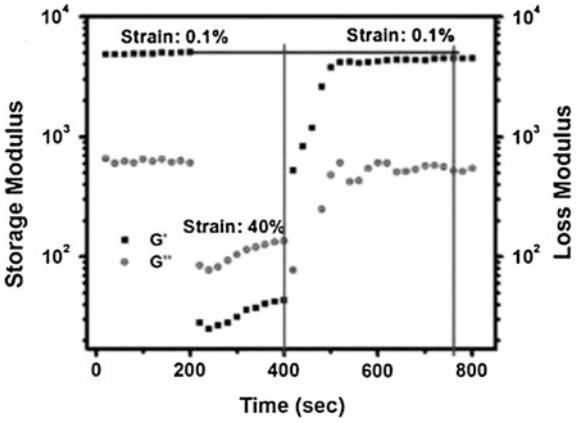

Fig. 8.14 Storage modulus (■) and loss modulus (●) as a function of time. Application of a strain of 40 % after 200 s leads to a sudden drop of the moduli by 2 orders of magnitude. After strain release the moduli nearly recover their initial values. From Baral et al. [23]

8.8 Summary

The overview presented in this chapter about current and potential applications of organogels is admittedly a limited one. Yet, it highlights the broad range of domains where organogels can contribute to create new materials and/or new processes in medicinal treatments to quote but a few. Although no current applications exist for hybrid materials involving polymers and organogels of the type as those detailed in Chap. 7, it is felt that these may flourish in a near future.

References

1. Thierry, A., Straupe, C., Lotz, B., Wittmann, J.C.: Physical gelation: a path towards ideal dispersion of additives in polymers polym. Commun. **31**, 299 (1990)
2. Wittmann, J.C., Lotz, B.: Polymer decoration: The orientation of polymer folds as revealed by the crystallization of polymer vapors. J. Polym. Sci. Polym. Phys. Ed. **23**, 205 (1985)
3. Thierry, A., Straupe, C., Wittmann, J.C., Lotz, B.: Organogelators and polymer crystallisation. Macromol. Symp. **241**, 103 (2006)
4. Fillon, B., Wittmann, J.C., Lotz, B., Thierry, A.: Self-nucleation and recrystallization of isotactic polypropylene (α phase) investigated by differential scanning calorimetry. J. Polym. Sci., Part B: Polym. Phys. **31**, 1383 (1993); Fillon, B., Lotz, B., Thierry, A.,Wittmann, J.C.: ibid. Self-nucleation and enhanced nucleation of polymers. Definition of a convenient calorimetric Efficiency scale and evaluation of nucleating additives in isotactic polypropylene (α phase) **31**, 1395 (1993)
5. Srinivasan, S., Praveen, V.K., Philip, R., Ajayaghosh, A.: Bioinspired superhydrophobic coatings of carbon nanotubes and linear p systems based on the "bottom-up" self-assembly approach. Angew Chem. Int. Ed. **47**, 5750 (2008)
6. Ajayaghosh, A., Srinivasan, S., Pravin, V.K.: Process for the development of superhydrophobic carbon nanotubes coatings, granted in US, patent no: 8323732, date of grant: 04/12/2012
7. Sun, T., Feng, L., Gao, X., Jiang, L.: Bioinspired surfaces with special wettability. Acc. Chem. Res. **38**, 644 (2005)

8. Öner, D., McCarthy, T.J.: Ultrahydrophobic. Surfaces effects of topography length scales on wettability. Langmuir **16**, 7777 (2000)
9. Kartha, K.K., Babu, S.S., Srinivasan, S., Ajayaghosh, A.: Attogram sensing of trinitrotoluene with a self-assembled molecular gelator. J. Am. Chem. Soc. **134**, 4834 (2012)
10. Kresge, C., Leonowicz, M., Roth, W., Vartuli, J., Beck, J.: Ordered mesoporous sieves synthesized by a liquid-template mechanism. Nature **359**, 710 (1992)
11. Nguyen, T.T.T., Simon, F.X., Khelfallah, N.S., Schmutz, M., Mésini, P.J.: Mesoporous polymeric catalysts synthesized from self-assembled organic nanotubes as templates. J. Mater. Chem. **20**, 3831 (2010)
12. Kloetstra, K.R., van Bekkum, H.: Base and acid catalysis by the alkali-containing MCM-41 mesoporous molecular sieve. J. Chem. Soc. Chem. Commun. 1005–1006 (1995)
13. Armao IV, J.J., Maaloum, M., Ellis, T., Fuks, G., Rawiso, M., Moulin, E., Giuseppone, N.: Healable supramolecular polymers as organic metals. J. Am. Chem. Soc. **136**, 11382 (2014)
14. Faramarzi, V., Niess1, F., Moulin, E., Maaloum, M., Dayen, J.F., Beaufrand, J.B., Zanettini, S., Doudin, B., Giuseppone, N.: Light-triggered self-construction of supramolecular organic nanowires as metallic interconnects. Nat. Chem. **4**, 485 (2012)
15. Giuseppone, N., Dayen, J.-F., Doudin, B., Faramarzi, V., Moulin, E., Niess, F.: Electrical conductivity by means of supramolecular polymers self-assemblies of triaryl amines, *patent* WO 2012093210
16. Armao, J.J., Domoto, Y., Umehara, T., Maaloum, M., Contal, C., Fuks, G., Moulin, E., Decher, G., Javahiraly, N., Giuseppone, N.: Supramolecular Organic Nanowires as Plasmonic Interconnects. ACS Nano, **10**, 2082–2090 (2016)
17. Moulin, E., Niess, F., Maaloum, M., Buhler, E., Nyrkova, I., Giuseppone, N.: The hierarchical self-assembly of charge nanocarriers: a highly cooperative process promoted by visible light. Angew. Chem. Int. Ed. **49**, 6974 (2010)
18. Bhattacharya, S., Krishnan-Ghosh, Y.: First report of phase selective gelation of oil from oil/water mixtures. Possible implications toward containing oil spills. Chem. Commun. 185 (2001)
19. Jadhav, S.R., Vemula, P.K., Kumar, R., Raghavan, S.R., John, G.: Sugar-derived phase-selective molecular gelators as model solidifiers for oil spills. Angew. Chem. Int. Ed. **49**, 7695 (2010)
20. Silva, G.A., Czeisler, C., Niece, K.L., Beniash, E., Harrington, D.A., Kessler, J.A., Stupp, S.I.: Selective differentiation of neural progenitor cells by high-epitope density nanofibers. Science **303**, 1352 (2004)
21. Zhang, Y., Gu, H., Yang, Z., Xu, B.: Supramolecular hydrogels respond to ligand-receptor interaction. J. Am. Chem. Soc. **125**, 13680 (2003)
22. Haines-Butterick, L., Rajagopal, K., Branco, M., Salick, D., Rughani, R., Pilarz, M., Lamm, M.S., Pochan, D.J., Schneider, J.P.: Controlling hydrogelation kinetics by peptide design for three-dimensional encapsulation and injectable delivery of cells. Proc. Natl. Acad. Sci. U. S. A. **104**, 7791 (2007)
23. Baral, A., Roy, S., Dehsorkhi, A., Hamley, I.W., Mohapatra, S., Ghosh, S., Banerjee, A.: Assembly of an injectable noncytotoxic peptide-based hydrogelator for sustained release of drugs. Langmuir **30**, 929 (2014)

General Summary

This monograph has hopefully provided the reader with some basic elements on the physical aspects of organogels that may be helpful for further investigations. Some general conclusions deserve to be developed particularly about the way these fascinating systems organogels should be studied, and in many case evaluated against their "cousins" the polymer thermoreversible gels.

Possibly, the first conclusion to be drawn for this comparison is that the fibrillary morphology of these two types of physical gels, despite being the same, originates in two different mechanisms: *1D crystallization* for the former against *chain-folding impediment* in the latter. As was highlighted in the introduction, these gels are just like birds and bats: they both have wings but the path of evolution was different. In spite of these differing origins, their investigation definitely relies on the same philosophy and approach.

In particular, it must be first checked that one is dealing with a gel according to the definition discussed in Chap. 1. The tube tilting is definitely a poor approach as toothpaste, humid sand, butter, and the like would pass the test. The fibrillary morphology should clearly be the first criterion, and then followed by the thermal behavior, namely the occurrence of first-order transitions for the gel formation and gel melting.

In the second place, the temperature-phase diagram should be mapped out. In the case of thermoreversible gels, many controversies occurred because scientists were not working at the same concentrations and therefore were not investigating the same phases. In many cases, Gibbs phase rules apply, but still one has to check that no size effect comes into play. Conclusions from the *T-C* phase diagram may be deceiving if such were the case.

This leads one to perform a deep study of the structure at different levels from the *microscopic range*, the crystal structure, to the *macroscopic range*, the morphology, not to mention the *mesoscopic structures*, namely the fibrils shape and how they interact so as to form the gel junctions. The junction type is not unique: many types exist, from side-by-side aggregation to intertwining, something which is still not clearly understood. Attempts have been made to predict whether a molecule would give an organogel through crystal engineering [1]. While this constitutes a first step to a better understanding of gelation, one remains far from

J.-M. Guenet, *Organogels*, SpringerBriefs in Materials,
DOI 10.1007/978-3-319-33178-2

being in a position to predict the appropriate design of a molecule possessing a very high probability to produce a gel. To do so, one should be able to find out whether this molecule will show the propensity to crystallize in a 1-D fashion in a given solvent. Further, as was presented in Chap. 3, the same molecule may form fibrillary structures in a given range of temperature but may produce spherulites in another range. The molecule–solvent interaction is probably the trickiest aspect to be mastered for obtaining adequate organogelation. In particular, the formation of molecular compound is an important issue that should be more seriously considered.

Finally, the question of the potential application of organogels should be raised. As a rule, their synthesis process is often long, tedious, and complex, so that the effective cost is high. Clearly, organogels have most probably little future in mass production but rather whenever high-tech materials are sought out for specific use. Thanks to their similar morphologies, hybrid gels prepared from polymers and organogelators may be of interest as they can combine the properties of both types of molecules. Polymers are usually much cheaper and can be used as a matrix for embedding the organogel, the latter bringing the functional properties. Similarly, both systems may bear a functional property, the possibilities being limited simply by imagination in view of the number of polymers and organogelators available nowadays. Although the making of materials with both systems appears obvious, little investigations have been carried out so far. This is most probably because ideas and results coming from either field have not cross-diffused so far. Hopefully, this monograph will achieve this goal.

Reference

1. Dastidar, P.: Supramolecular gelling agents: can they be designed? Chem. Soc. Rev. **37**, 2699 (2008)

Index

J.-M. Guenet, *Organogels*, SpringerBriefs in Materials,
DOI 10.1007/978-3-319-33178-2